NBS

Technical Note No. 319

NUMERICAL VALUES OF THE PATH INTEGRALS FOR LOW AND VERY LOW FREQUENCIES

By

LESLIE A. BERRY AND MARY E. CHRISMAN

U. S. DEPARTMENT OF COMMERCE
NATIONAL BUREAU OF STANDARDS

THE NATIONAL BUREAU OF STANDARDS

The National Bureau of Standards is a principal focal point in the Federal Government for assuring maximum application of the physical and engineering sciences to the advancement of technology in industry and commerce. Its responsibilities include development and maintenance of the national standards of measurement, and the provisions of means for making measurements consistent with those standards; determination of physical constants and properties of materials; development of methods for testing materials, mechanisms, and structures, and making such tests as may be necessary, particularly for government agencies; cooperation in the establishment of standard practices for incorporation in codes and specifications; advisory service to government agencies on scientific and technical problems; invention and development of devices to serve special needs of the Government; assistance to industry, business, and consumers in the development and acceptance of commercial standards and simplified trade practice recommendations; administration of programs in cooperation with United States business groups and standards organizations for the development of international standards of practice; and maintenance of a clearinghouse for the collection and dissemination of scientific, technical, and engineering information. The scope of the Bureau's activities is suggested in the following listing of its four Institutes and their organizational units.

Institute for Basic Standards. Applied Mathematics. Electricity. Metrology. Mechanics. Heat. Atomic Physics. Physical Chemistry. Laboratory Astrophysics.* Radiation Physics. Radio Standards Laboratory:* Radio Standards Physics; Radio Standards Engineering. Office of Standard Reference Data.

Institute for Materials Research. Analytical Chemistry. Polymers. Metallurgy. Inorganic Materials. Reactor Radiations. Cryogenics.* Materials Evaluation Laboratory. Office of Standard Reference Materials.

Institute for Applied Technology. Building Research. Information Technology. Performance Test Development. Electronic Instrumentation. Textile and Apparel Technology Center. Technical Analysis. Office of Weights and Measures. Office of Engineering Standards. Office of Invention and Innovation. Office of Technical Resources. Clearinghouse for Federal Scientific and Technical Information.**

Central Radio Propagation Laboratory.* Ionospheric Telecommunications. Tropospheric Telecommunications. Space Environment Forecasting. Aeronomy.

---

* Located at Boulder, Colorado 80301.

** Located at 5285 Port Royal Road, Springfield, Virginia 22171.

NATIONAL BUREAU OF STANDARDS

Technical Note 319

ISSUED September 2, 1965

NUMERICAL VALUES OF THE PATH INTEGRALS FOR LOW AND VERY LOW FREQUENCIES

Leslie A. Berry and Mary E. Chrisman
Central Radio Propagation Laboratory
National Bureau of Standards
Boulder, Colorado

NBS Technical Notes are designed to supplement the Bureau's regular publications program. They provide a means for making available scientific data that are of transient or limited interest. Technical Notes may be listed or referred to in the open literature.

For sale by the Superintendent of Documents, U. S. Government Printing Office
Washington, D.C. 20402
Price: 55 cents

Table of Contents

NUMERICAL VALUES OF THE PATH INTEGRALS FOR LOW AND VERY LOW FREQUENCIES

Leslie A. Berry and Mary E. Chrisman

ABSTRACT

Numerical values of the path integrals for the first five hops are given as a function of distance from 1000 km to 8000 km, for frequencies of 10, 20, 30, 60, 100, 150, and 200 kHz,, for sea paths, and for land paths with conductivities of 0.01 and 0.001 mhos/m, assuming reflection heights of 60, 70, 80, 90, and 100 km. For convenience, ground wave curves for the same parameters are given. Using these values, and any ionospheric reflection coefficients, the individual time modes, and the total field can be calculated simply. The calculation is valid near the caustic and in the shadow region. The path integrals can also be used to extract ionospheric reflection coefficients from experimental data.

Key words: path integrals, wave hops, low frequencies, propagation, diffraction.

Numerical Values of the Path Integrals for Low and Very Low Frequencies

Leslie A. Berry and Mary E. Chrisman

1. Introduction

This paper presents numerical results, in graphical form, which make possible simple full-wave calculations of LF and VLF field strengths. The theory used is analytically and numerically equivalent to VLF mode theory, but the concepts are asymptotically related to HF ray-hop theory, or geometric optics. The ray theory itself is not adequate at low frequencies because diffraction around the curvature of the earth is important for these wave lengths. The cutback factor [Wait and Conda, 1958] can be used to correct the first hop for diffraction, and there have also been attempts to provide diffractive corrections for the higher order hops [Norton, 1959] but these corrections are as difficult to calculate as the full wave hops [Berry, 1964; Berry and Chrisman, 1965], and more difficult to use in LF field strength calculations.

The theory used here was suggested by Rydbeck [1944] and Bremmer [1949], and developed in detail by Wait [1961]. Wait discussed the propagation characteristics of the hops and techniques for evaluating them, and Wait and Conda [1961] evaluated the path integral for the first hop. Berry [1964] showed the propagation characteristics of the first three hops graphically, and Berry and Chrisman [1965] developed detailed methods for calculating the path integrals. This paper is essentially a numerical supplement to the last mentioned paper.

The vertical electric field is written

$$E_r = E_o + \sum_{j=1}^{\infty} \gamma_j I_j , \qquad (1)$$

where E_o is the ground wave, γ_j is the ionospheric reflection coefficient, and I_j is the path integral [Wait, 1961]. Each term of the series in (1) is called a wave hop since it reduces, in the saddle point approximation, to the corresponding ray-hop of the geometric optics series. Thus the familiar geometry of ray theory is used, as shown in figure 1. The vertical electric dipole source is located on the surface of the spherical earth of radius a, with conductivity σ, and permittivity ϵ. The field is found on the surface at a great circle distance $d = a\theta$. The ray paths of the first two hops are shown for a reflection height h. The jth hop is incident on the earth at an angle τ_j, and on the ionosphere at an angle φ_j. Its phase path length is D_j. The lit region is $\tau_j < \frac{\pi}{2}$; $\tau_j = \frac{\pi}{2}$ is the caustic; and beyond the caustic is the shadow region. In the shadow region the "ray path" is assumed to run along the surface of the earth.

Section 2 describes the graphs of the path integrals and of the other parameters necessary to use them. Sources of ionospheric reflection coefficients to be used in (1) are discussed in section 3. A sample calculation, illustrating the use of the graphs, is given in section 4, and the formulas and methods of calculation are given in section 5.

2. Description of figures

The main results are the amplitudes and phase lags of the path integrals, I_j, $j = 1, \ldots, 5$, for frequencies of 10, 20, 30, 60, 100, 150,

and 200 kHz. Three kinds of paths are assumed; sea water ($\sigma = 5$, $\epsilon = 80$) where σ is the ground conductivity, in mhos/m, and ϵ is the dielectric constant relative to free space, and two land paths ($\sigma = 0.001$, $\epsilon = 10$, and $\sigma = 0.01$, $\epsilon = 15$). The curves are given for reflection heights of 60, 70, 80, 90, and 100 km. It is hoped that this set of parameters covers most cases of interest, and that the points are sufficiently close together as a function of frequency and height to allow interpolation. The space between the earth and the ionosphere is assumed to be free space, and the actual earth's radius, $a \cong 6.367 (10^6)$m, is used.

Also included are graphs of the ground wave, E_o, for the same set of parameters (figures 6, 7, and 8); a graph of $\cos\varphi$ as a function of distance parametric in height (figure 3); a graph to determine D_j (figure 4); and a graph to convert measured field strength to the equivalent dipole current moment (figure 5).

2.1 The path integrals

Figures 9 through 23 show the calculated path integrals. The figures are grouped first by conductivity; then each group is arranged by ascending reflection height. The wave hop number, j, is indicated by the digit after the decimal point; e.g., figure 14.3 shows the third hop. Each figure shows both the amplitude (divided by the frequency in kHz) and the phase lag, β_j, of the wave hop for the set of frequencies mentioned above. The phase lag is defined by

$$\beta_o = -\{\text{ph } E_o + kd + \pi/2\} \quad \text{for the ground wave,} \qquad (2)$$

and

$$\beta_j = -\{\text{ph } I_j + kD_j + \pi/2\} \quad \text{for the wave hops.} \qquad (3)$$

There is, of course, an ambiguity of an integral multiple of 2π. This definition was chosen so that $\beta_j \to 0$ for perfectly conducting earth in the saddle point (ray-hop) limit [Berry and Chrisman, 1965].

Figure 14.1 shows the amplitude and phase of I_1 for a path conductivity of 0.01 mhos/m. For this reflection height the caustic is at d = 1740 km -- beyond this is the shadow region. However, the first wave hop propagates into the shadow region by diffraction. Deep in the shadow region the propagation characteristics are much like a ground wave as demonstrated by Wait [1961]. Thus, the diffraction loss increases with frequency and is less for higher conductivities (compare figures 9.1 and 19.1).

The amplitude of I_2 for the same parameters is shown in figure 14.2. There is a relative minimum in the amplitude near 3000 km. This is caused by the pseudo-Brewster angle in the ground reflection coefficient [Bremmer, 1949]. The minimum is very sharp for a frequency of 150 kHz, showing that there is nearly perfect matching of characteristic and surface impedances for this set of parameters [Wait, 1962]. Corresponding to the sharp minimum in the amplitude, there is a sudden phase shift of 180°. The location of the psuedo-Brewster angle varies with frequency, conductivity, and, of course, reflection height. The pseudo-Brewster angle minimum also occurs on the third and higher hops at appropriately greater distances.

From geometrical considerations it is clear that the width of the neighborhood of the pseudo-Brewster angle and of the caustic region is proportional to the hop number. Figures 9.4 and 9.5 show that the very low frequency high-order wave hops have an oscillatory behavior in the vicinity of the caustic and the pseudo-Brewster angle. These are perhaps related to the interference fringes of optics, although, if so, it is not clear to the authors why they only occur for the high-order hops.

Figure 19.1 illustrates an interesting phenomenon that occurs on sea paths -- the amplitude curves cross over each other just beyond the caustic. The same crossover occurs in the geometric optics cut-back factor [Hyovalti, 1965]. In figure 19.3, there appears to be a double crossover in the third hop. The first is due to the frequency variation of the location of the pseudo-Brewster angle, and the second is the true crossover beyond the caustic.

Bremmer [1949] shows that the ground wave at a distant point does not increase monotonically with conductivity. Rather, for a fixed frequency, the field first increases with conductivity, goes through a broad maximum, and then decreases slowly with increasing conductivity. The path integrals behave the same way. For example, for h = 60 km, d = 7000 km, and f = 20 kHz, $|I_1(\sigma = .001)| = 2.85(10^{-11})$, $|I_2(\sigma = .01)| = 3.79(10^{-11})$, and $|I_1(\sigma = 5.)| = 3.5(10^{-11})$.

The phase lag, β_j, is a very sensitive indicator of computational accuracy since the first few significant digits are lost in (3). In some cases, especially hops 4 and 5, there is a slight discontinuity in the phase lag curves where the computer switches from the saddle point approximation (23) to numerical integration of (17). The worst example of this is the top curve in figure 18.5, where there is a discontinuity of about 40°. In most cases, the discontinuity is less than 5°, and it is not difficult to draw a smooth curve to eliminate the discontinuity.

There are undoubtedly features of the wave hop calculations of more interest to some readers than those described above. It is not the intent to exhaust the possibilities here -- the calculations are being presented in hopes they will be used and studied by others interested in LF and VLF propagation.

2.2 The ground wave

For completeness, the amplitude and phase lag of the ground wave are shown in figures 6, 7, and 8, for the same set of parameters used to calculate the path integrals. The only difference is the distance range covered -- the ground wave is important only at shorter distances, so the curves are shown from 100 km to 3500 km.

2.3 Normalization

The calculations have been made for a unit dipole current moment. (Refer to (19) of section 5.) Figure 5 shows the field of such a dipole at one mile as a function of frequency. The field strength increases below about 30 kHz because the induction and electrostatic fields extend out to one mile at these frequencies. The equivalent dipole current moment to be used for an existing transmitter is found by dividing the value given by figure 5 by the measured field strength at one mile.

3. Reflection coefficients

To use (1) to predict field strengths, ionospheric reflection coefficients must be available. Calculation of such coefficients is outside the scope of this paper; however, several sources of reflection coefficients will be listed, and instructions given for their use.

In general, the reflection coefficients are functions of angle of incidence, φ, which varies with distance and reflection height according to [Bremmer, 1949]:

$$\cos\varphi_j = \left[a\left(1 - \cos\frac{\theta}{2j}\right) + h\right]\left[2a(a+h)\left(1 - \cos\frac{\theta}{2j}\right) + h^2\right]^{-\frac{1}{2}} \qquad (4)$$

$$\cong \left[\frac{h}{a} + 4\left(\frac{jh}{d}\right)^2\right]^{\frac{1}{2}}, \text{ if } \frac{jh}{d} \ll 1.. \qquad (5)$$

The subscript j indicates the hop. Figure 3 shows $\cos\varphi$ as a function of d/j for various heights.

For propagation into the shadow region, the reflection coefficient for maximum φ (minimum $\cos\varphi$) is used. A useful approximation for the great circle distance to the caustic is

$$d_c \cong 225\sqrt{h}\, j \ , \tag{6}$$

where h and d_c are both in kilometers, and the angle of incidence for this distance is given approximately by

$$\varphi_c \cong 89.9 - \sqrt{h} \quad \text{degrees}, \tag{7}$$

where again h is in kilometers.

3.1 Isotropic ionosphere

If the effect of the earth's magnetic field is ignored, the ionosphere is isotropic, and

$$\gamma_j = T_{ee}^{\,j} = {}_{\|}R_{\|}^{\,j}, \tag{8}$$

where T_{ee} is the ratio of the incident field in the plane of incidence to the reflected field in the same plane. (The T notation is used by Bremmer [1949], Johler and Harper [1962], etc.; the R notation is used by Budden [1961], Wait [1962], etc.) For a sharply-bounded, homogeneous, locally plane ionosphere [Bremmer, 1949],

$$T_{ee} = \frac{\eta_i \cos\varphi - \sqrt{1 - (\sin\varphi/\eta_i)^2}}{\eta_i \cos\varphi + \sqrt{1 - (\sin\varphi/\eta_i)^2}} \ , \tag{9}$$

where $\eta_i^2 = 1 - i\,\omega_r/\omega$, $\omega_r = \frac{\omega_o^2}{\nu + i\omega}$, ω_o is the plasma frequency, and ν is the collision frequency.

Wait and Walters [1963a,b,c] show many results for continuously varying models of the ionosphere.

3.2 Anisotropic ionosphere

If the effect of the earth's magnetic field is included, γ_j is given by

$$\begin{bmatrix} \gamma_j & \alpha_{12} \\ \alpha_{21} & \alpha_{22} \end{bmatrix} = \begin{bmatrix} T_{ee} & T_{em} \\ -R_m T_{me} & -R_m T_{mm} \end{bmatrix}^j = \begin{bmatrix} {}_{\parallel}R_{\parallel} & {}_{\parallel}R_{\perp} \\ -R_{m\perp}R_{\parallel} & -R_{m\perp}R_{\perp} \end{bmatrix}^j , \tag{10}$$

where R_m is the Fresnel ground reflection coefficient for horizontal polarization [Bremmer, 1949]:

$$R_m = \frac{\cos\tau - \sqrt{\eta_g^2 - \sin^2\tau}}{\cos\tau + \sqrt{\eta_g^2 - \sin^2\tau}} , \tag{11}$$

where η_g is the index of refraction of the ground, given by (21). In (T_{mm} is the ratio of the incident field perpendicular to the plane of incidence to the reflected field perpendicular to the plane of incidence; T_{em} is the ratio of the incident field in the plane of incidence to the reflected field perpendicular to it; and T_{me} is the ratio of the incident field perpendicular to the plane of incidence to the reflected field in the plane of incidence.

Explicitly,

$$\gamma_1 = T_{ee}$$

$$\gamma_2 = T_{ee}^2 - R_m T_{em} T_{me}, \text{ and}$$

$$\gamma_3 = T_{ee}^3 - 2R_m T_{em} T_{me} + R_m^2 T_{em} T_{me} T_{mm}. \tag{12}$$

Clearly, (12) reduces to (8) if the terms containing the coupling coefficients T_{em} and T_{me} are neglected. This is usually a good approximation at grazing incidence for LF and VLF radio waves.

Johler, Walters, and Harper [1960] show reflection coefficients for a sharply bounded, homogeneous anisotropic ionosphere with arbitrary magnetic field, and Johler and Harper [1962] calculate them for a continuously stratified ionosphere with arbitrary magnetic field, as do Walters and Wait [1963] for a horizontal, transverse magnetic field.

Belrose [1964] shows average magnitude and the seasonal variation of measured reflection coefficients for several LF and VLF frequencies over various paths.

3.3 Extrapolation of reflection coefficients

It is sometimes convenient to extrapolate a reflection coefficient measured at a given frequency and distance to other frequencies and/or distances. The following empirical formulas have been suggested.

For an exponential model ionosphere and very low frequencies, Wait and Walters [1963a] have shown that

$$T_{ee} \cong - e^{-\alpha_1 \cos\varphi} e^{i\alpha_2 \cos\varphi} , \qquad (13)$$

where α_1 and α_2 are positive constants (for a fixed frequency). This is a very good approximation especially over moderate variations of φ.

Allcock [1955] suggested that

$$|T_{ee}| \cong \alpha_3 f \cos\varphi , \qquad (14)$$

which can be used to extrapolate in the frequency domain. Belrose [1964] has compiled data that tends to confirm (14) in the winter, but not in the summer.

4. Sample calculation

Using (2), (3), (17), and (42), (1) can be written

$$E_r \cong I_o \ell \, e^{-i(kd + \pi/2)} \left\{ |E_o|^{-i\beta_o} + \sum_{j=1}^{\infty} |\gamma_j| \, |I_j| e^{-i(\beta_j + k(D_j - d) - \text{ph}\,\gamma_j)} \right\} \tag{15}$$

All quantities in (15) except $|\gamma_j|$ and $\text{ph}\,\gamma_j$ are shown in figures in this paper, as discussed in section 2. Sources for $|\gamma_j|$ and $\text{ph}\,\gamma_j$ were discussed in section 3.

A sample field strength calculation is described below for the parameters:

$$f = 20 \text{ kc/s}, \; h = 70 \text{ km}, \; \sigma = 0.001, \; d = 1000 \; (200) \; 4000 \text{ km}.$$

For simplicity, an exponential, isotropic ionosphere is used so that $\gamma_j = T_{ee}^{j}$ (see (8)), and [Wait and Walters, 1963a]

$$T_{ee} \cong -\exp((-3 + 3.5i)\cos\varphi), \text{ i.e.,}$$

$$|\gamma_j| \cong e^{-3j\cos\varphi}, \text{ and } \text{ph}\,\gamma_j \cong j(\pi + 3.5\cos\varphi). \tag{16}$$

(1) For each distance and each hop, $\cos\varphi$ is found from figure 3. Since the first hop caustic is at $d \cong 1880$ km, $\cos\varphi$ is held constant for the first hop for all greater distances. Similarly, $\cos\varphi$ is constant for the second hop beyond 3760 km. Only three hops are necessary for this distance range.

(2) $|\gamma_j|$ and $\text{ph}\,\gamma_j$ are calculated using (16).

(3) $|E_o|$ and β_o are read from figure 6. $|I_j|$ and β_j, $j = 1, 2, 3$, are read from figures 10.1, 10.2, and 10.3

(4) For f = 20 kHz, $k \cong .419$. $(D_j - d) = j\left(\frac{D_j - d}{j}\right)$ is found from figure 4. Note that β_j is given in degrees while $k(D_j - d)$ and $\text{ph}\,\gamma_j$ are in radians.

(5) The individual terms of (15) are calculated and the sum of the series is found.

(6) If desired, the series can be multiplied by $I_o \ell e^{-i(kd + \pi/2)}$ as shown in (15). This was not done in the sample calculation.

The calculated amplitudes of the wave hops, the ground wave, and the total field for this example are shown in figure 2. As would be expected, it is not necessary to consider the ground wave at great distances. Indeed, for this daytime model, reasonably good results are obtained by including only the two largest wave hops at each point. At night, it would probably be necessary to include three, four, or more, hops.

The path integrals can also be used to extract ionospheric reflection coefficients from measured data [Berry and Chrisman, 1965].

5. Formulas used

A previous paper [Berry and Chrisman, 1965] discussed the calculation of the path integrals in detail and compared the methods of calculating them. The formulas used are repeated here for completeness.

5.1 The path integrals

The path integral I_j is given by

$$I_j \cong (-1)^j 4K e^{i\pi/4} \frac{e^{-ikd}}{\sqrt{\sin\theta}} \oint_c (1+zt)^{5/2} e^{-ixt} \frac{E_2^{j-1}(t)\, F^j(t)}{E_1^{j+1}(t)}\, dt, \quad (17)$$

where $k = 2\pi/\lambda = \frac{\omega}{c}$, $\omega = 2\pi f$, and c is the speed of light.

$$x = v\theta, \; z = \frac{1}{2v^2}, \text{ and } v = \left(\frac{ka}{2}\right)^{1/3}. \quad (18)$$

$$K = 11.96\, I_0 \ell \sqrt{\frac{k}{a^3}}\; v^2, \quad (19)$$

where $I_0\ell$ is the dipole current moment.

$$E_k(t) = W_k'(t) - qW_k(t), \text{ where} \quad (20)$$

$$q = -v\sqrt{1 - \eta_g^2} \;/\; \eta_g^2, \quad \text{and} \quad (21)$$

$\eta_g^2 = \epsilon - i\mu_0 c^2 \sigma/\omega$, where ϵ is the relative permittivity of the earth and σ is its conductivity.

The Airy function, $W_k(x)$, is discussed by Spies and Wait [1961] and formulas for its calculation are in section 5.3.

$$F(t) = \frac{W_1(t-y)}{W_2(t-y)} \quad (22)$$

where $y = kh/v$.

The saddle point approximation to (17) is

$$I_j \cong -i2K e^{-ikd} \sqrt{\frac{\pi}{x \sin\theta}} \left(1 + \frac{x}{2j\alpha}\right)^{\frac{1}{2}} (1+R)^2 e^{-i\Omega} R^{j-1} H(\alpha), \quad (23)$$

$$\text{where } \alpha = \frac{4j^2 y - x^2}{4xj} \quad , \tag{24}$$

$$\Omega = -x\alpha^2 + \frac{4}{3} j (y + \alpha^2)^{3/2} - \frac{4}{3} j \alpha^3 \quad , \tag{25}$$

$$R = \frac{\alpha M(is) - iqL(is)}{\alpha M(-is) + iqL(-is)} \cdot \frac{L(-is)}{L(is)} \quad , \tag{26}$$

$$s = \frac{2}{3} \alpha^3 \quad , \tag{27}$$

$$H(\alpha) = (1-\alpha^2 z)^{5/2} L^2(is) \left\{ \frac{L(is)}{L(-is)} \right\}^{j-1} , \tag{28}$$

and L(x) and M(x) are defined in (55).

The saddle point approximation is valid if $\alpha^2 >> 1$.

For most cases of interest $H(\alpha) \cong 1$, in which case Wait [1961] has shown that (23) is the jth geometrical optics ray-hop.

The integral in (17) can also be calculated by summing the residues at the poles, t_s, such that

$$E_1(t_s) = 0. \tag{29}$$

The calculation is intricate since the poles are of order j+1, but it can be done on a computer with the following formulas:

Rewrite (17) as

$$I_j \cong (-1)^{j-1} 4K e^{i\pi/4} \frac{e^{-ikd}}{\sqrt{\sin\theta}} \int \frac{D(t)\, E_2^{j-1}(t)\, F^j(t)\, dt}{E_1^{j+1}(t)} \tag{30}$$

$$\cong (-1)^{j-1} 4K e^{i\pi/4} \frac{e^{-ikd}}{\sqrt{\sin\theta}} \int \frac{A_j(t)}{B_j(t)} \, dt$$

$$\text{where } D(t) \cong (1 + \tfrac{5}{2} zt)\, e^{-ixt}, \text{ since } |zt| << 1. \tag{31}$$

Let $\mathrm{Res}(j,t_s)$ be the residue of the integrand of (17) at t_s. Then

$$I_j \cong (-1)^{j-1} 8\pi i \, K e^{i\pi/4} \frac{e^{-ikd}}{\sqrt{\sin\theta}} \sum_{s=o}^{\infty} \mathrm{Res}(j,t_s), \tag{32}$$

$$\mathrm{Res}(j,t_s) = \frac{(-1)^j}{b_{jo}^{j+1}} \begin{vmatrix} a_{jo} & a_{j_1} & a_{j_2} & \cdots & a_{jj} \\ b_{jo} & b_{j_1} & b_{j_2} & \cdots & b_{jj} \\ 0 & b_{jo} & b_{j_1} & \cdots & b_{jj-1} \\ 0 & 0 & b_{jo} & \cdots & b_{jj-2} \\ \cdot & \cdot & \cdot & \cdots & \cdot \\ \cdot & \cdot & \cdot & \cdots & \cdot \\ \cdot & \cdot & \cdot & \cdots & \cdot \\ 0 & 0 & . & b_{jo} & b_{j_1} \end{vmatrix}, \tag{33}$$

where $a_{jn}(t_s) = A_j^{(n)}(t_s)/n!$, and $b_{jn}(t_s) = B_j^{(n+j+1)}(t_s)/(n+j+1)!$. (34)

The superscript (n) denotes the nth derivative.

Using Liebnitz's rule for the nth derivative of a product [Kaplan, 1952],

$$(gh)^{(n)} = \sum_{m=1}^{n} \frac{n!}{m!(n-m)!} g^{(m)} h^{(n-m)}, \tag{35}$$

the necessary derivatives of $[E_2(t)F(t)]$ and

$$A_j(t) = A_{j-1}(t)[E_2(t)F(t)] \tag{36}$$

are found recursively. The necessary derivatives of D, E_2, and F for the first five I_j are

$$D^{(n)}(t) = (-ix)^{n-1} e^{-ixt}[n\tfrac{5}{2} z - ix(1+\tfrac{5}{2} zt)] \tag{37}$$

$$\begin{aligned}
E_2'(t) &= tW_2(t) - qW_2'(t), \\
E_2''(t) &= tW_2'(t) + (1-qt)W_2(t), \\
E_2^{(3)}(t) &= (t^2 - q)W_2(t) + (2-qt)W_2'(t), \\
E_2^{(4)}(t) &= (4t-qt^2)W_2(t) + (t^2-2q)W_2'(t), \text{ and} \\
E_2^{(5)}(t) &= (4-4qt+t^3)W_2(t) + (6t-qt^2)W_2'(t);
\end{aligned} \tag{38}$$

$$\begin{aligned}
F'(t) &= 2i[W_2(t-y)]^{-2}, \\
F''(t) &= -2GF'(t), \\
F^{(3)} &= \{-2(t-y) + 6G^2\} F'(t) \\
F^{(4)}(t) &= \{-2+16(t-y)G-24G^3\} F'(t), \text{ and} \\
F^{(5)}(t) &= \{16(t-y)^2 +20G-120\,(t-y)G^2 + 120G^4\} F'(t).
\end{aligned} \tag{39}$$

In (39), $G = W_2'(t-y)/W_2(t-y)$; a single prime indicates a first derivative and a double prime indicates a second derivative.

The b_{jn} can be found by repeated use of (36) and (29), but are given explicitly here for the first five hops.

$$
\begin{aligned}
b_{jo} &= (E_1'(t_s))^{j+1}, \quad j = 1,\ldots,5 , \\
b_{j1} &= \frac{j+1}{2}(E_1'(t_s))^{j} E_1''(t_s), \quad j = 1,\ldots,5, \\
E_1'(t_s) b_{j2} &= \frac{j}{4} E_1''(t_s)\, b_{j1} + \frac{j+1}{6} E_1^{(3)}(t_s)\, b_{jo}, \quad j = 2,\ldots,5, \\
E_1'(t_s) b_{j3} &= \frac{j-1}{6} E_1''(t_s)\, b_{j2} + \frac{2j+1}{18} E_1^{(3)}(t_s)\, b_{j1} \\
&\quad + \frac{j+1}{24} E_1^{(4)}(t_s)\, b_{jo}, \quad j = 3, 4, 5 , \\
E_1'(t_s) b_{j4} &= \frac{j-2}{8} E_1''(t_s)\, b_{j3} + \frac{j}{12} E_1^{(3)}(t_s)\, b_{j2} \\
&\quad + \frac{3j+2}{96} E_1^{(4)}(t_s)\, b_{j1} + \frac{j+1}{120} E_1^{(5)}(t_s)\, b_{jo}, \quad j = 4,5 ,
\end{aligned}
\tag{40}
$$

$$
\begin{aligned}
b_{55} &= \frac{3}{16} E_1'(t_s)(E_1''(t_s))^5 + \frac{5}{4}(E_1'(t_s))^2 (E_1''(t_s))^3 E_1^{(3)}(t_s) \\
&\quad + \frac{5}{6}(E_1'(t_s))^3 E_1''(t_s)(E_1^{(3)}(t_s))^2 \\
&\quad + \frac{5}{8}(E_1'(t_s))^3 (E_1''(t_s))^2 E_1^{(4)}(t_s) \\
&\quad + \frac{5}{24}(E_1'(t_s))^4 E_1^{(3)}(t_s) E_1^{(4)}(t_s) \\
&\quad + \frac{1}{8}(E_1'(t_s))^4 E_1''(t_s) E_1^{(5)}(t_s) \\
&\quad + \frac{1}{120}(E_1'(t_s))^5 E_1^{(6)}(t_s),
\end{aligned}
$$

and $b_{jn} = 0$, if $j < n$.

The necessary derivatives of $E_1(t_s)$ are

$$\begin{aligned}
E_1'(t_s) &= (t_s - q^2)\, W_1(t_s), \\
E_1''(t_s) &= W_1(t_s), \\
E_1^{(3)}(t_s) &= (t_s^2 - q^2 t_s + q)\, W_1(t_s), \\
E_1^{(4)}(t_s) &= (4t_s - 2q^2)\, W_1(t_s), \\
E_1^{(5)}(t_s) &= (t_s^3 - q^2 t_s^2 + 2t_s q + 4)\, W_1(t_s), \text{ and} \\
E_1^{(6)}(t_s) &= (9t_s^2 - 6q^2 t_s + 6q)\, W_1(t_s).
\end{aligned} \tag{41}$$

In general, the saddle point approximation is valid in the lit region except near the caustic; numerical integration of (17) is necessary in the vicinity of the caustic on the lit side; and the residue series is used in the shadow region.

5.2 The ground wave

In the notation used in this paper, the ground wave is [Wait, 1962]

$$E_o \cong 2iKe^{-i\pi/4} \frac{e^{-ikd}}{\sqrt{\sin\theta}} \int \frac{D(t)\, W_1(t)}{E_1(t)}\, dt \tag{42}$$

$$\cong -4\pi K e^{-i\pi/4} \frac{e^{-ikd}}{\sqrt{\sin\theta}} \sum_{s=o}^{\infty} \frac{D(t_s)}{t_s - q^2}\,, \tag{43}$$

where, again, t_s is a zero of $E_1(t)$.

5.3 The Airy functions, $W_k(x)$

Let [Spies and Wait, 1961]

$$y_1(t) = 1 + \sum_{n=1}^{\infty} \frac{(1)(4)(7)\ldots(3n-2)}{(3n)!} t^{3n}, \text{ and} \tag{44}$$

$$y_2(t) = t + \sum_{n=1}^{\infty} \frac{(2)(5)(8)\ldots(3n-1)}{(3n+1)!} t^{3n+1} \tag{45}$$

so that

$$y_1'(t) = \sum_{n=1}^{\infty} \frac{(1)(4)(7)\ldots(3n-2)}{(3n-1)!} t^{3n-1}, \text{ and} \tag{46}$$

$$y_2'(t) = 1 + \sum_{n=1}^{\infty} \frac{(2)(5)(8)\ldots(3n-1)}{(3n)!} t^{3n}. \tag{47}$$

Then

$$W_k(t) = u(t) + (-1)^k iv(t), \tag{48}$$

where

$$u(t) = (a_1 y_1(t) + a_2 y_2(t))\sqrt{3}, \tag{49}$$

$$v(t) = a_1 y_1(t) - a_2 y_2(t), \tag{50}$$

$$a_1 = \frac{\sqrt{\pi}}{\sqrt[3]{9}\,\Gamma(\frac{2}{3})}, \text{ and } a_2 = \frac{\sqrt{\pi}}{\sqrt[3]{3}\,\Gamma(\frac{1}{3})} \tag{51}$$

These convergent expansions are adequate for small $|t|$. For large $|t|$, the plane is divided into four regions:

Region I: $|\text{ph } t| < 20°$

Region II: $|\text{ph } t| > 100°$

Region IIIa: $-100° \leq \text{ph } t \leq -20°$, and (52)

Region IIIb: $20° \leq \text{ph } t \leq 100°$.

In region I, let $z = \frac{2}{3} t^{3/2}$, then [Olver, 1954]

$$W_k(t) \cong t^{-\frac{1}{4}} \left[e^z (L(z) + (-1)^k \frac{i}{2} e^{-z} L(-z)\right], \text{ and} \tag{53}$$

$$W_k'(t) \cong t^{\frac{1}{4}} \left[e^z M(z) + (-1)^{k+1} \frac{i}{2} e^{-z} M(-z)\right], \tag{54}$$

where

$$L(z) = \sum_{j=o}^{\infty} U_j z^{-j}, \quad M(z) = \sum_{j=o}^{\infty} V_j z^{-j}, \tag{55}$$

$U_o = V_o = 1$, and for $j \geq 1$

$$U_j = \frac{(2j+1)(2j+3)\ldots(6j-1)}{j!(216)^j}, \text{ and } V_j = - U_j \frac{6j+1}{6j-1}. \tag{56}$$

In region II, let $z = \frac{2}{3} (-t)^{3/2}$, then

$$W_k(t) \cong (-t)^{-\frac{1}{4}} \exp[i(-1)^k (z + \tfrac{\pi}{4})] \, L[(-1)^k iz], \text{ and} \tag{57}$$

$$W_k'(t) \cong (-t)^{\frac{1}{4}} \exp[i(-1)^k (z - \tfrac{\pi}{4})] \, M[(-1)^k iz]. \tag{58}$$

In region III, let $z = \frac{2}{3}(t)^{3/2}$, then, in IIIa

$$W_k(t) \cong t^{-\frac{1}{4}}[e^z L(z) + i(k-2)e^{-z}L(-z)], \text{ and} \tag{59}$$

$$W_k'(t) \cong t^{\frac{1}{4}}[e^z M(z) - i(k-2)e^{-z}M(-z)]. \tag{60}$$

In region IIIb

$$W_k(t) \cong t^{-\frac{1}{4}}[e^z L(z) + i(k-1)e^{-z}L(-z)], \text{ and} \tag{61}$$

$$W_k'(t) \cong t^{\frac{1}{4}}[e^z M(z) - i(k-1)e^{-z}M(-z)]. \tag{62}$$

These formulas are asymptotically valid in regions larger than those given here [Olver, 1954], but greater computational accuracy is achieved in the restricted regions.

6. References

Allcock, G. McK., (1955), Ionospheric absorption at low and medium frequencies in The Physics of the Ionosphere, Phil. Soc. London.

Belrose, J. S. (1964), The oblique reflection of CW low-frequency radio waves from the ionosphere, Propagation of radio waves at frequencies below 300 kc/s, AGARDograph 74 (Pergamon Press, New York, N.Y.).

Berry, L. A. (1964), Wave hop theory of long distance propagation of low frequency radio waves, Radio Sci. J. Res. NBS, 68D, No. 12, 1275-1284.

Berry, L. A. and M. E. Chrisman (1965), The path integrals of LF/VLF wave hop theory, Radio Sci. J. Res. NBS, 69D, No. 11.

Bremmer, H. (1949), Terrestrial radio waves. (Elsevier Publishing Co., New York, N.Y.).

Budden, K. G. (1961), Radio waves in the ionosphere (Cambridge at the University Press, London).

Hyovalti, D. C. (1965), Private communication.

Johler, J. R. and J. D. Harper, Jr. (1962), Reflection and transmission of radio waves at a continuously stratified plasma with arbitrary magnetic induction, J. Res. NBS 66D, (Radio Prop.), No. 1, 81-99.

Johler, J. R., L. C. Walters, and J. D. Harper, Jr. (1960), Low and very-low-frequency model ionosphere reflection coefficients, NBS Tech. Note. No. 69.

Kaplan, W. (1952), Advanced Calculus (Addison-Wesley Publishing Co., Inc., Reading, Mass.).

Norton, K. A. (1959), Transmission loss in Radio Propagation - II, NBS technical Note No. 12.

Olver, F.W.J. (1954), The asymptotic expansion of Bessel functions, Roy. Soc. of London, Phil. Trans. A, 247, 364-367.

Rydbeck, O.E.H. (1944), On the propagation of radio waves, Trans. of Chalmers Univ. of Tech., 34.

Spies, K. P. and J. R. Wait (1961), Mode calculations for VLF propagation in the earth-ionosphere waveguide, NBS Tech. Note No. 114.

Wait, J. R. (1960), Diffractive corrections to the geometrical optics of low frequency propagation, Electromagnetic Wave Propagation (Academic Press, London).

Wait, J. R. (1961), A diffraction theory of LF sky-wave propagation, J. Geophys. Res. 66, No. 6, 1713-1724.

Wait, J. R. (1962), Electromagnetic waves in stratified media (Pergamon Press, New York, N.Y.).

Wait, J. R. and A. M. Conda (1958), Pattern of an antenna on a curved lossy surface, IRE Trans. Ant. Prop. AP-6, No. 4, 348-359.

Wait, J. R., and A. M. Conda (1961), A diffraction theory of LF sky-wave propagation - an additional note, J. Geophys. Res. 66, No. 6, 1725-1729.

Wait, J. R. and L. C. Walters (1963a), Reflection of VLF radio waves from an inhomogeneous ionosphere, Part I, Exponentially varying isotropic models, J. Res. NBS 67D (Radio Prop.), No. 3, 361-367.

Wait, J. R. and L. C. Walters (1963b), Reflection of VLF radio waves from an inhomogeneous ionosphere. Part II, Perturbed exponential model, J. Res. NBS 67D (Radio Prop.), No. 5, 519-523.

Wait, J. R. and L. C. Walters (1963c), Reflection of VLF radio waves from an inhomogeneous ionosphere. Part III, Exponential model with hyperbolic transition, J. Res. NBS 67D (Radio Prop.), No. 6, 747-752.

Walters, L. C. and J. R. Wait (1963), Numerical calculations for reflection of electromagnetic waves from a lossy magneto plasma, NBS Tech. Note No. 205.

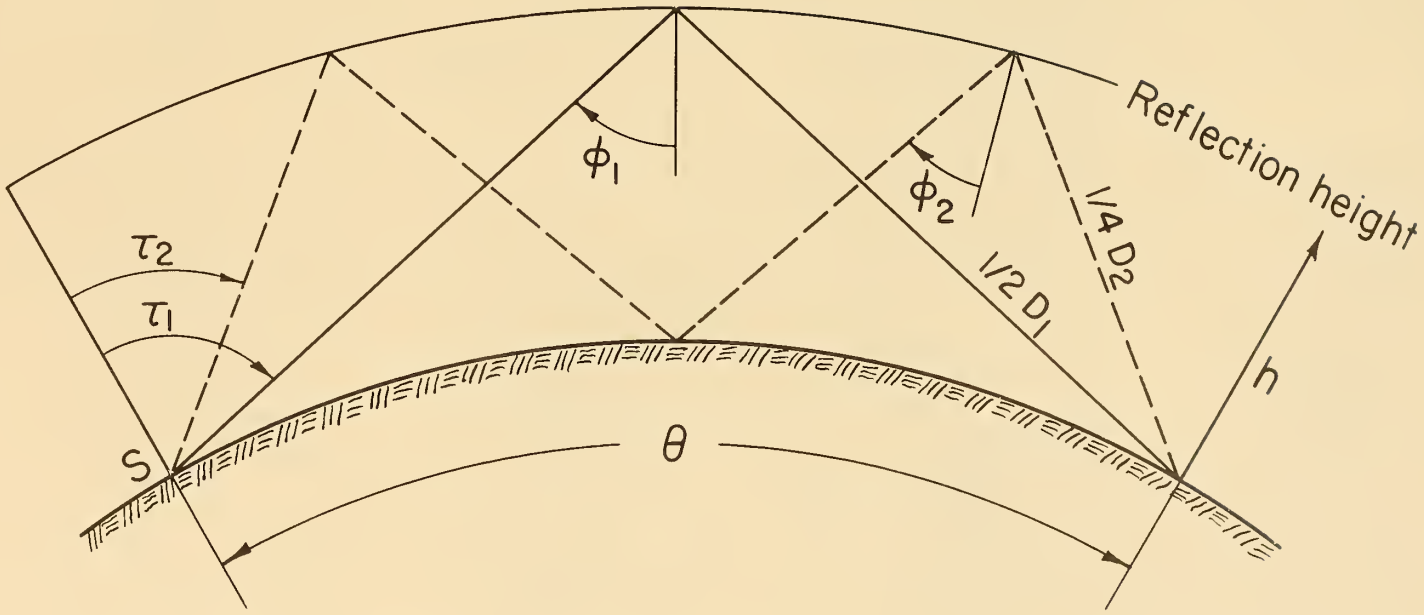

Figure 1. Geometry used.

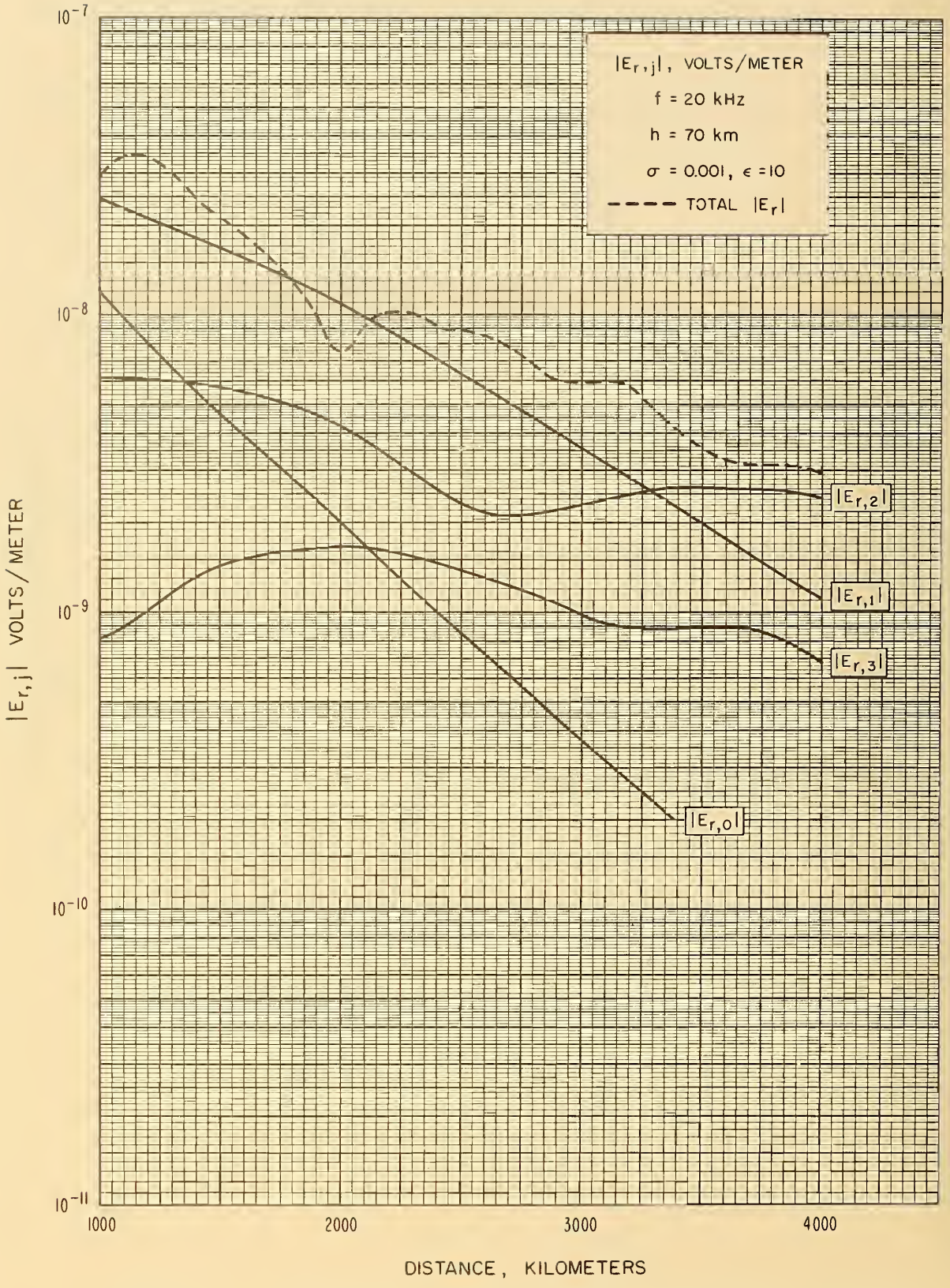

Figure 2. Amplitudes of the total field, ground wave, and first three wave hops showing the sample calculation of Section 4.

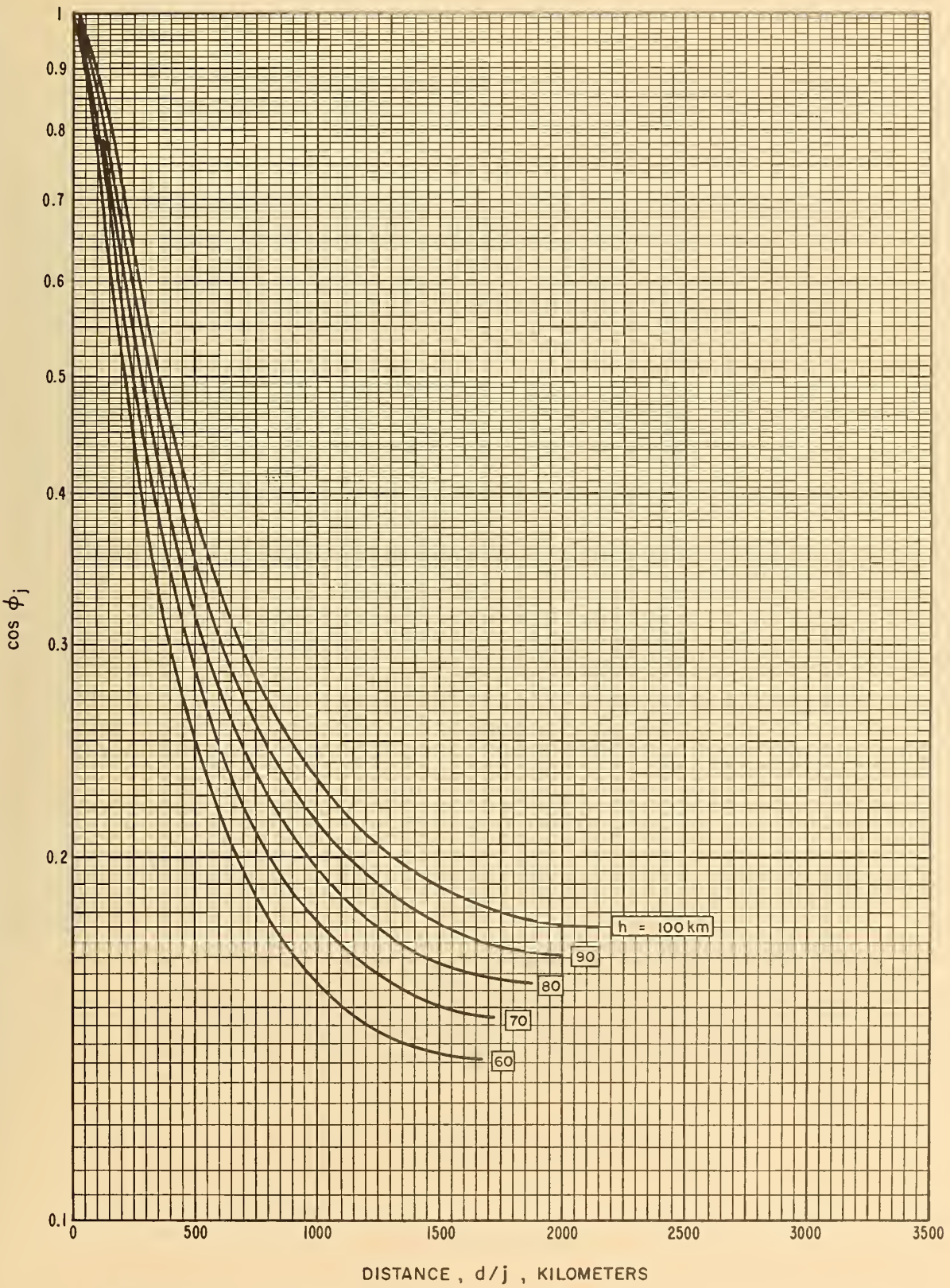

Figure 3. Cosine of the angle of incidence of a ray versus distance for various reflection heights.

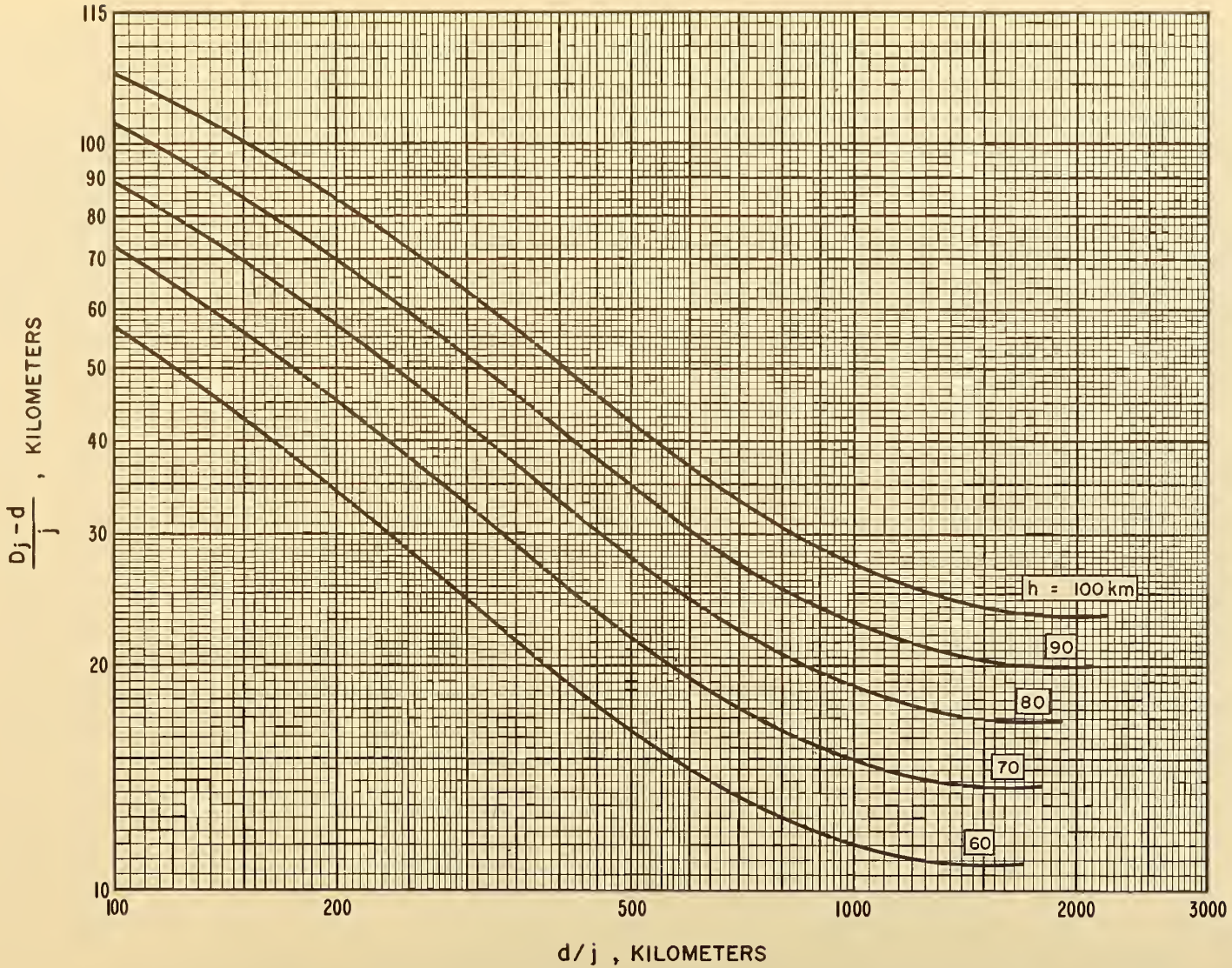

Figure 4. Values of $(D_j - d)/j$ versus d for various reflection heights, to be used in calculating the phase of the wave hop.

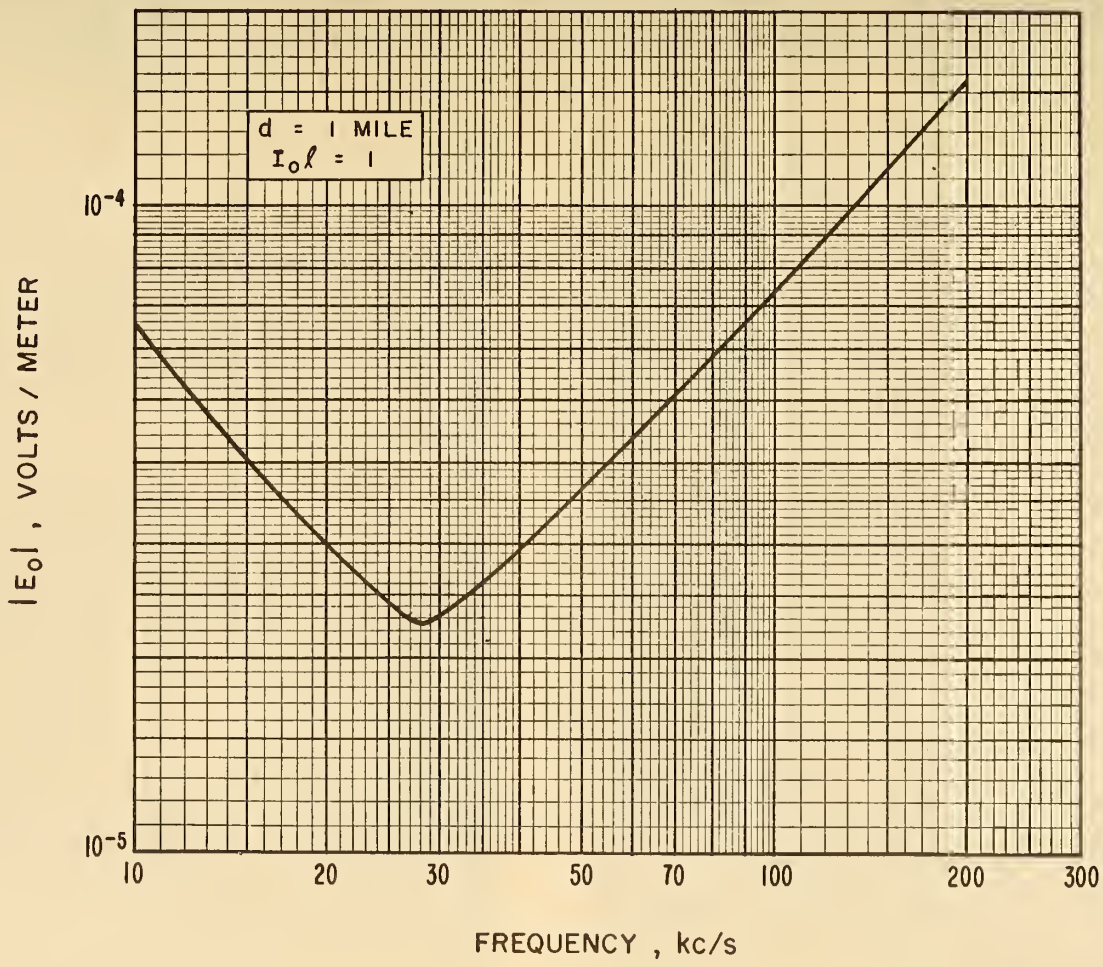

Figure 5. Vertical electric field at one mile of a vertical dipole with current moment $I_o\ell = 1$.

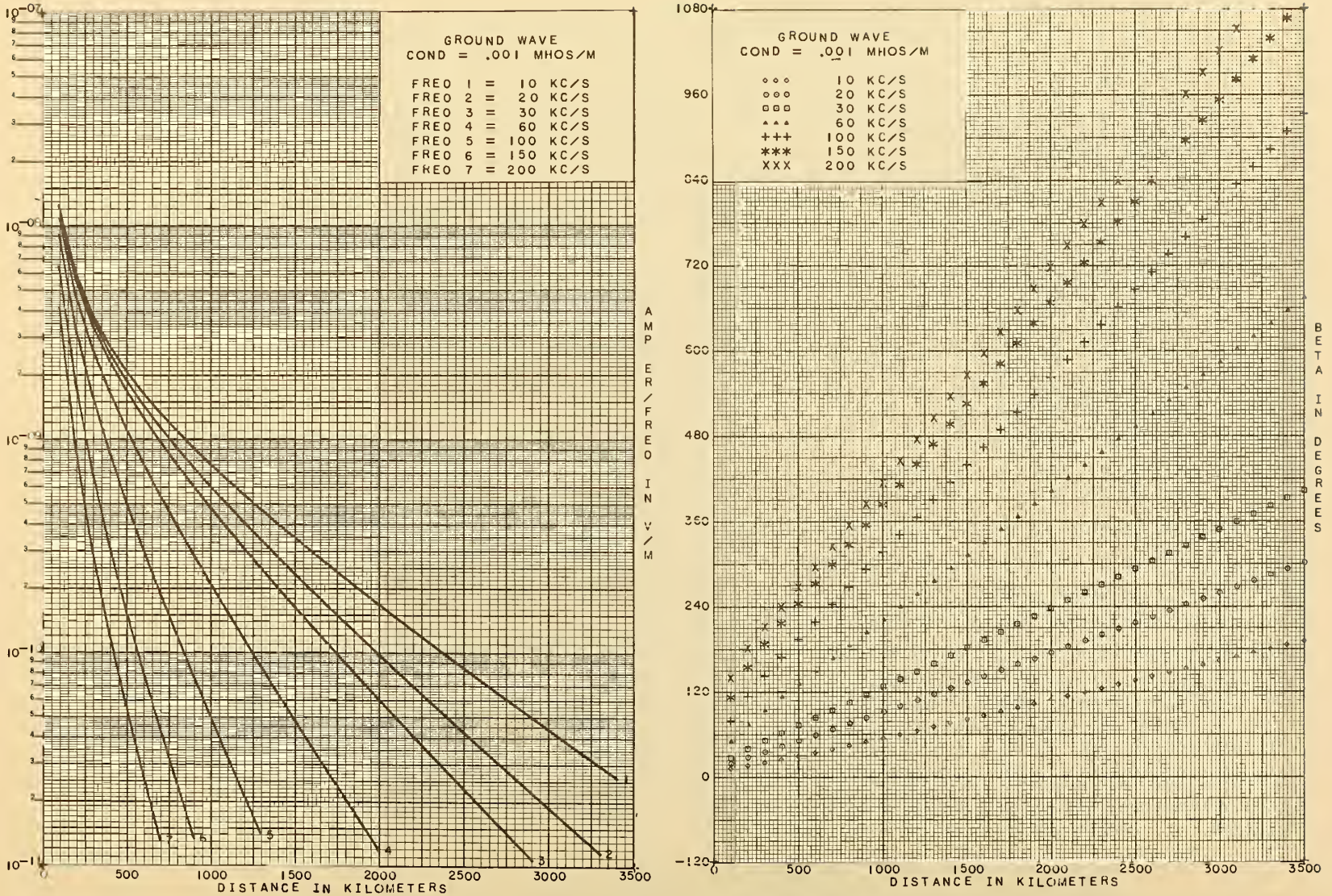

Figure 6. Amplitude and phase lag of the ground wave versus distance for various frequencies for poor ground.

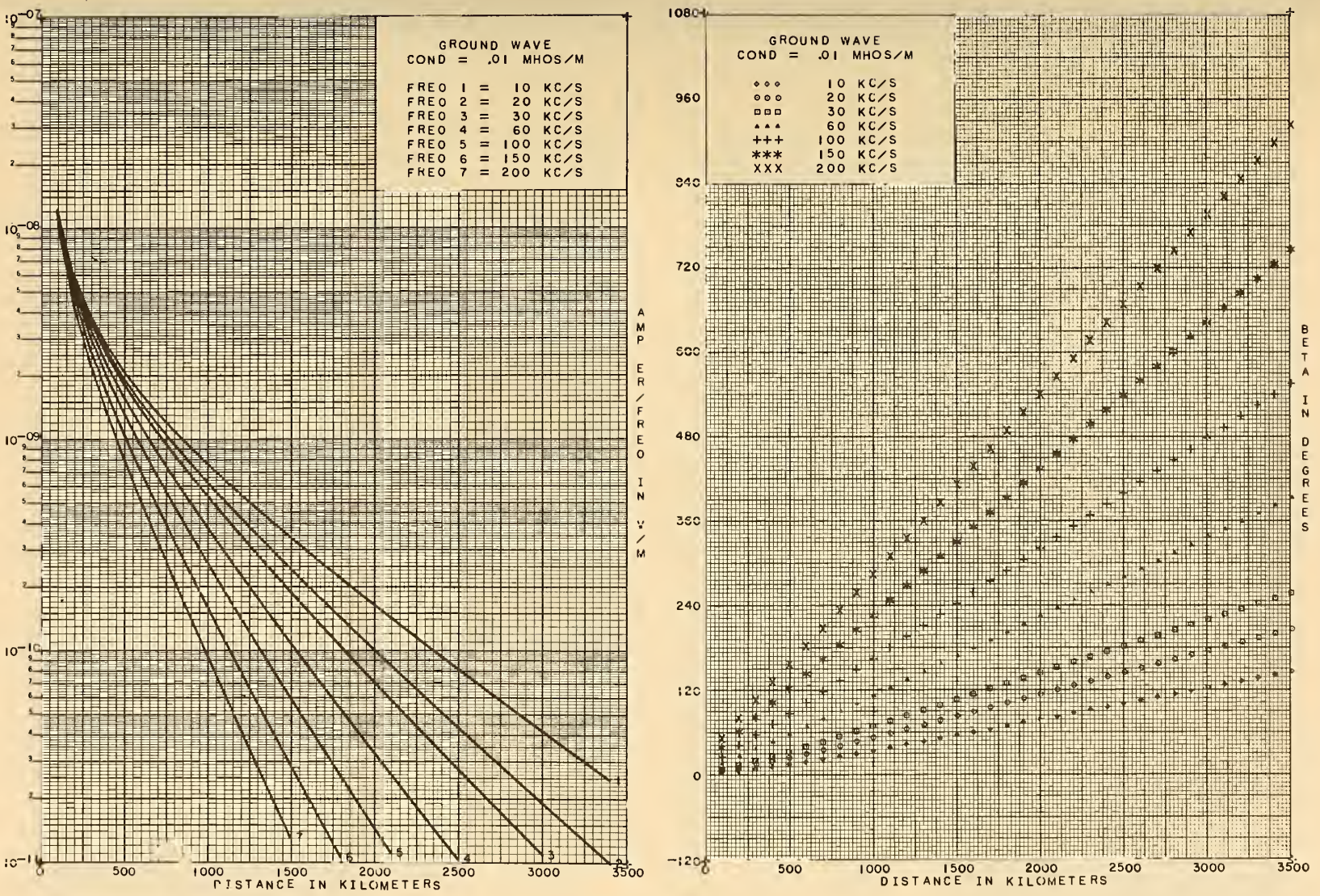

Figure 7. Amplitude and phase lag of the ground wave versus distance for various frequencies for typical ground.

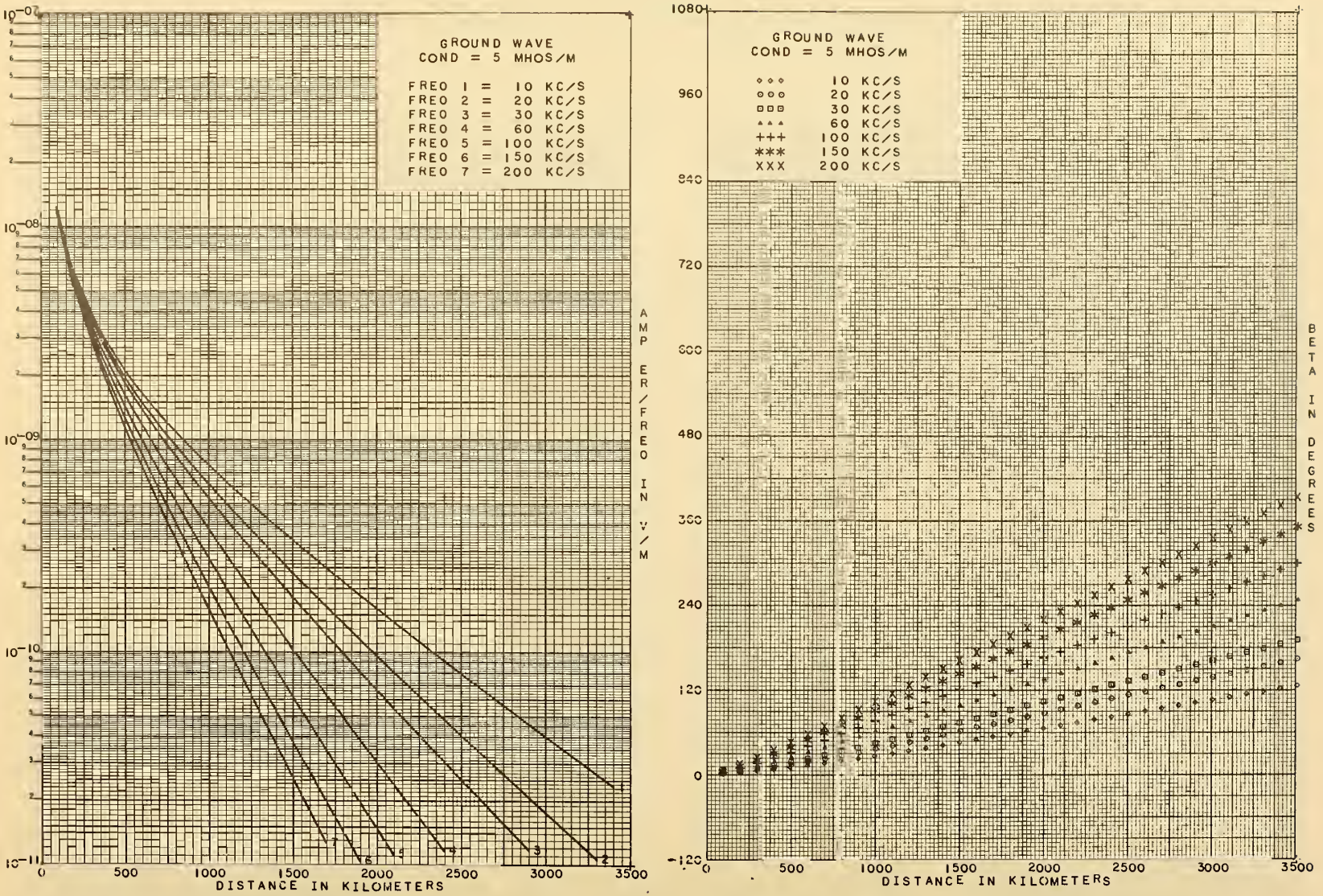

Figure 8. Amplitude and phase lag of the ground wave versus distance for various frequencies for sea water.

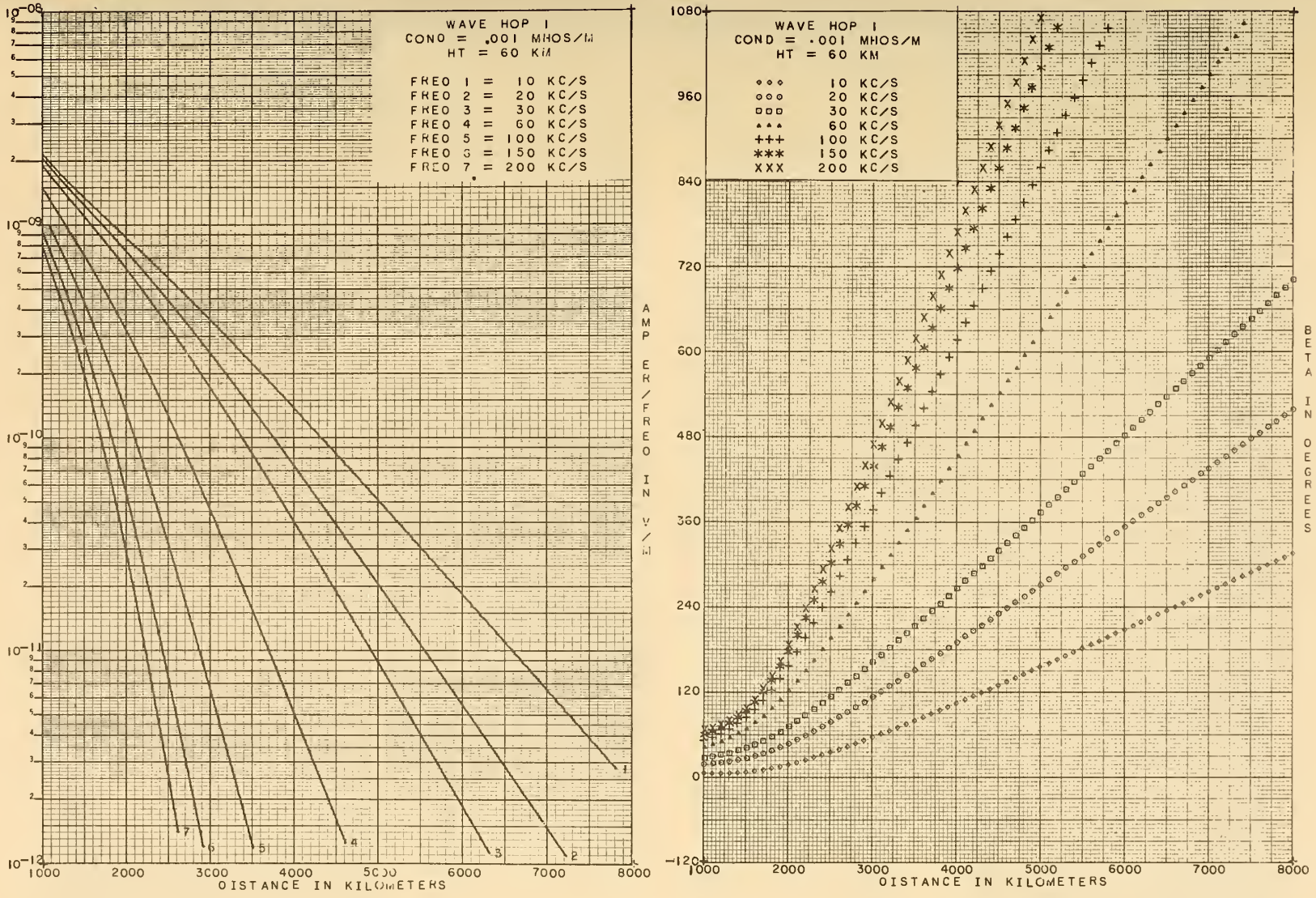

Figure 9.1 Amplitude, $|I_1/f_{kHz}|$, and phase lag, β_1, for parameters shown.

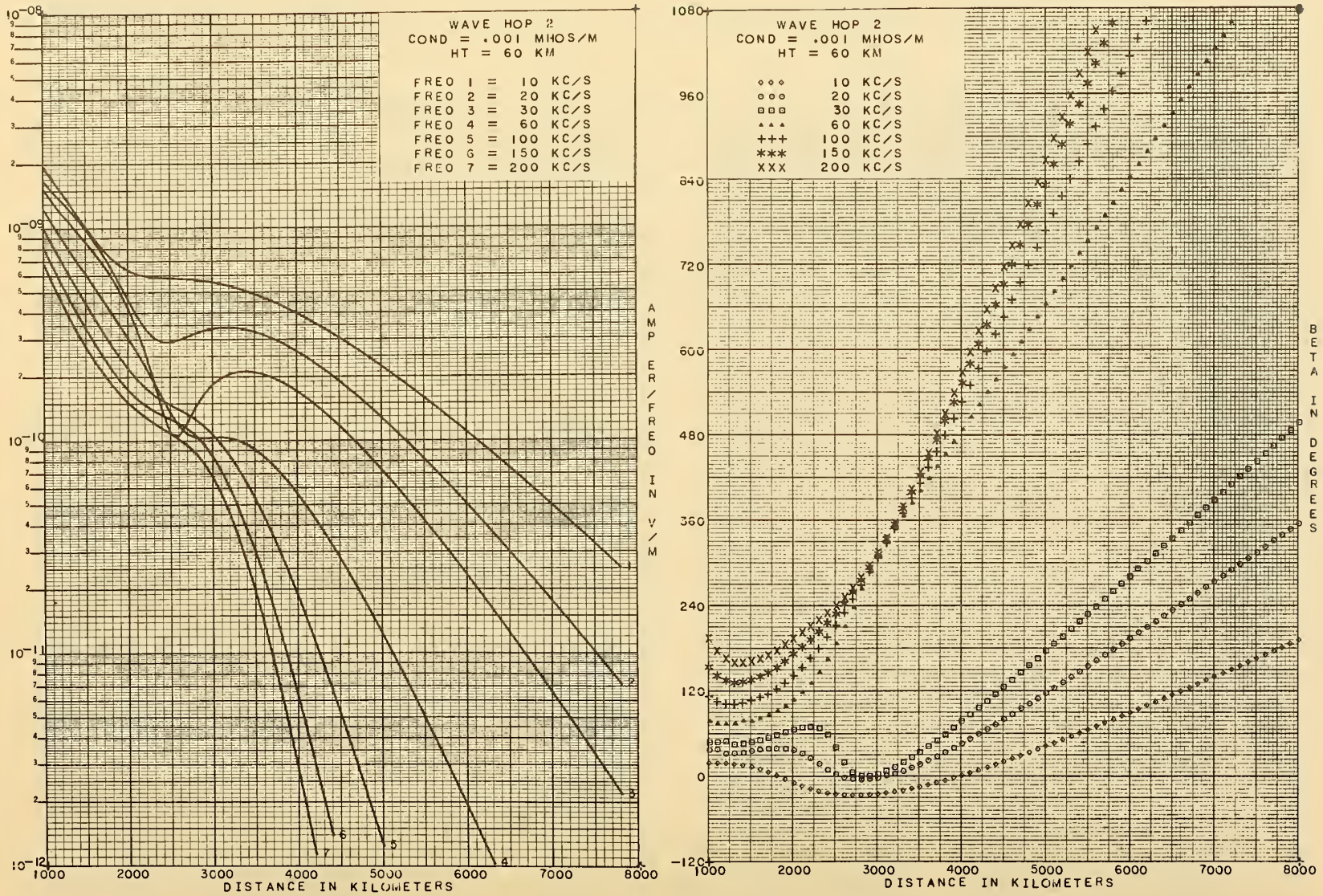

Figure 9.2 Amplitude, $|I_2/f_{kHz}|$, and phase lag, β_2, for parameters shown.

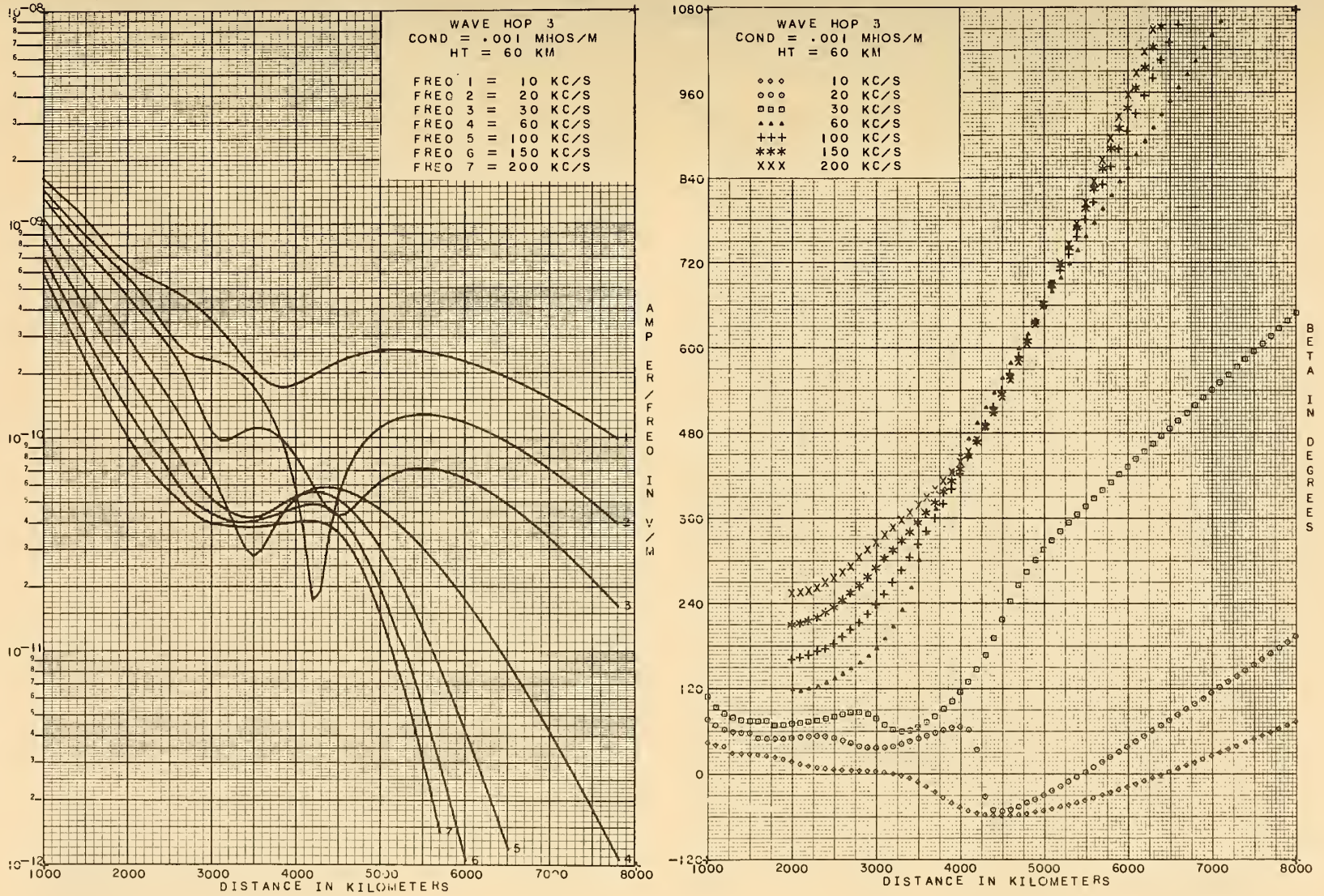

Figure 9.3 Amplitude, $|I_3/f_{kHz}|$, and phase lag, β_3, for parameters shown.

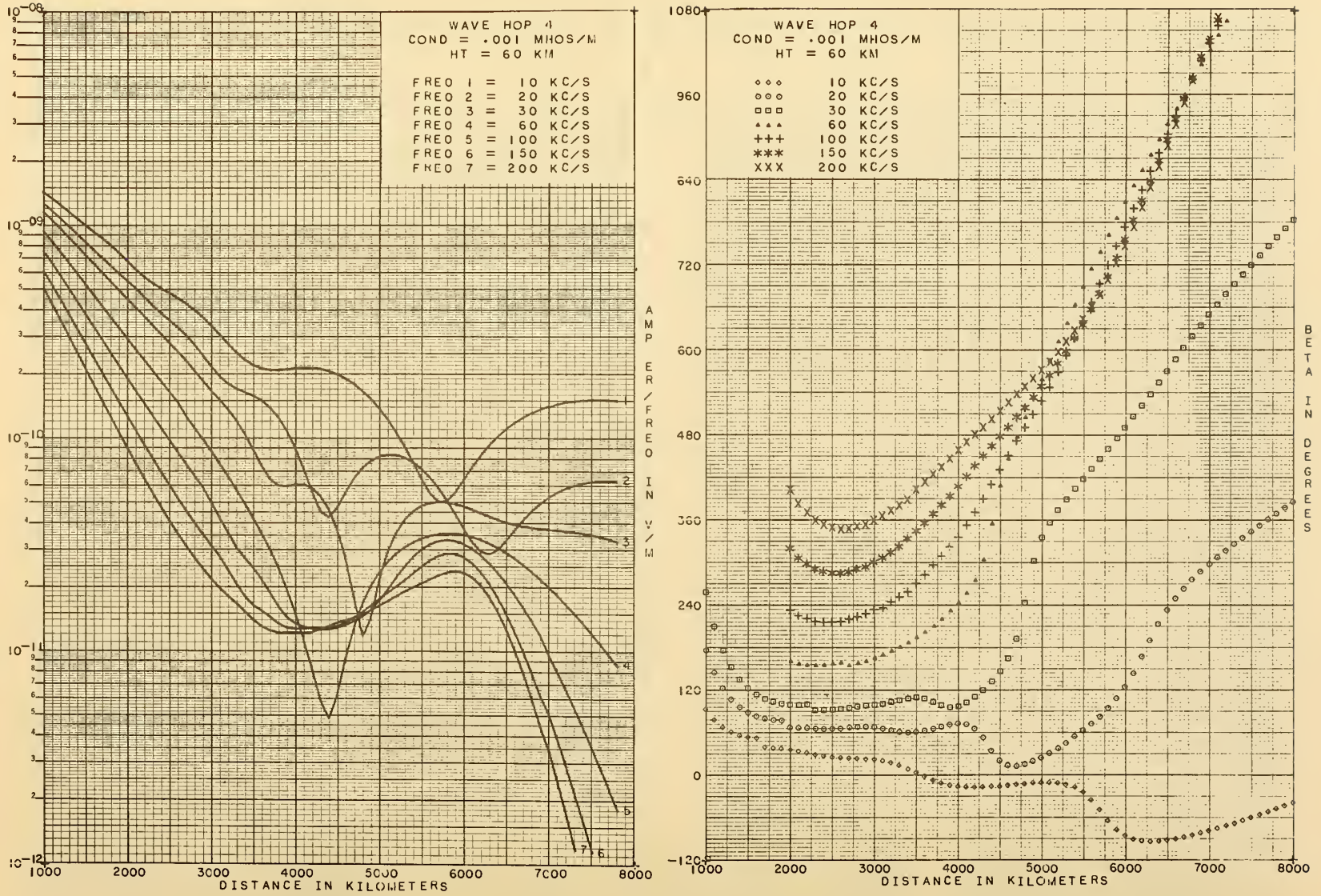

Figure 9.4 Amplitude, $|I_4/f_{kHz}|$, and phase lag, β_4, for parameters shown.

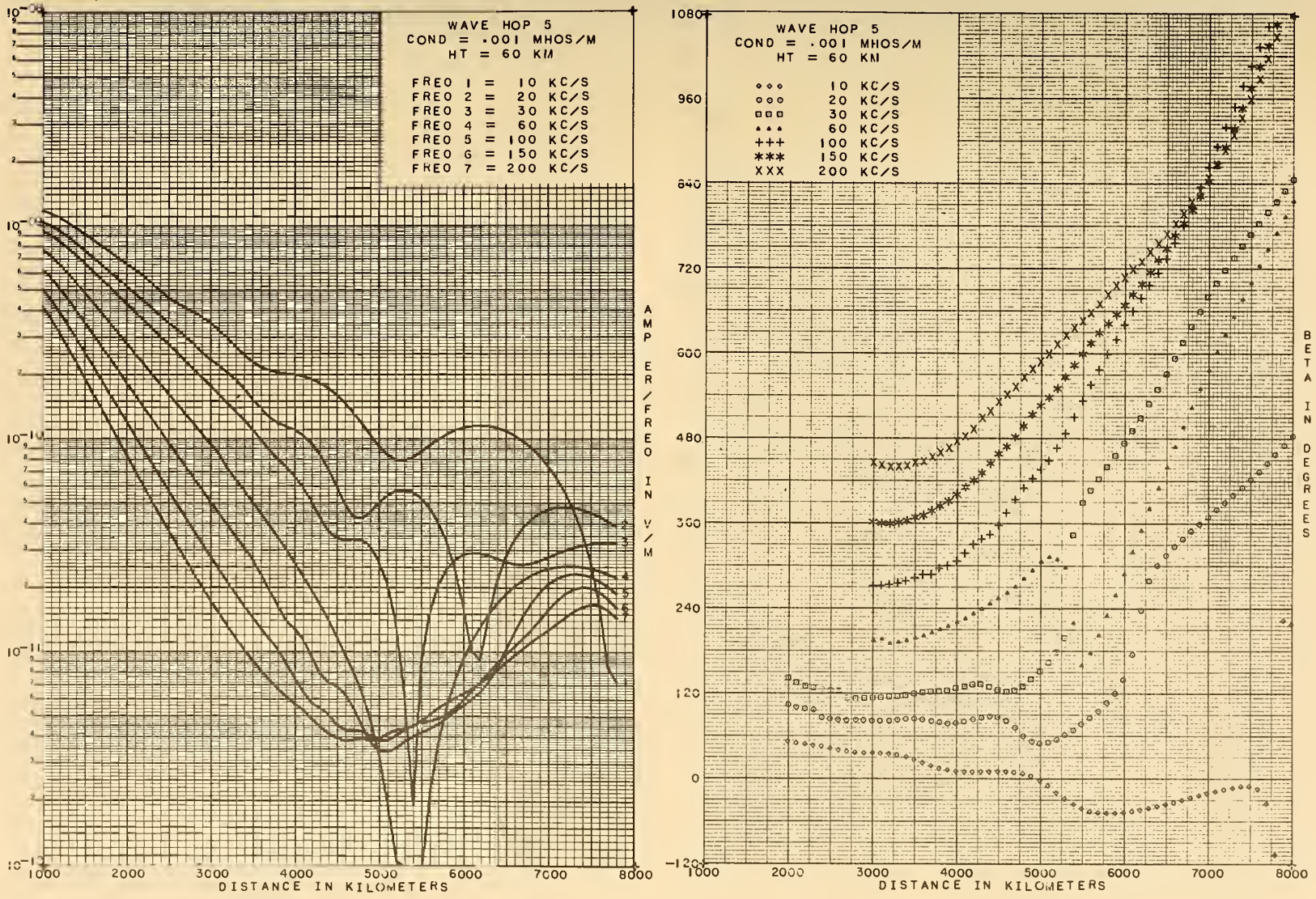

Figure 9.5 Amplitude, $|I_5/f_{kHz}|$, and phase lag, β_5, for parameters shown.

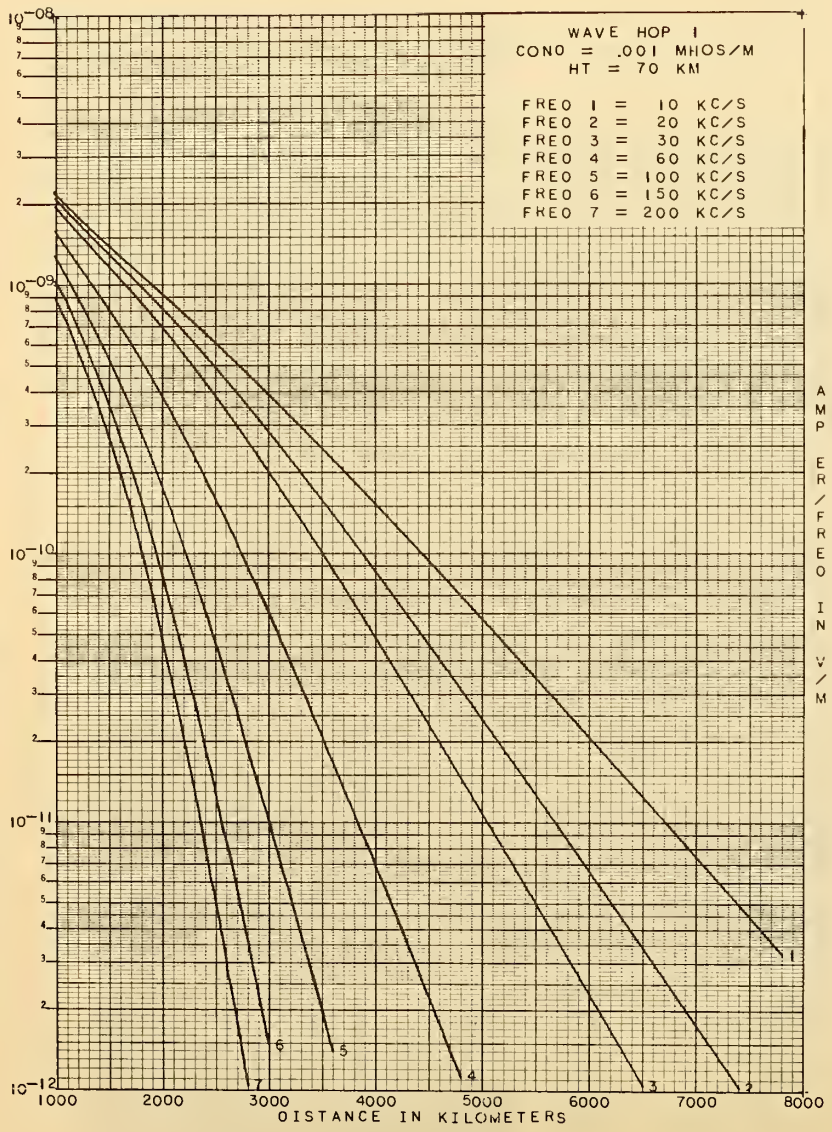

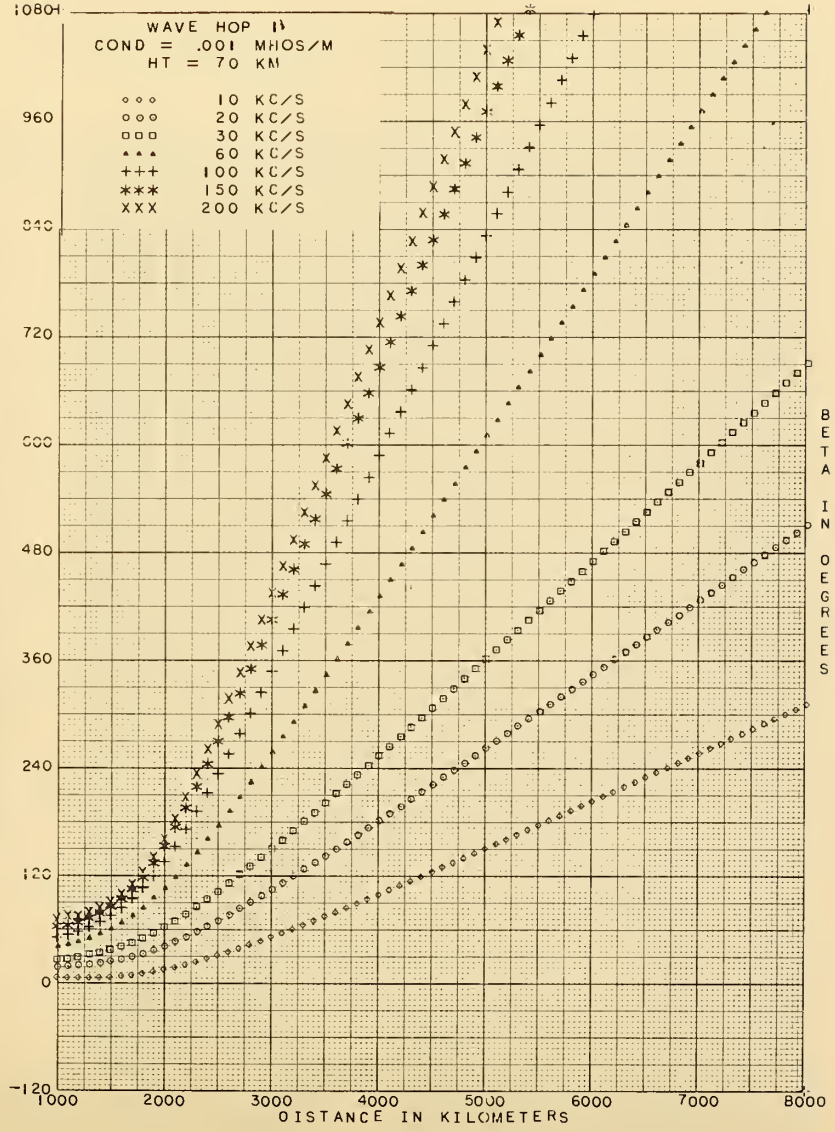

Figure 10.1 Amplitude, $|I_1/f_{kHz}|$, and phase lag, β_1, for parameters shown.

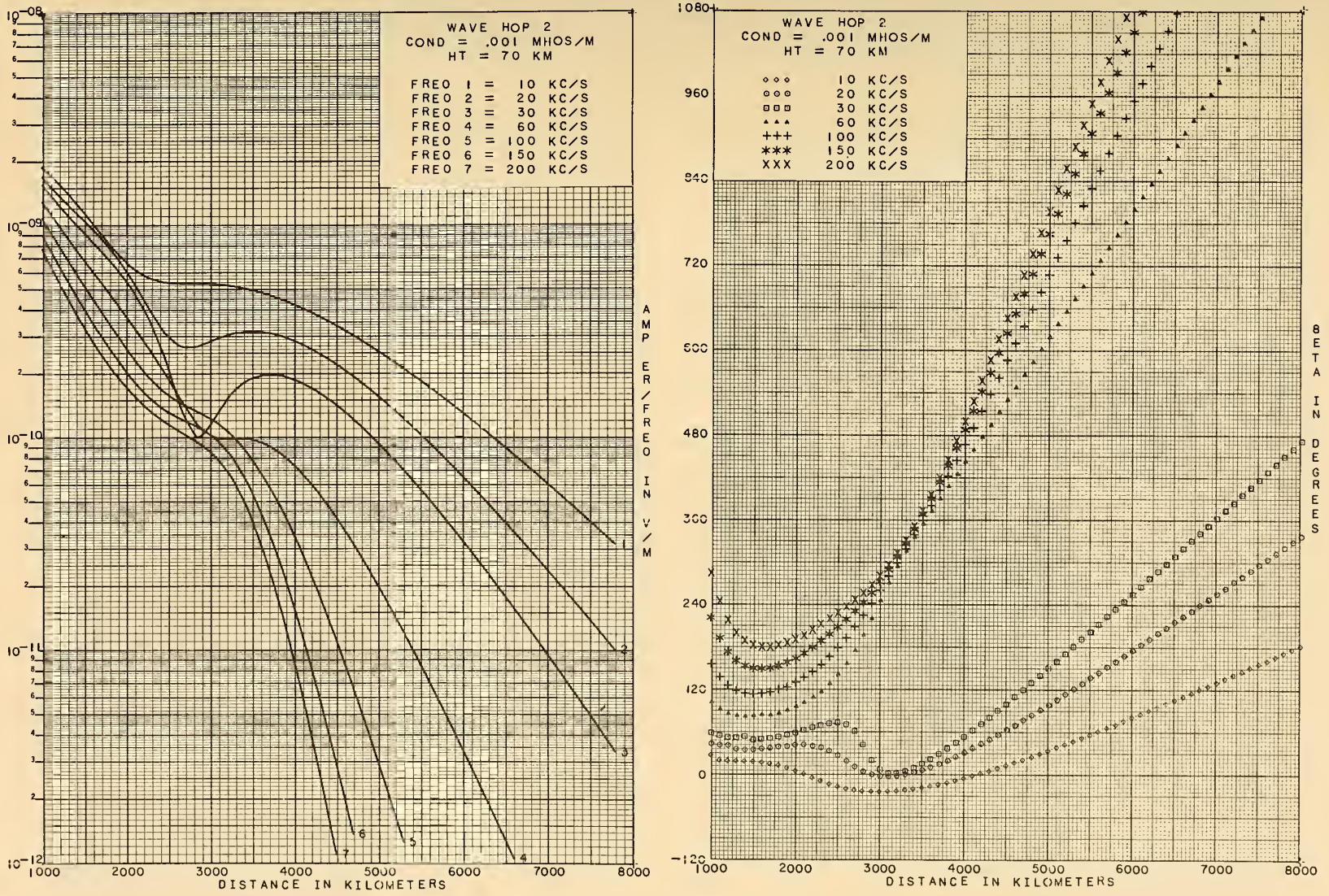

Figure 10.2 Amplitude, $|I_2/f_{kHz}|$, and phase lag, β_2, for parameters shown.

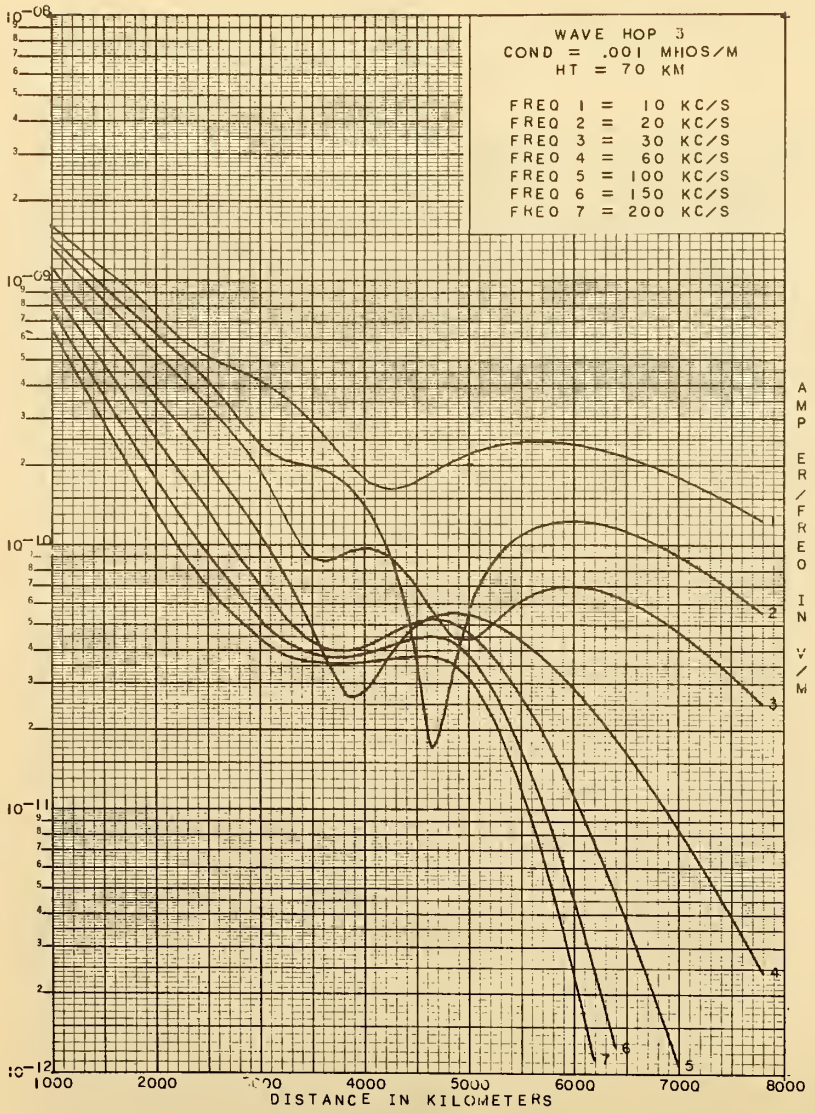

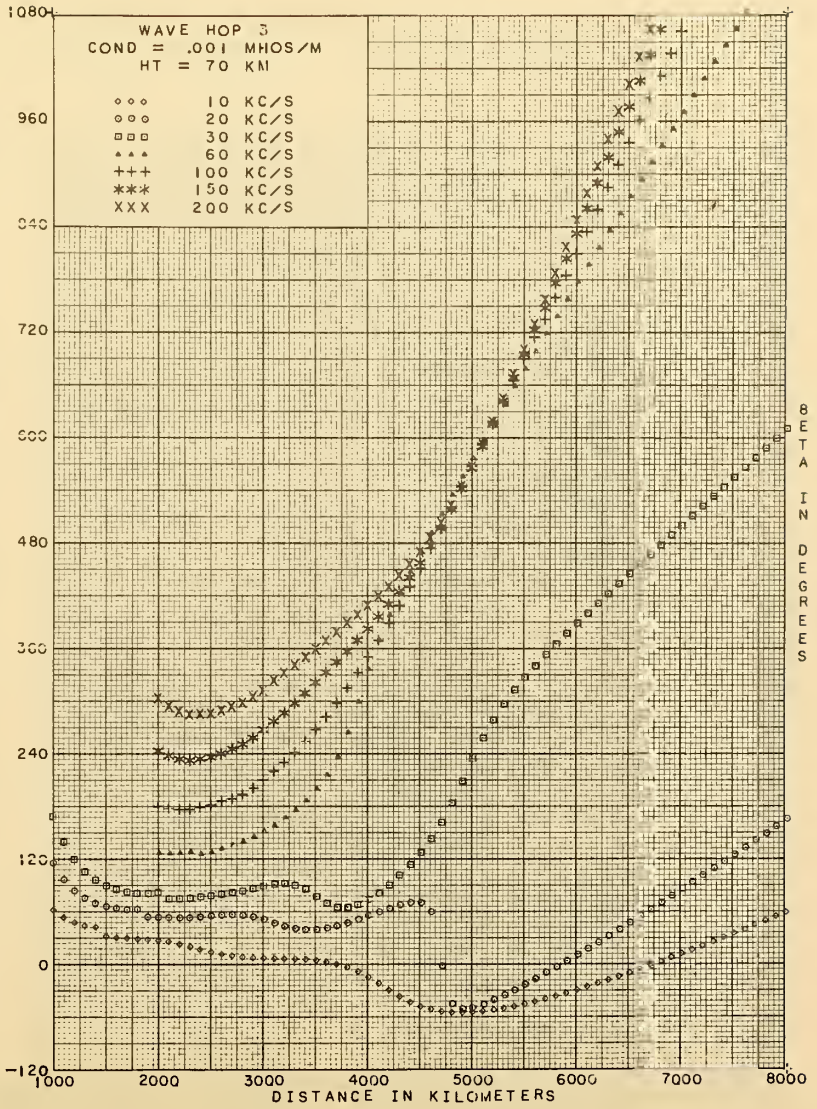

Figure 10.3 Amplitude, $|I_3/f_{kHz}|$, and phase lag, β_3, for parameters shown.

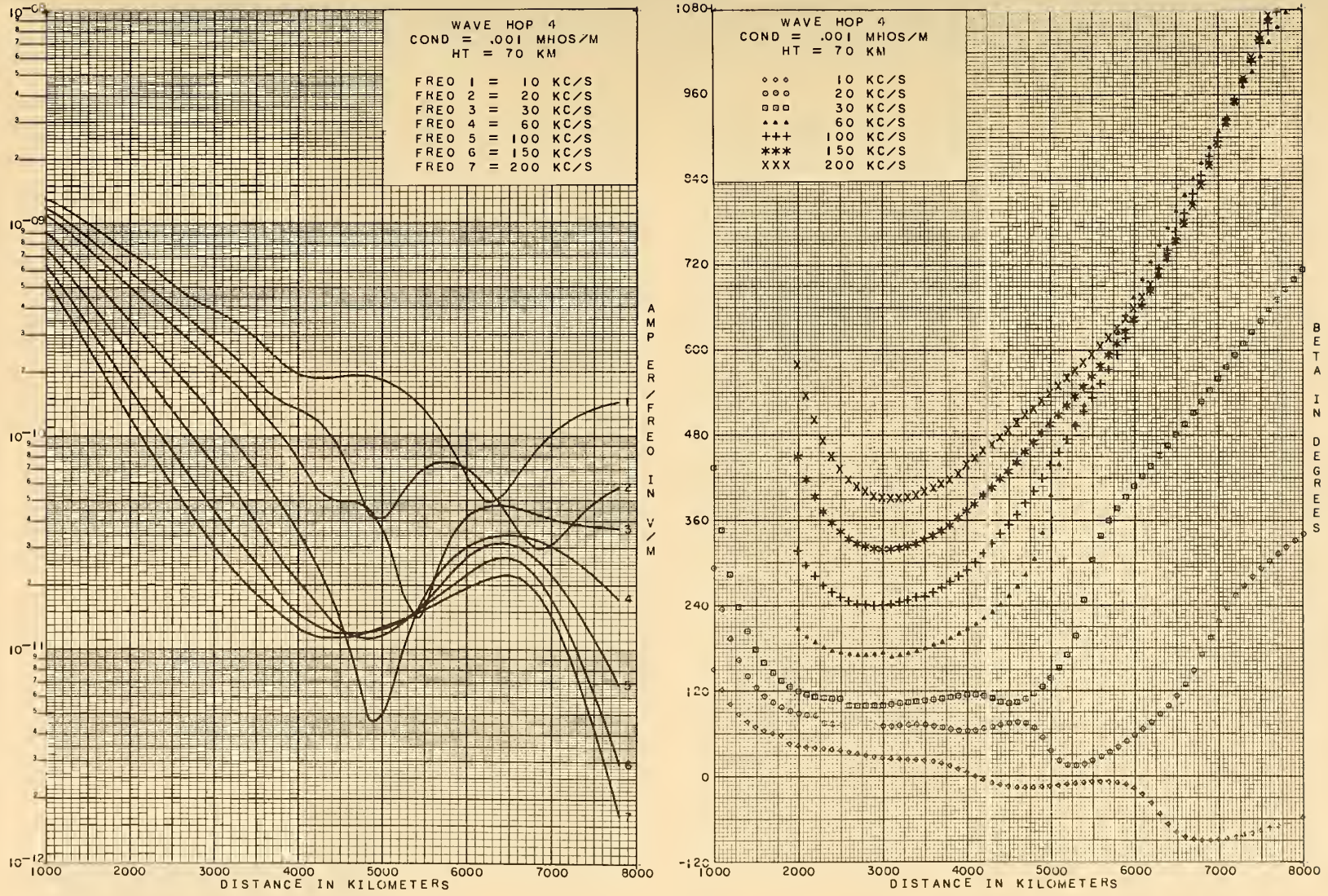

Figure 10.4 Amplitude, $|I_4/f_{kHz}|$, and phase lag, β_4, for parameters shown.

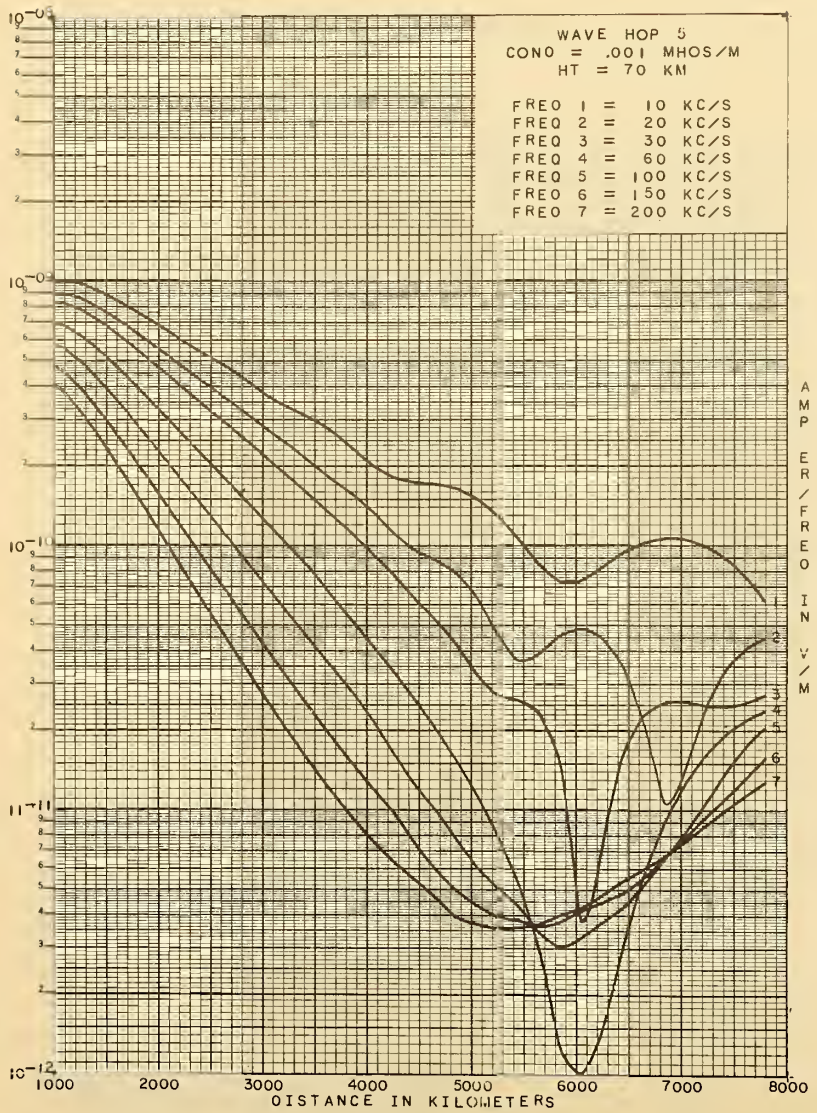

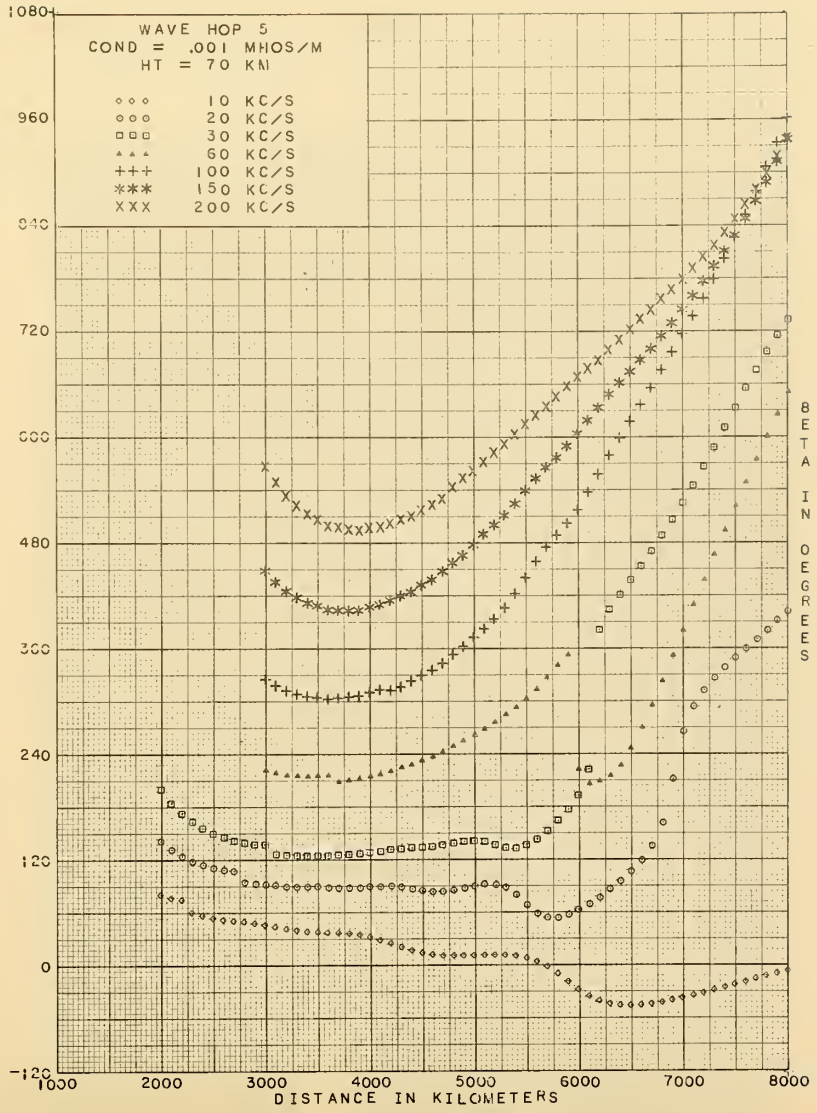

Figure 10.5 Amplitude, $|I_5/f_{kHz}|$, and phase lag, β_5, for parameters shown.

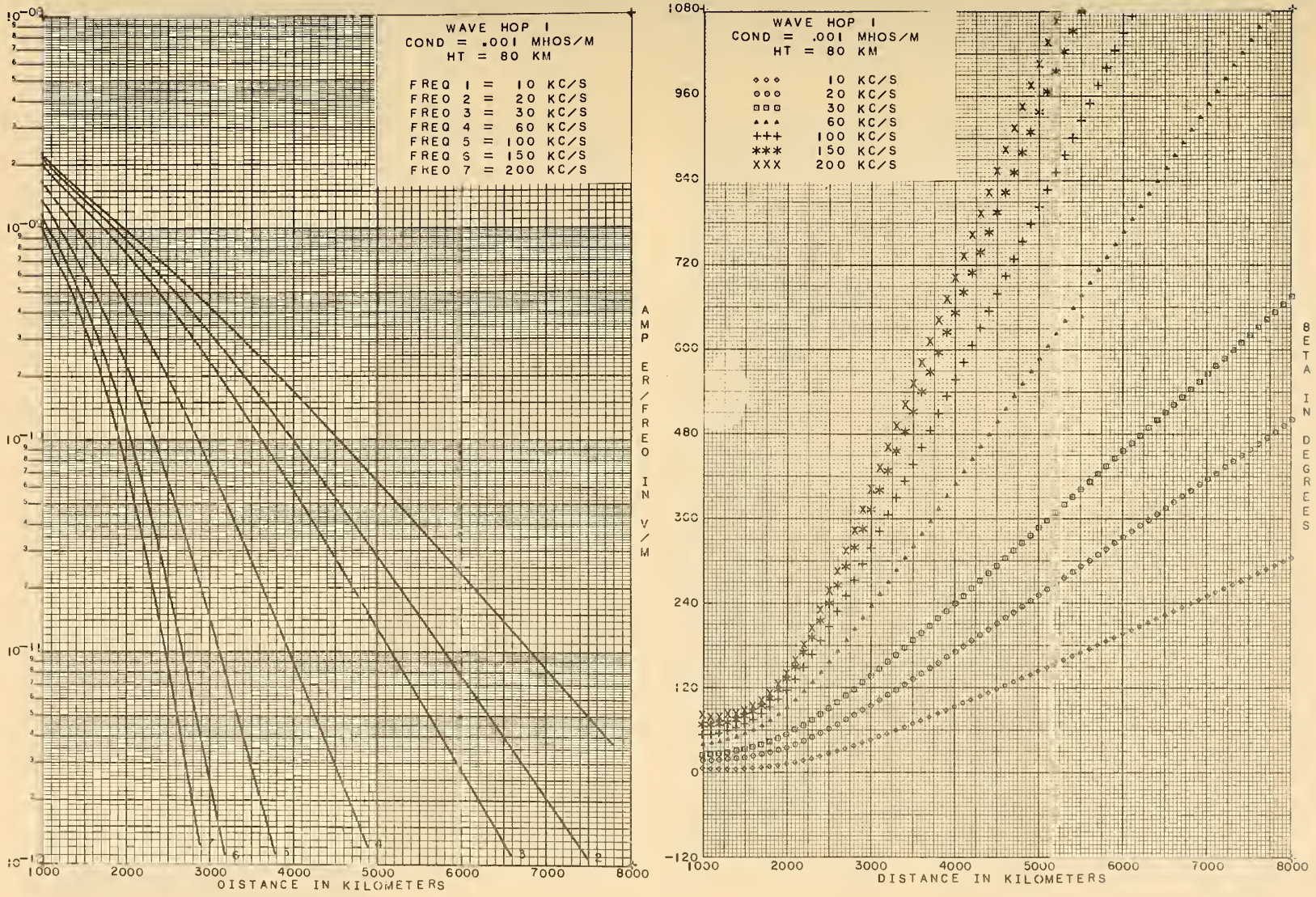

Figure 11.1 Amplitude, $|I_1/f_{kHz}|$, and phase lag, β_1, for parameters shown.

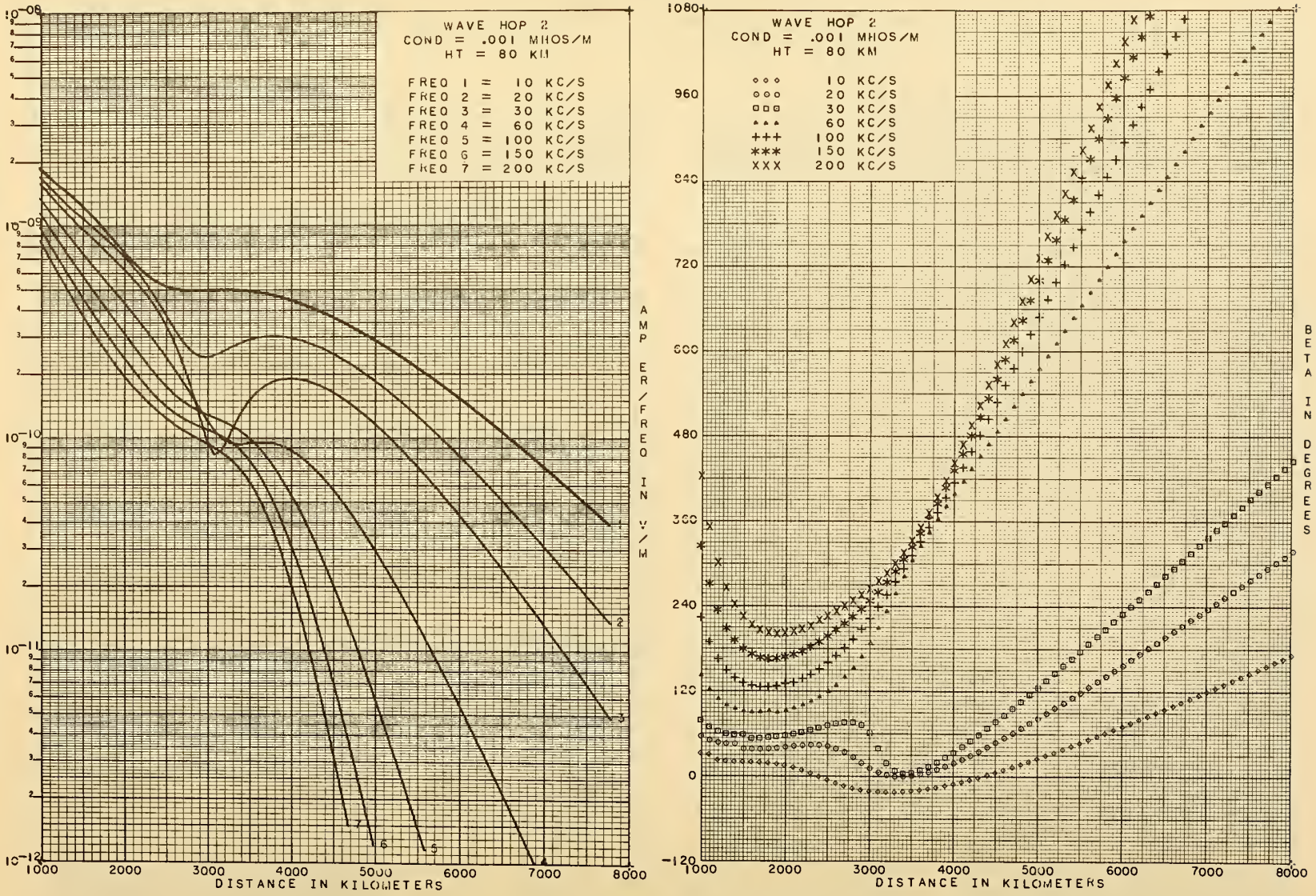

Figure 11.2 Amplitude, $|I_2/f_{kHz}|$, and phase lag, β_2, for parameters shown.

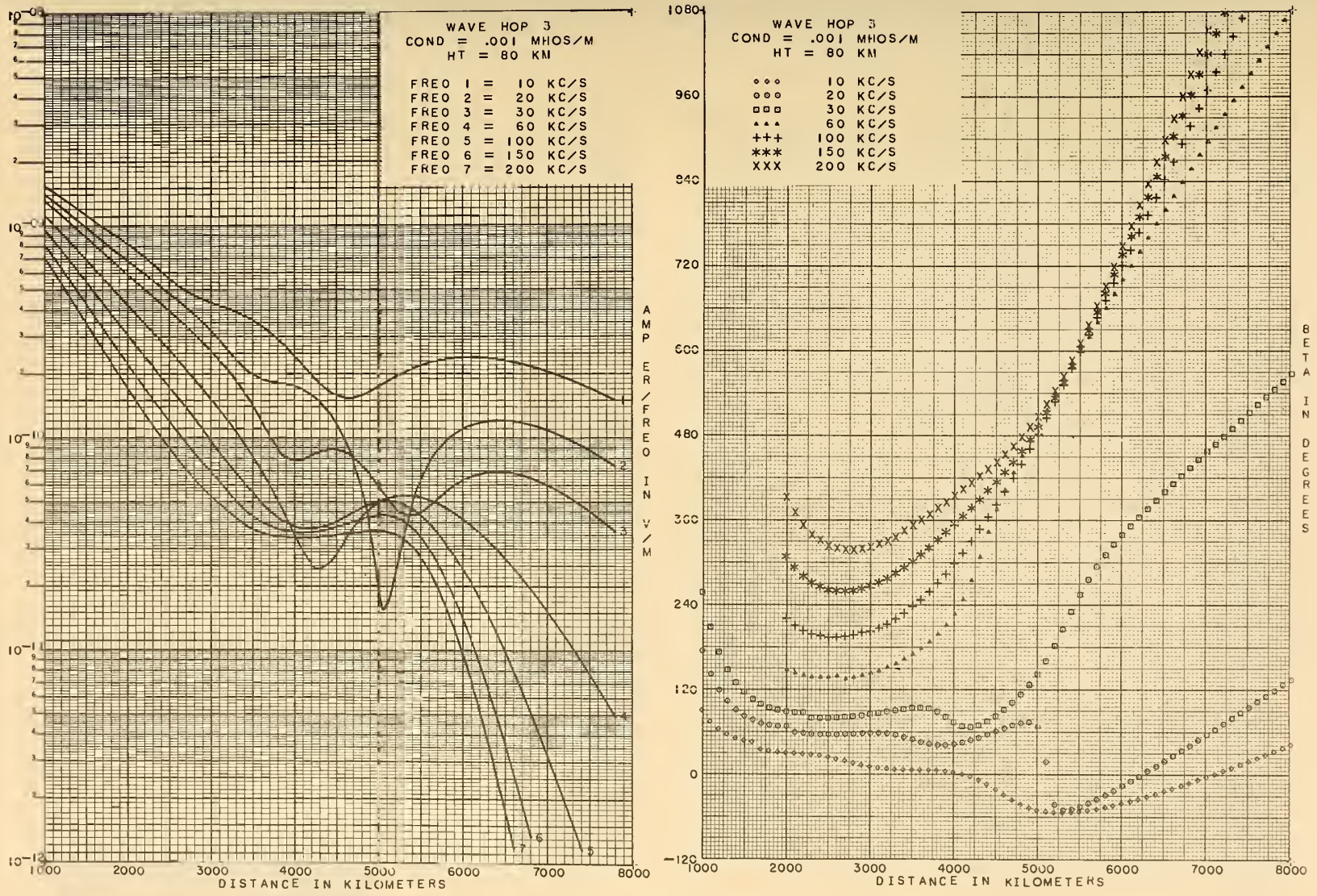

Figure 11.3 Amplitude, $|I_3/f_{kHz}|$, and phase lag, β_3, for parameters shown.

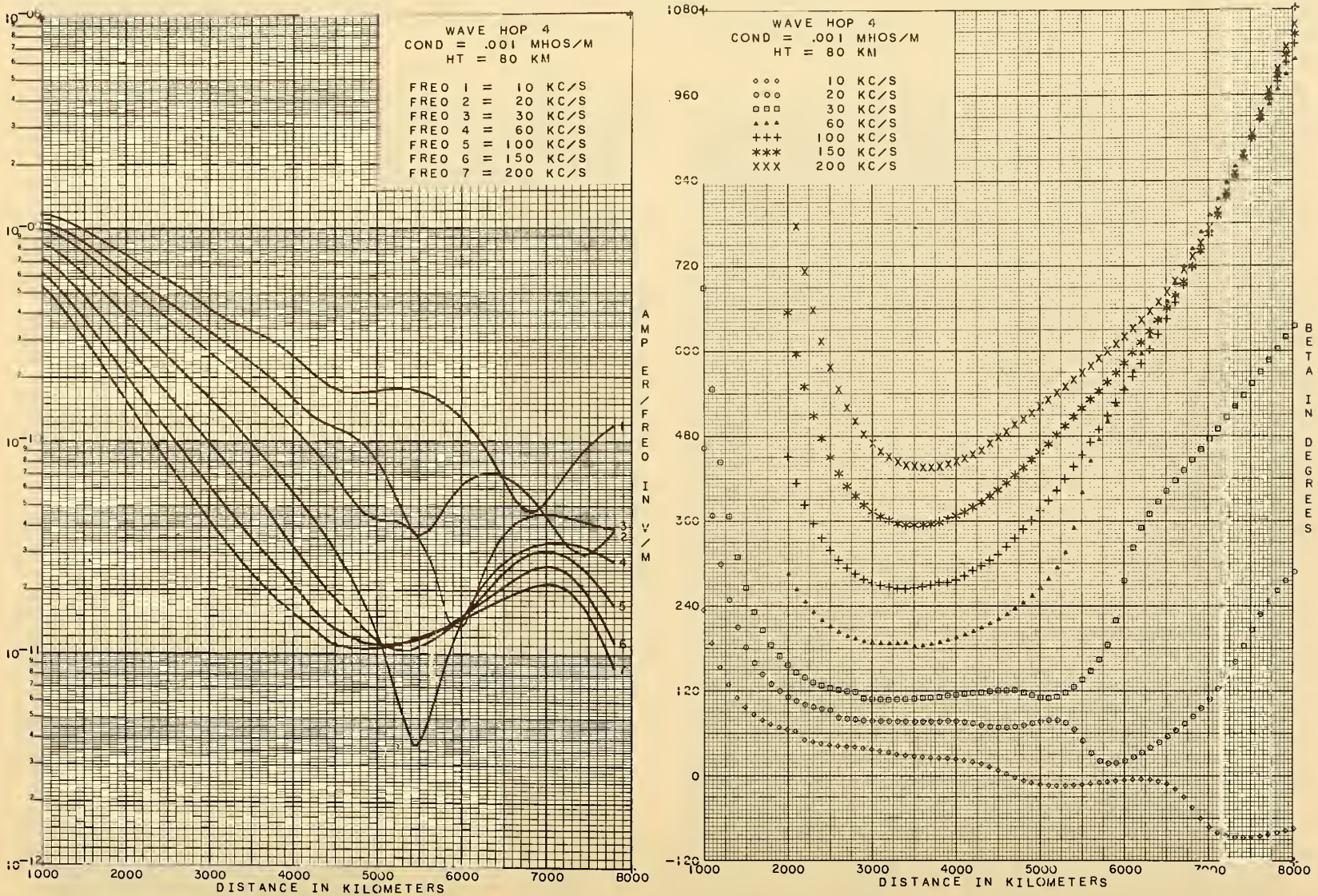

Figure 11.4 Amplitude, $|L_4/f_{kHz}|$, and phase lag, β_4, for parameters shown.

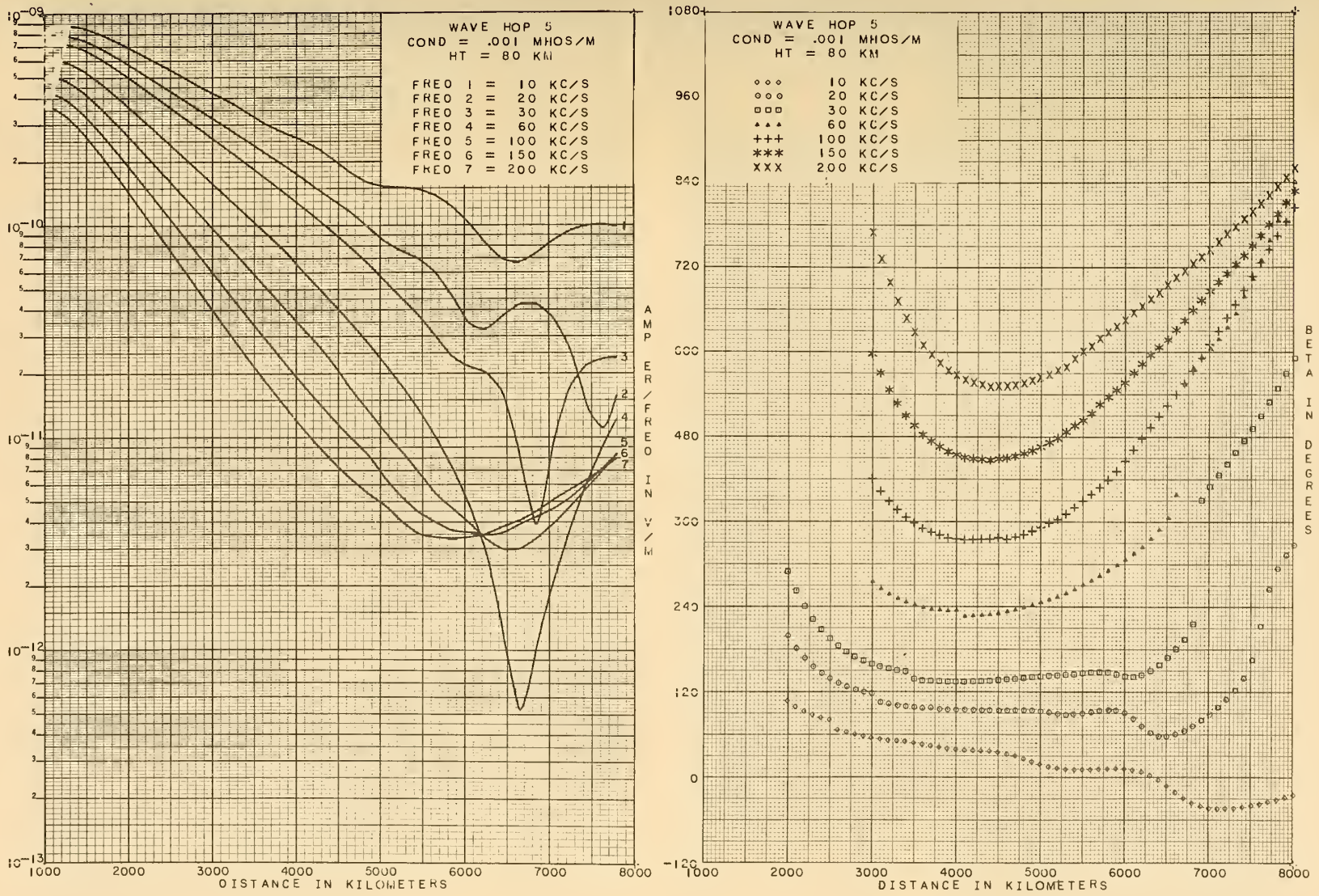

Figure 11.5 Amplitude, $|I_5/f_{kHz}|$, and phase lag, β_5, for parameters shown.

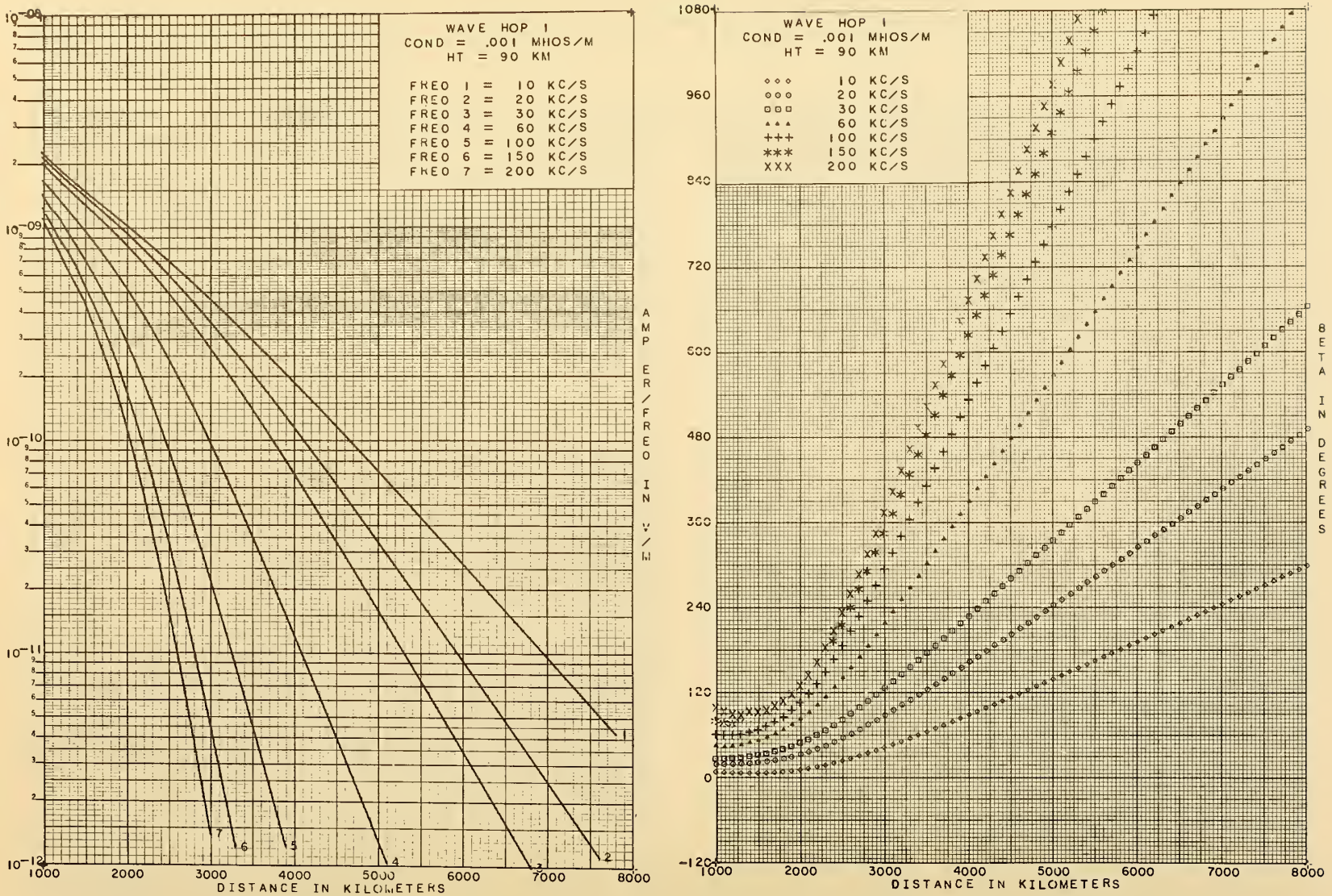

Figure 12.1 Amplitude, $|I_1/f_{kHz}|$, and phase lag, β_1, for parameters shown.

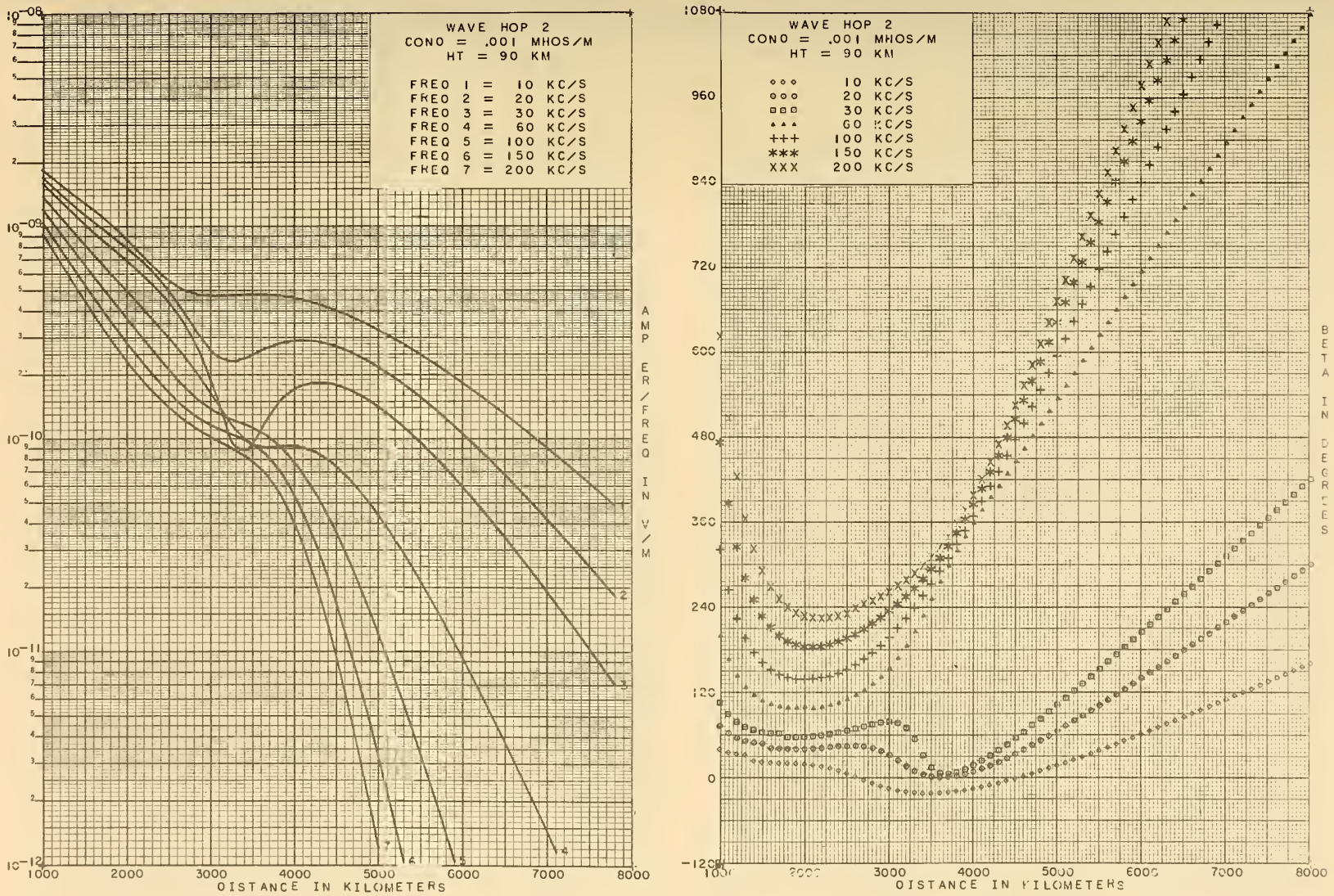

Figure 12.2 Amplitude, $|I_2/f_{kHz}|$, and phase lag, β_2, for parameters shown.

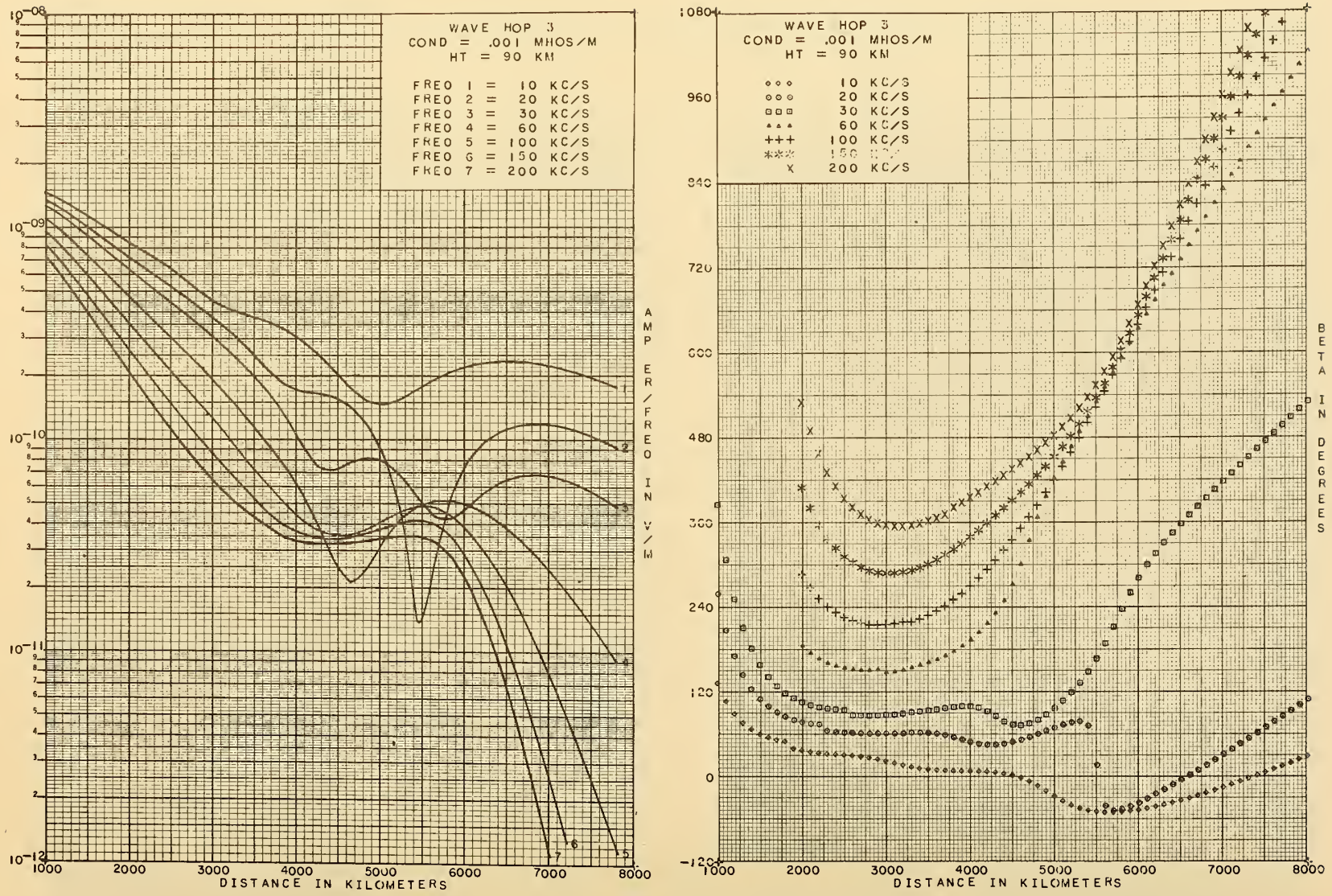

Figure 12.3 Amplitude, $|I_3/f_{kHz}|$, and phase lag, β_3, for parameters shown.

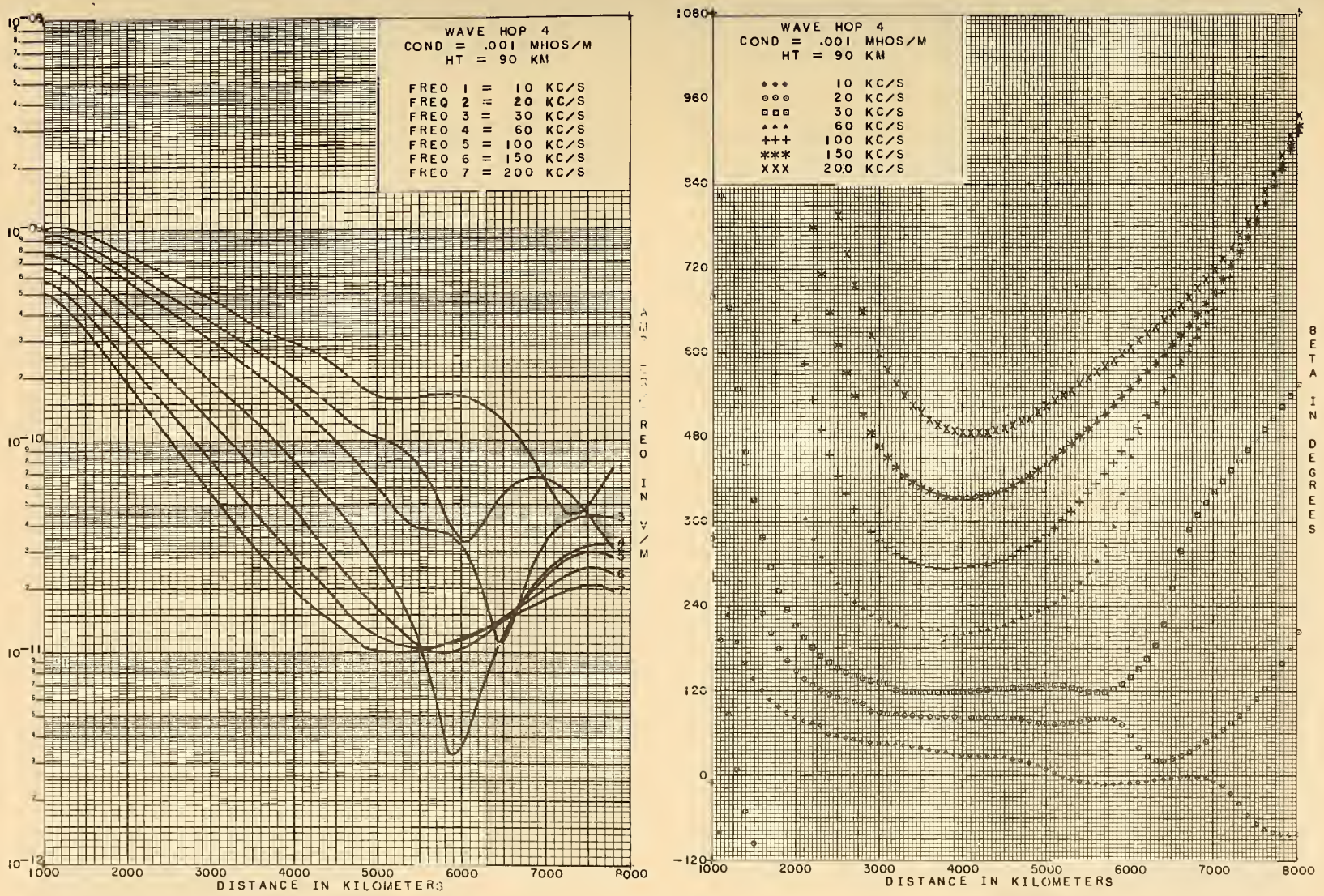

Figure 12.4 Amplitude, $|I_4/f_{kHz}|$, and phase lag, β_4, for parameters shown.

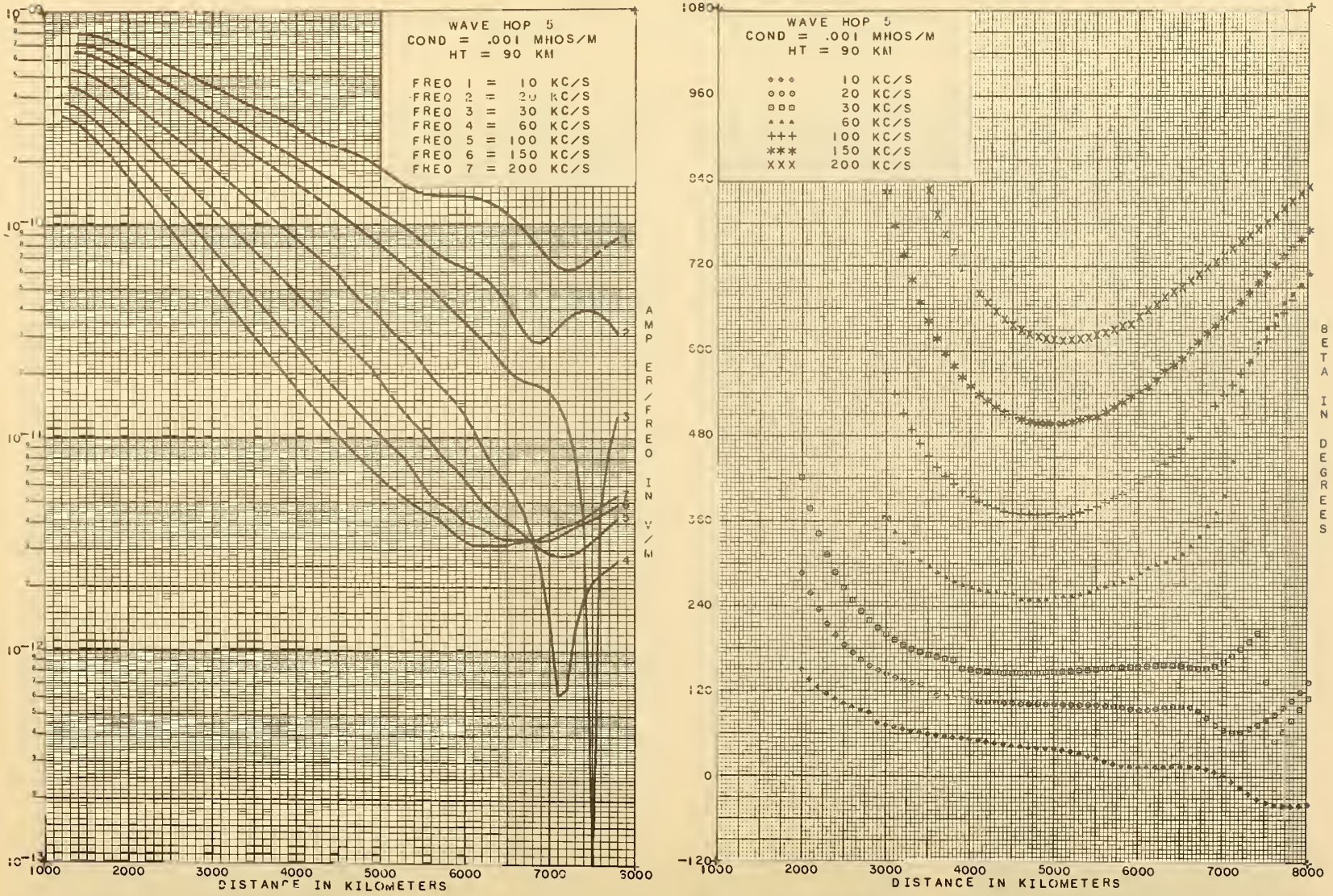

Figure 12.5 Amplitude, $|I_5/f_{kHz}|$, and phase lag, β_5, for parameters shown.

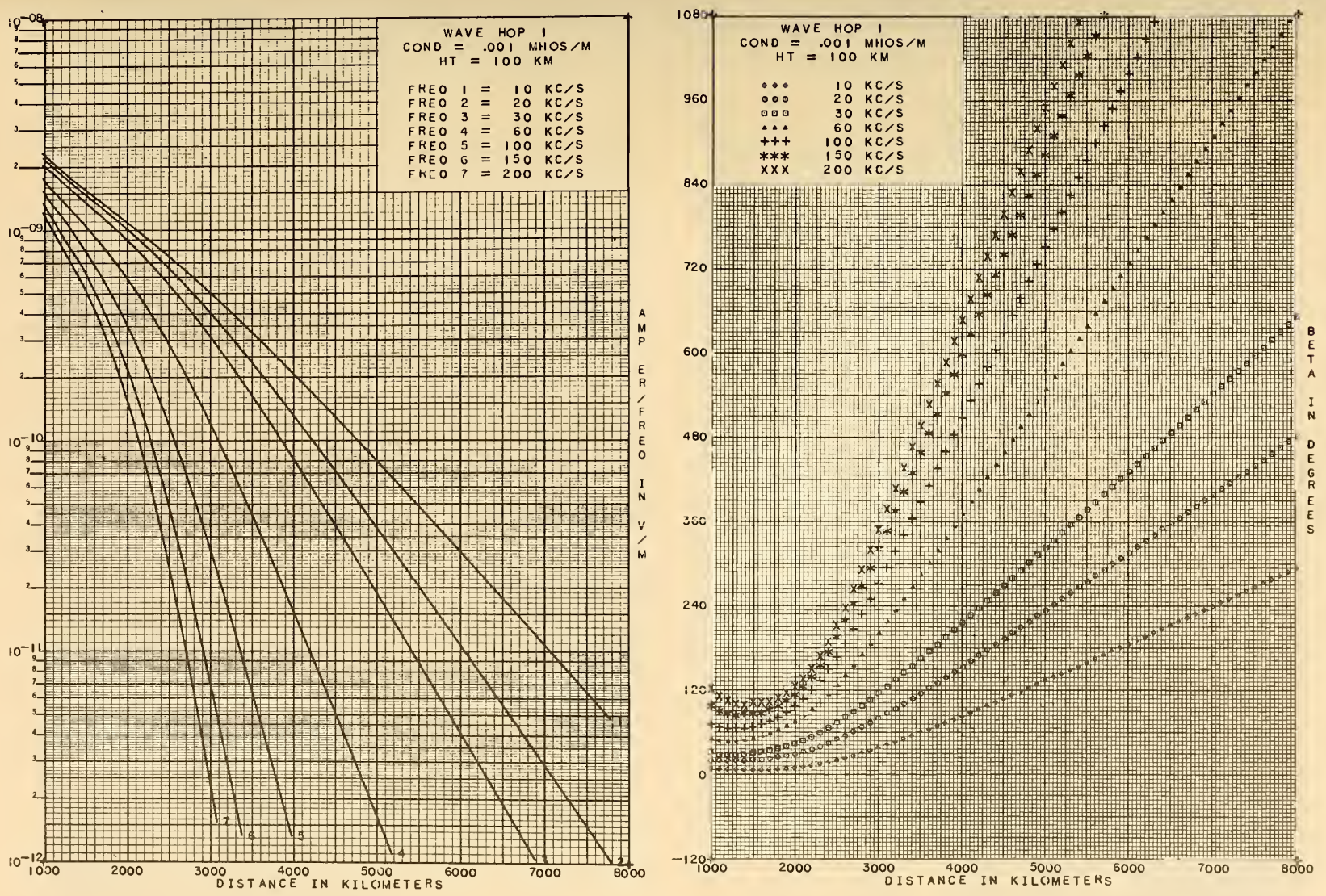

Figure 13.1 Amplitude, $|I_1/f_{kHz}|$, and phase lag, β_1, for parameters shown.

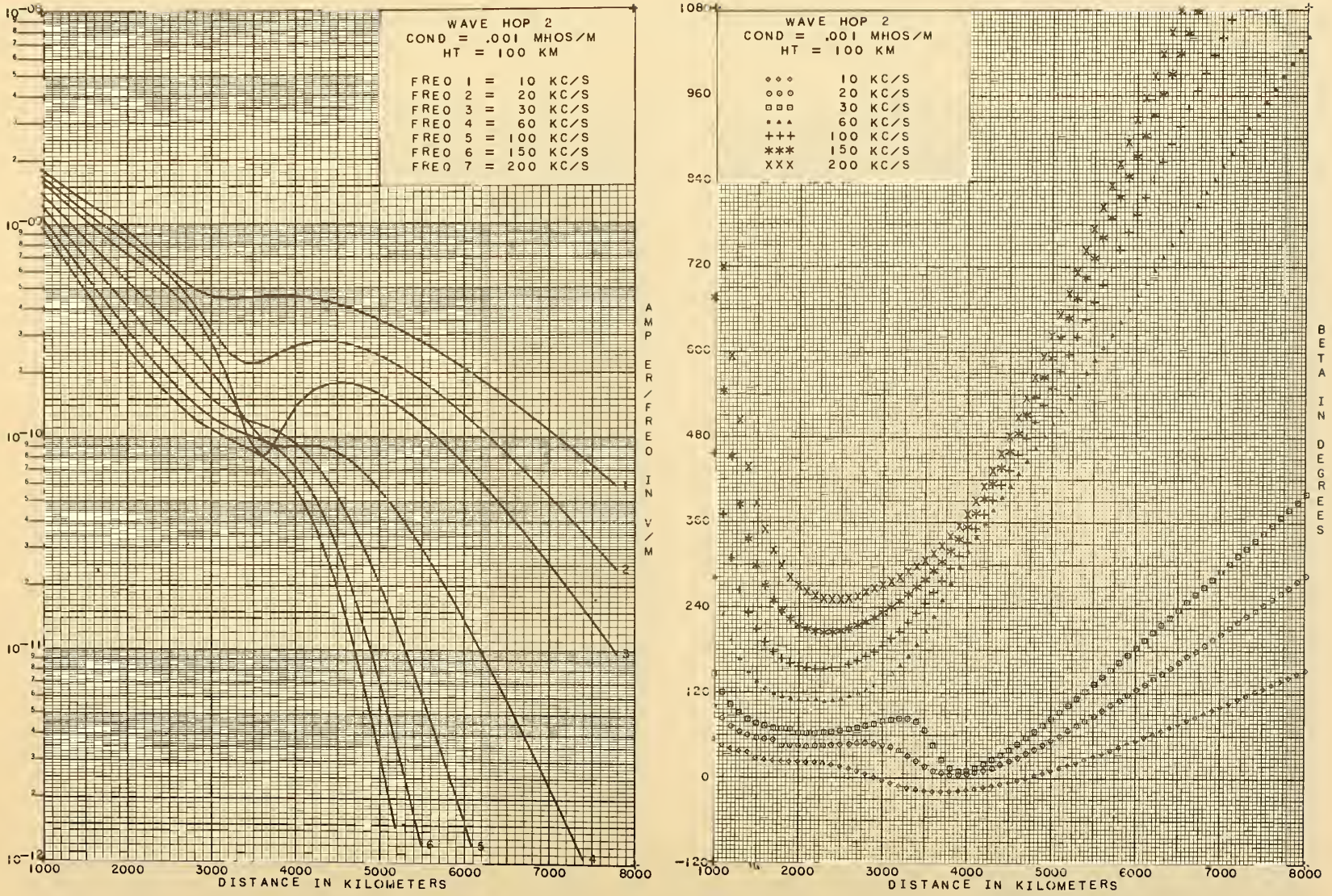

Figure 13.2 Amplitude, $|I_2/f_{kHz}|$, and phase lag, β_2, for parameters shown.

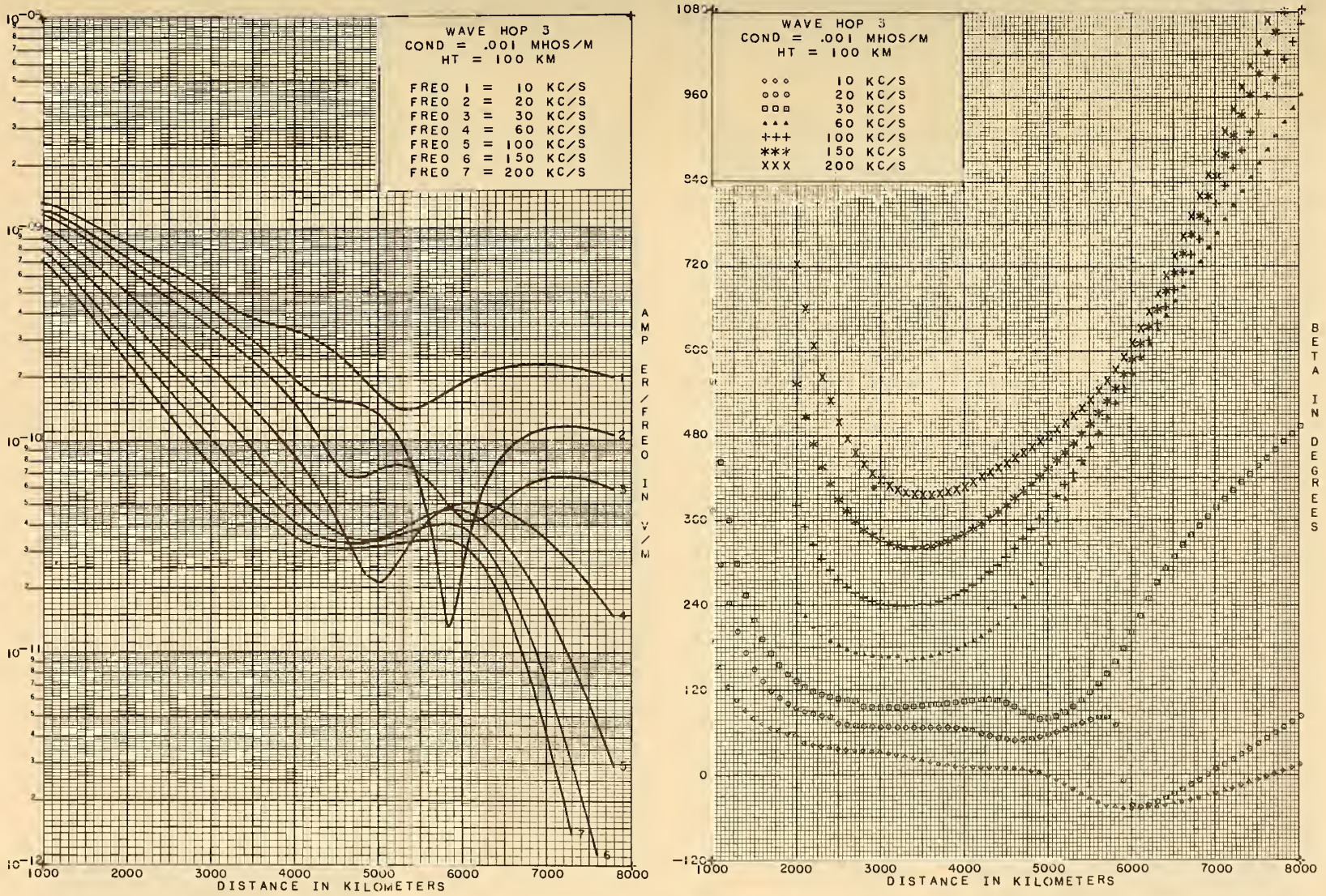

Figure 13.3 Amplitude, $|I_3/f_{kHz}|$, and phase lag, β_3, for parameters shown.

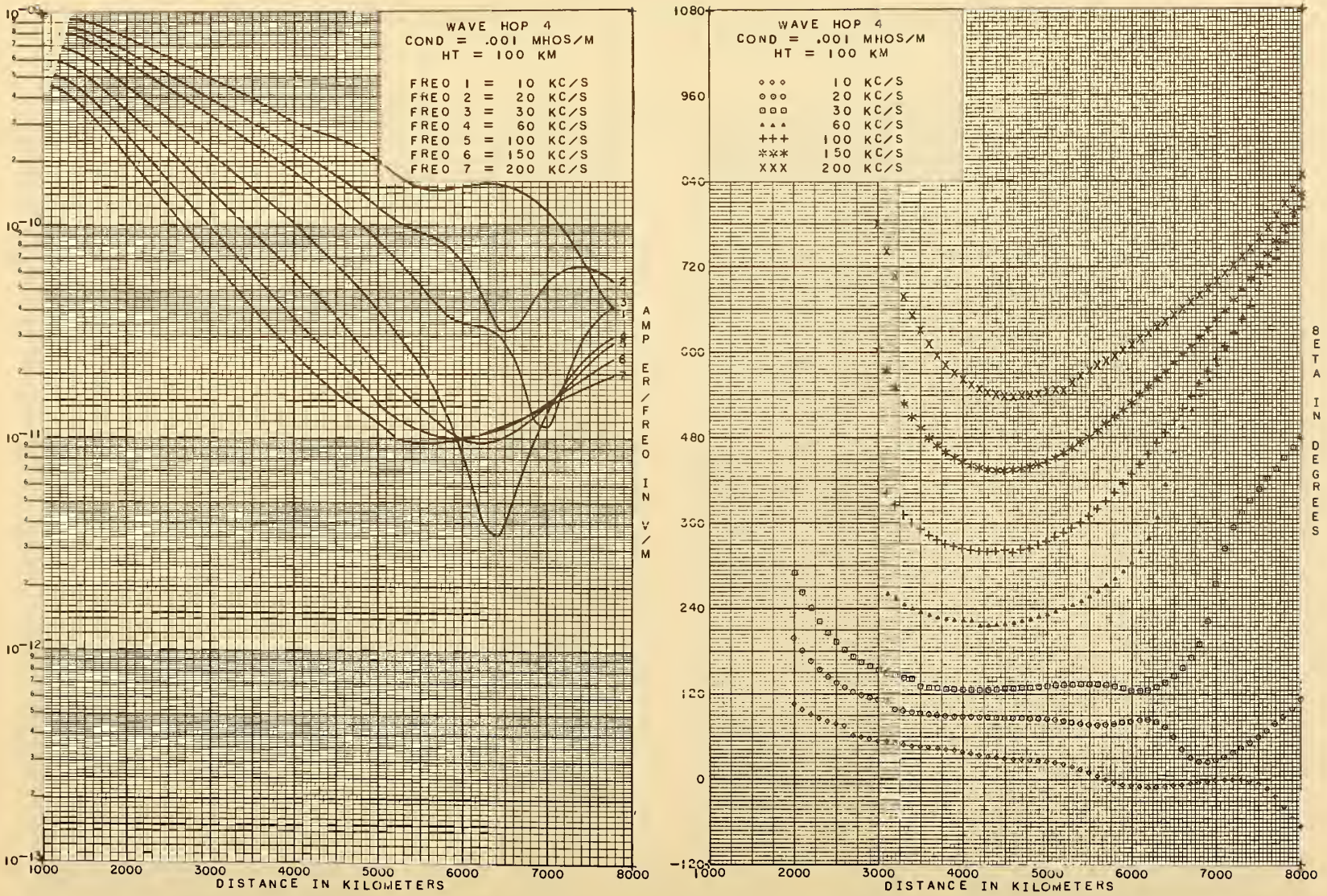

Figure 13.4 Amplitude, $|I_4/f_{kHz}|$, and phase lag, β_4, for parameters shown.

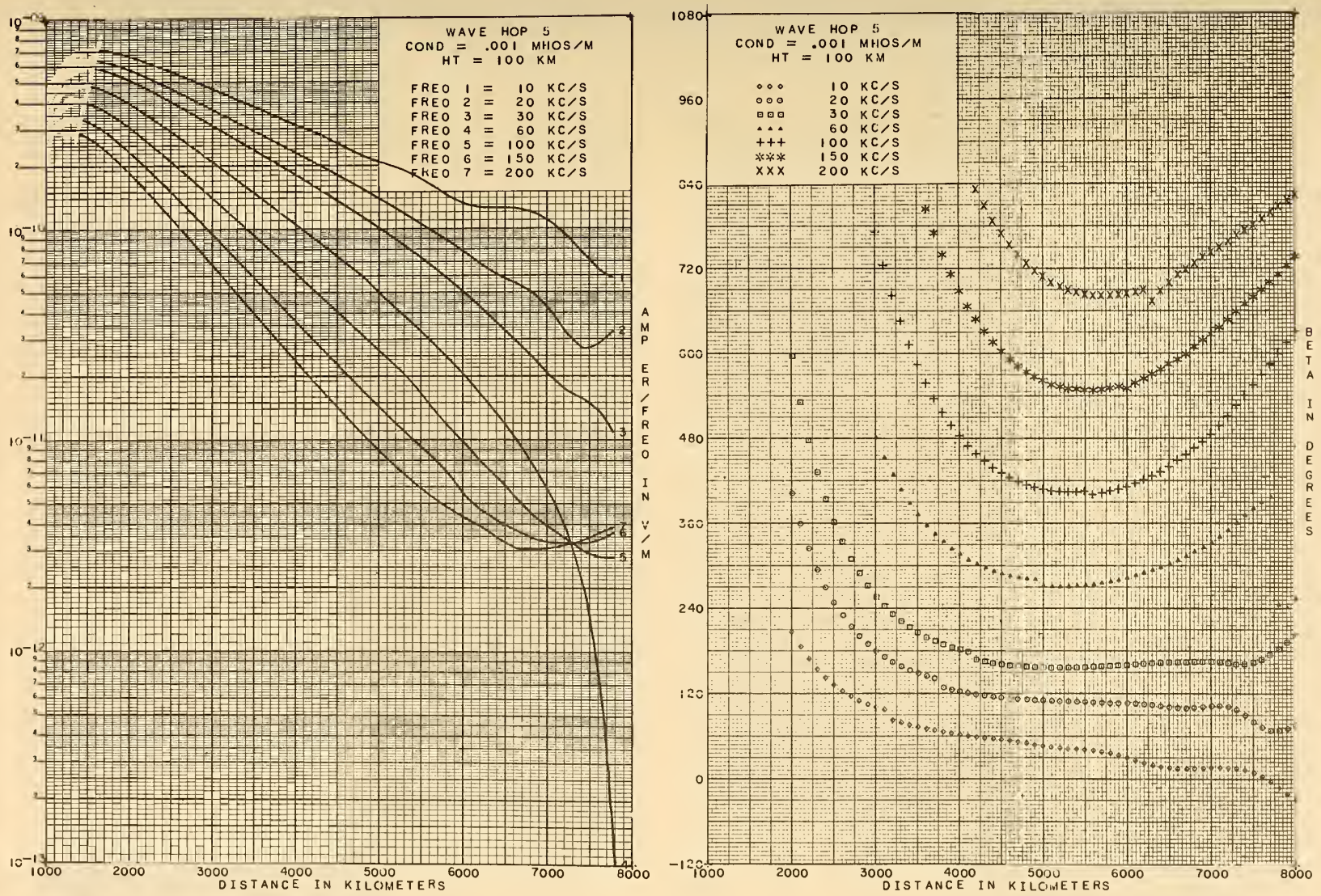

Figure 13.5 Amplitude, $|I_5/f_{kHz}|$, and phase lag, β_5, for parameters shown.

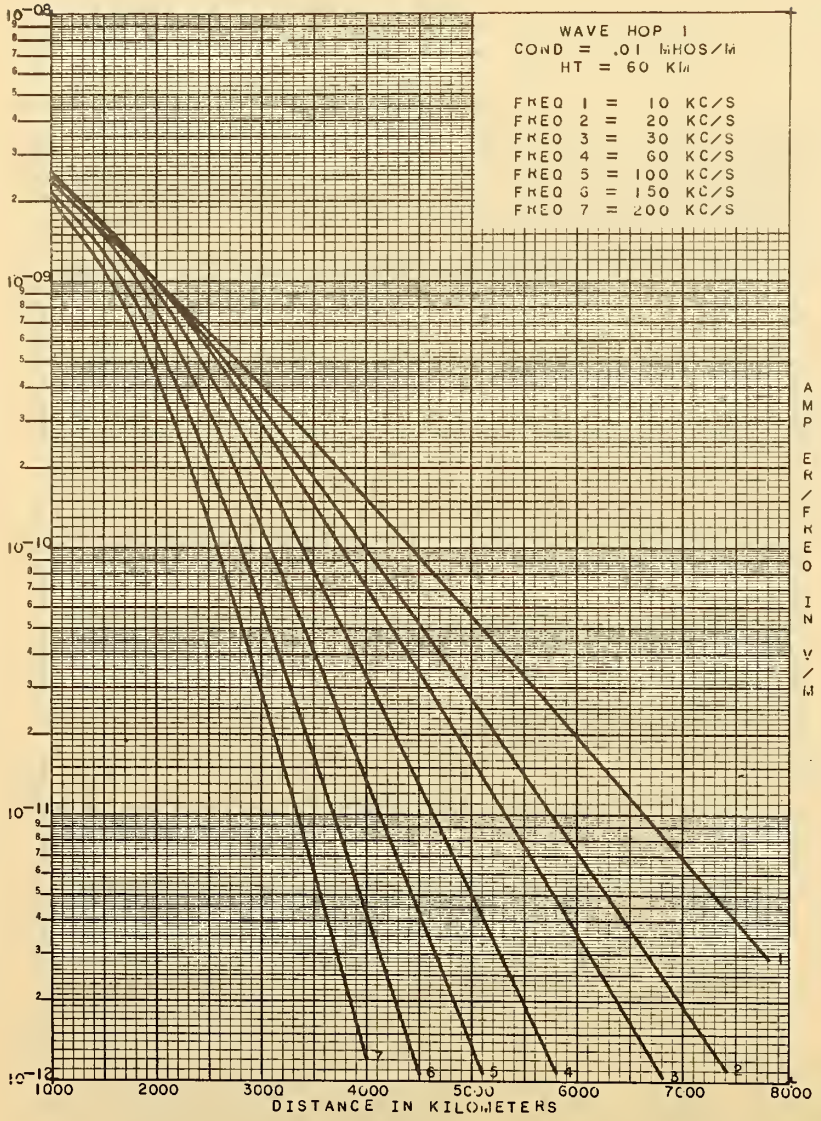

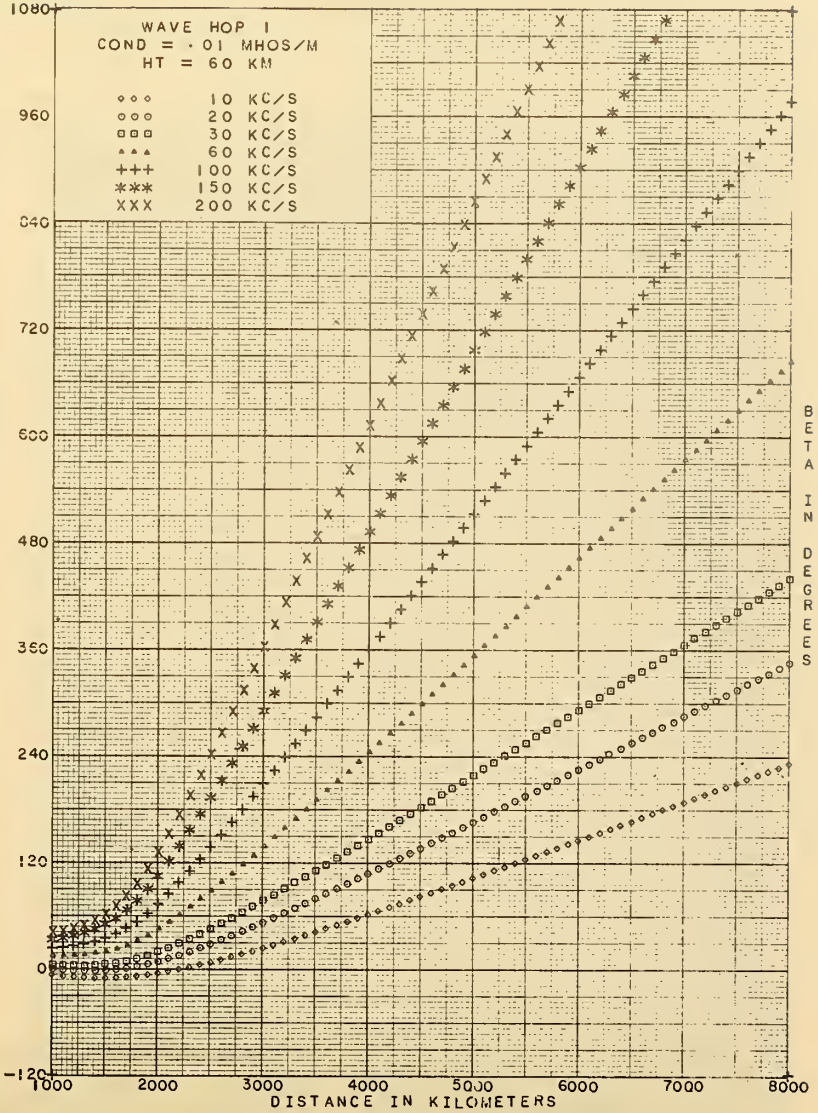

Figure 14.1 Amplitude, $|I_1/f_{kHz}|$, and phase lag, β_1, for parameters shown.

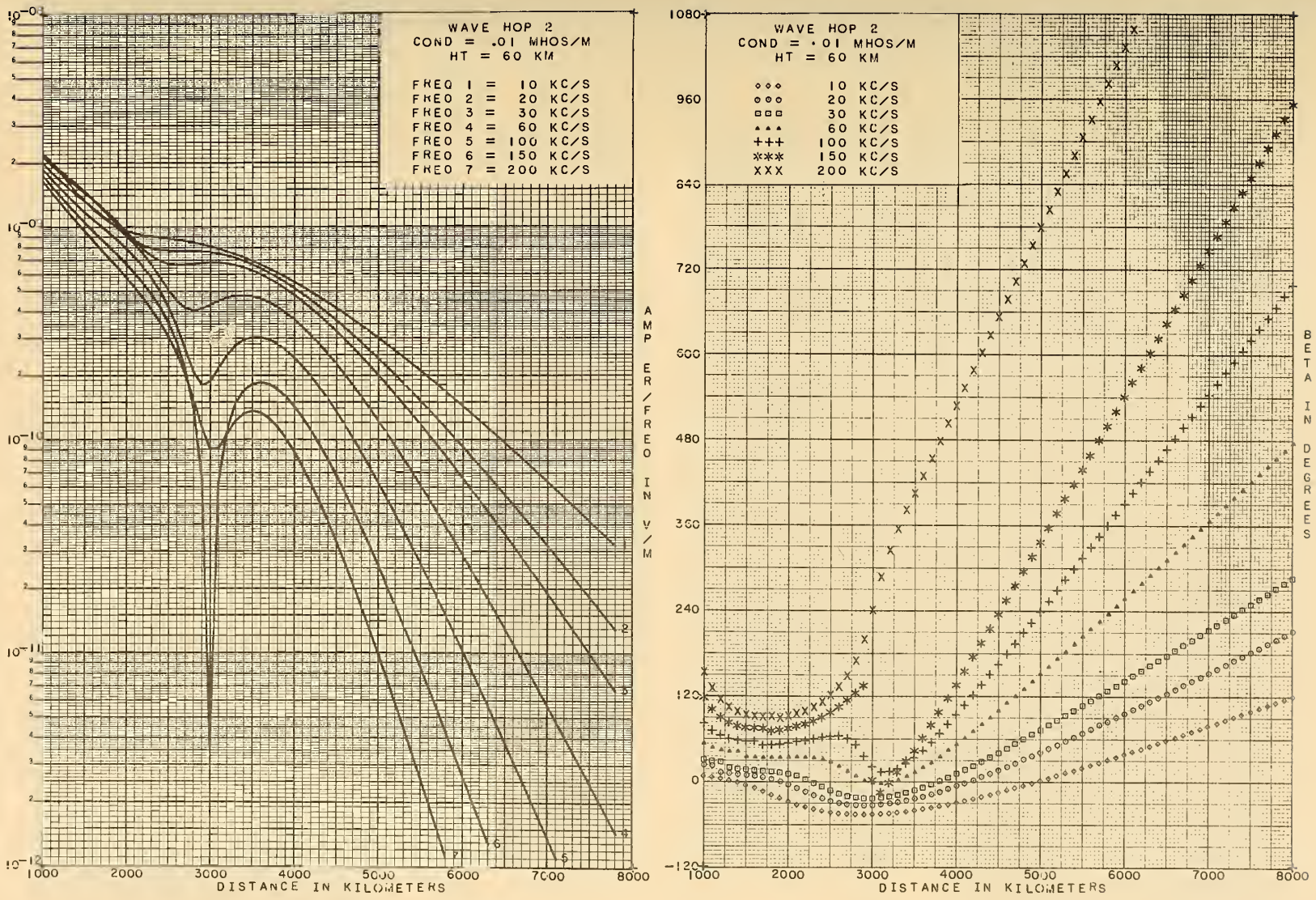

Figure 14.2 Amplitude, $|I_2/f_{kHz}|$, and phase lag, β_2, for parameters shown.

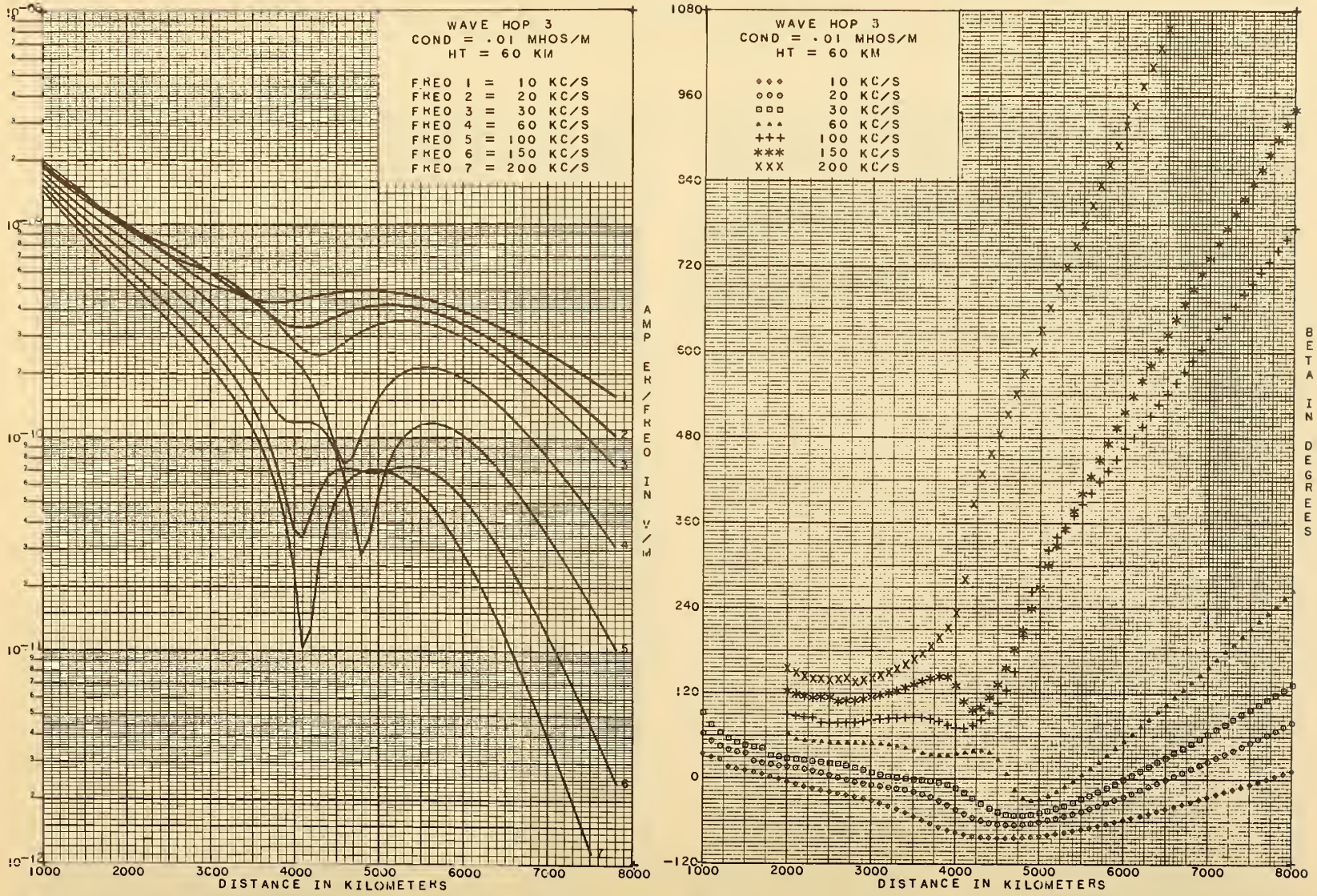

Figure 14.3 Amplitude, $|I_3/f_{kHz}|$, and phase lag, β_3, for parameters shown.

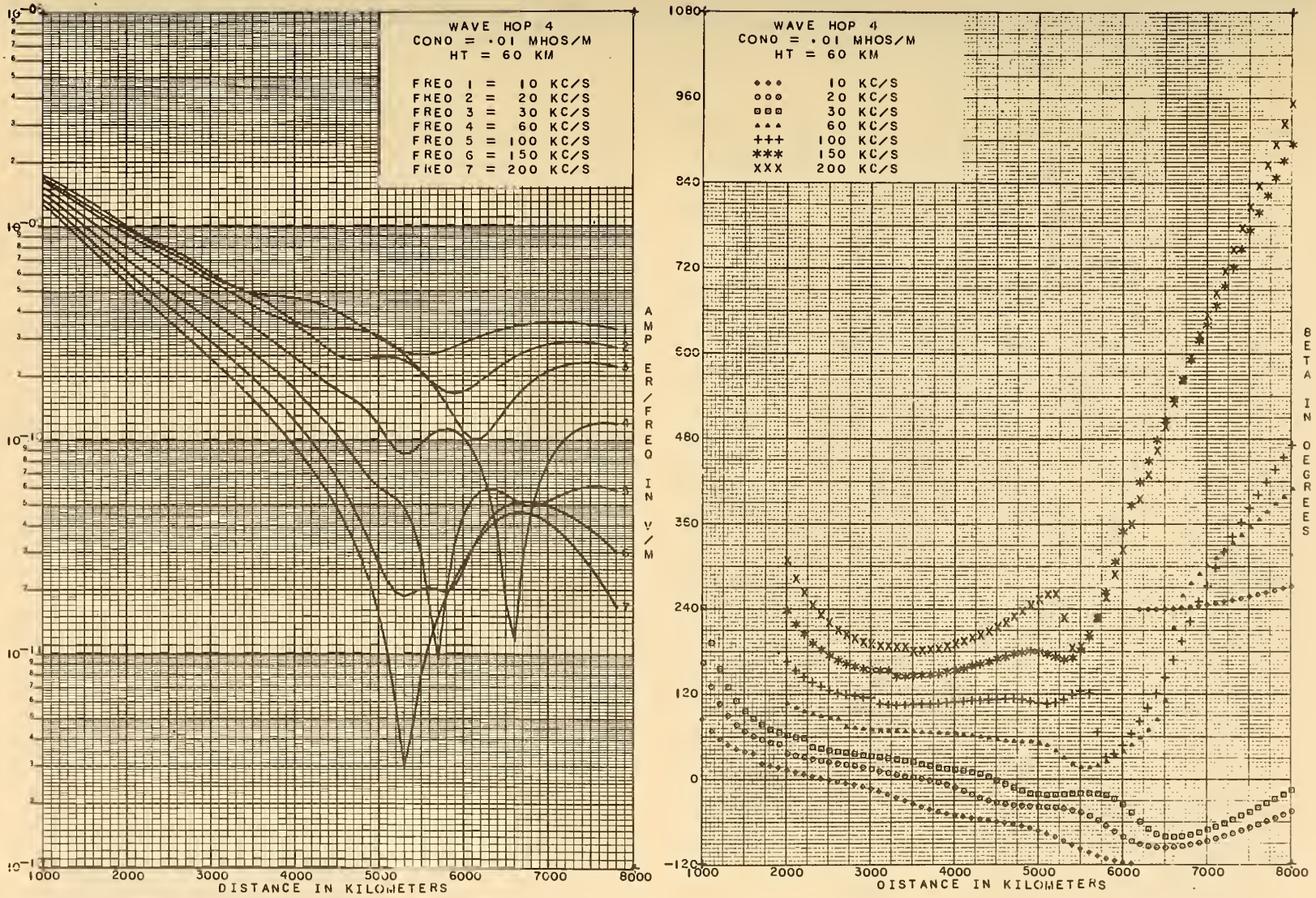

Figure 14.4 Amplitude, $|I_4/f_{kHz}|$, and phase lag, β_4, for parameters shown.

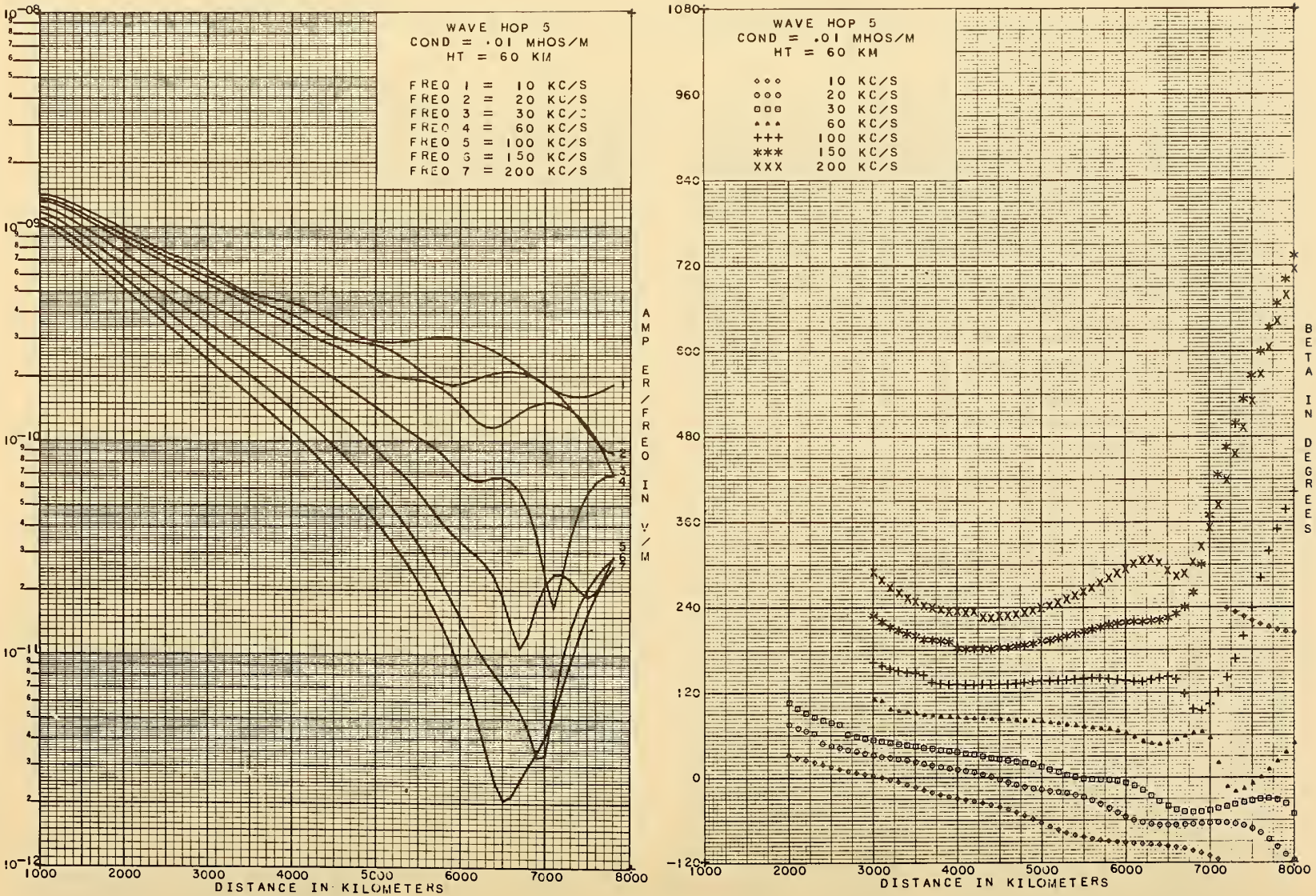

Figure 14.5 Amplitude, $|I_5/f_{kHz}|$, and phase lag, β_5, for parameters shown.

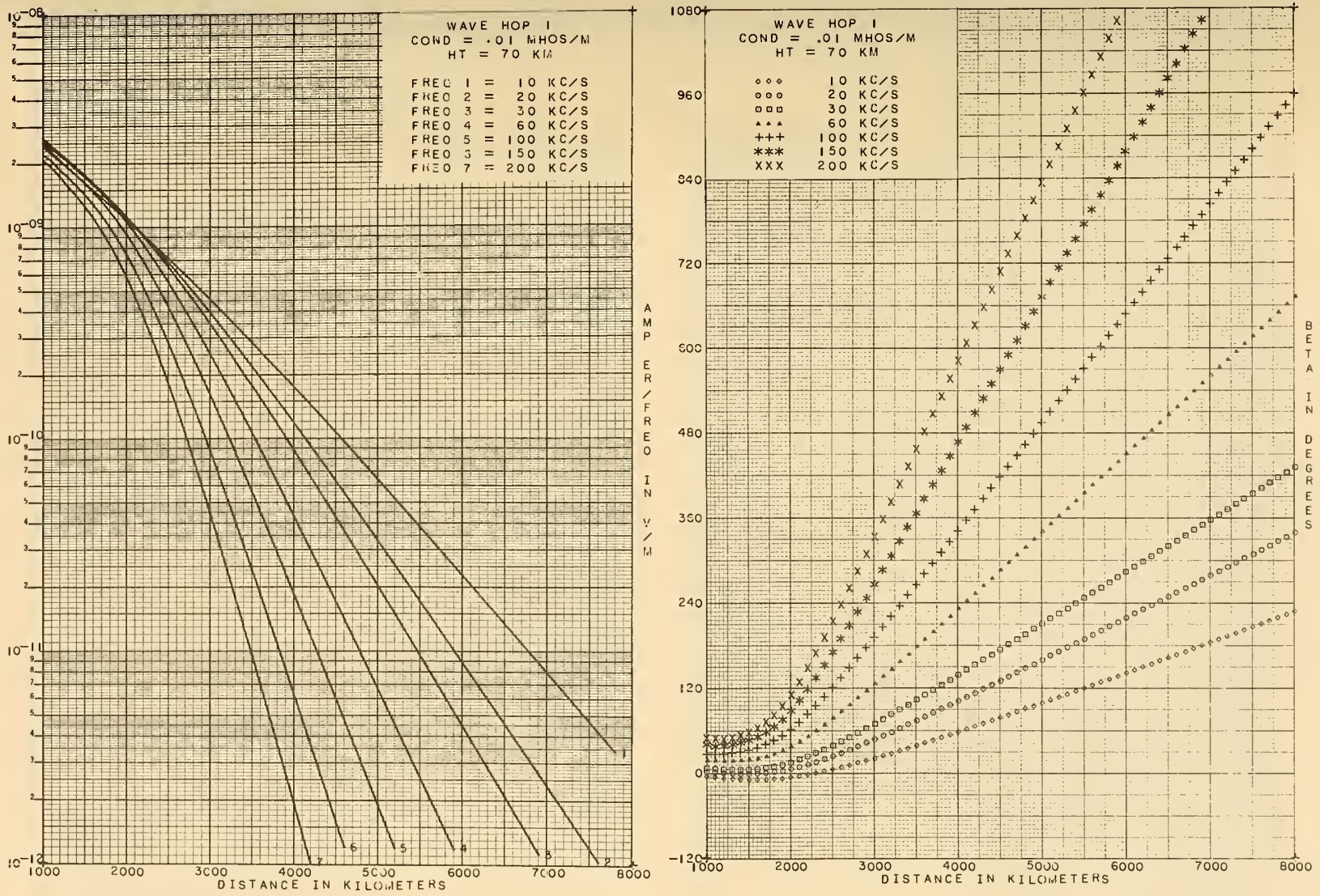

Figure 15.1 Amplitude, $|I_1/f_{kHz}|$, and phase lag, β_1, for parameters shown.

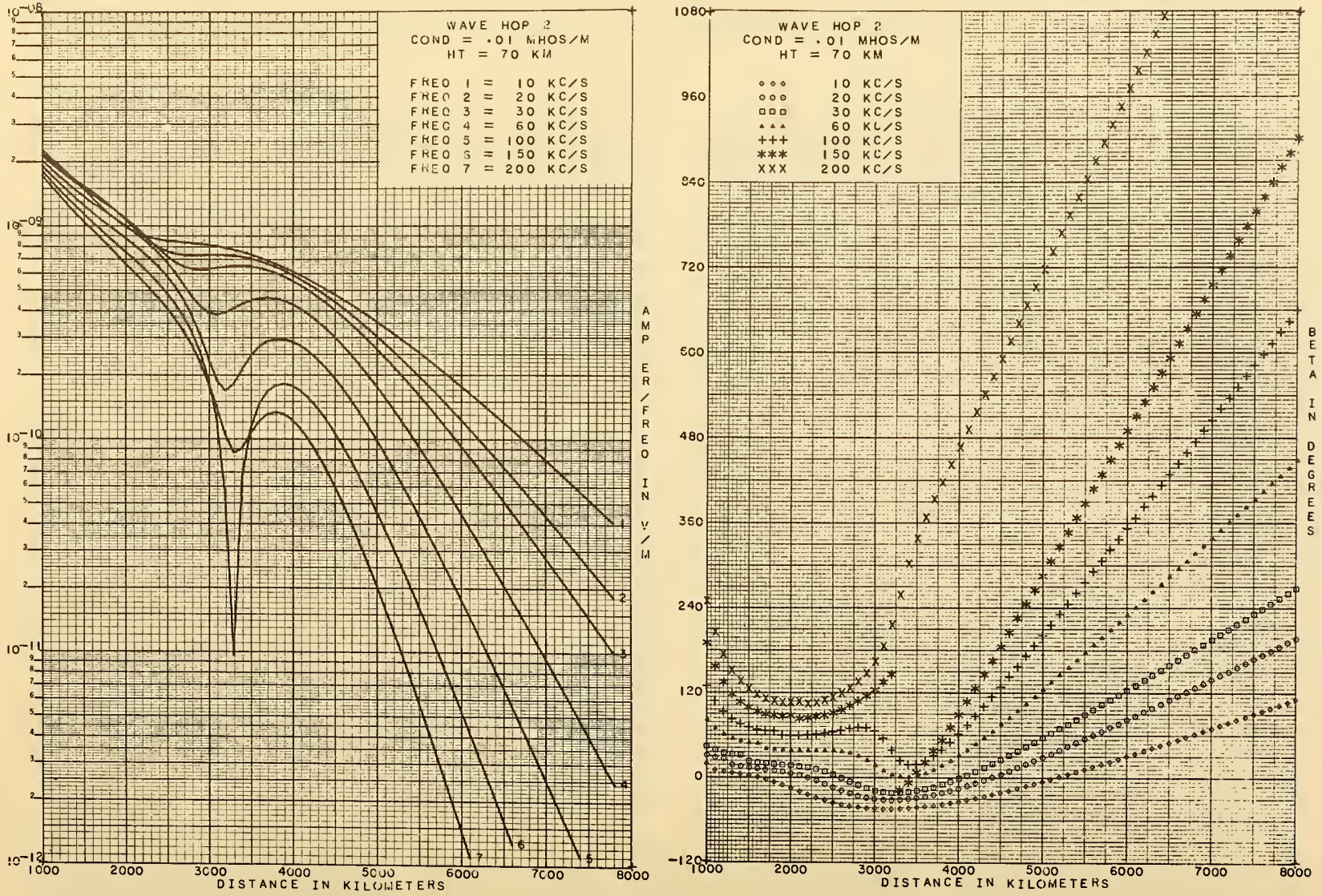

Figure 15.2 Amplitude, $|I_2/f_{kHz}|$, and phase lag, β_2, for parameters shown.

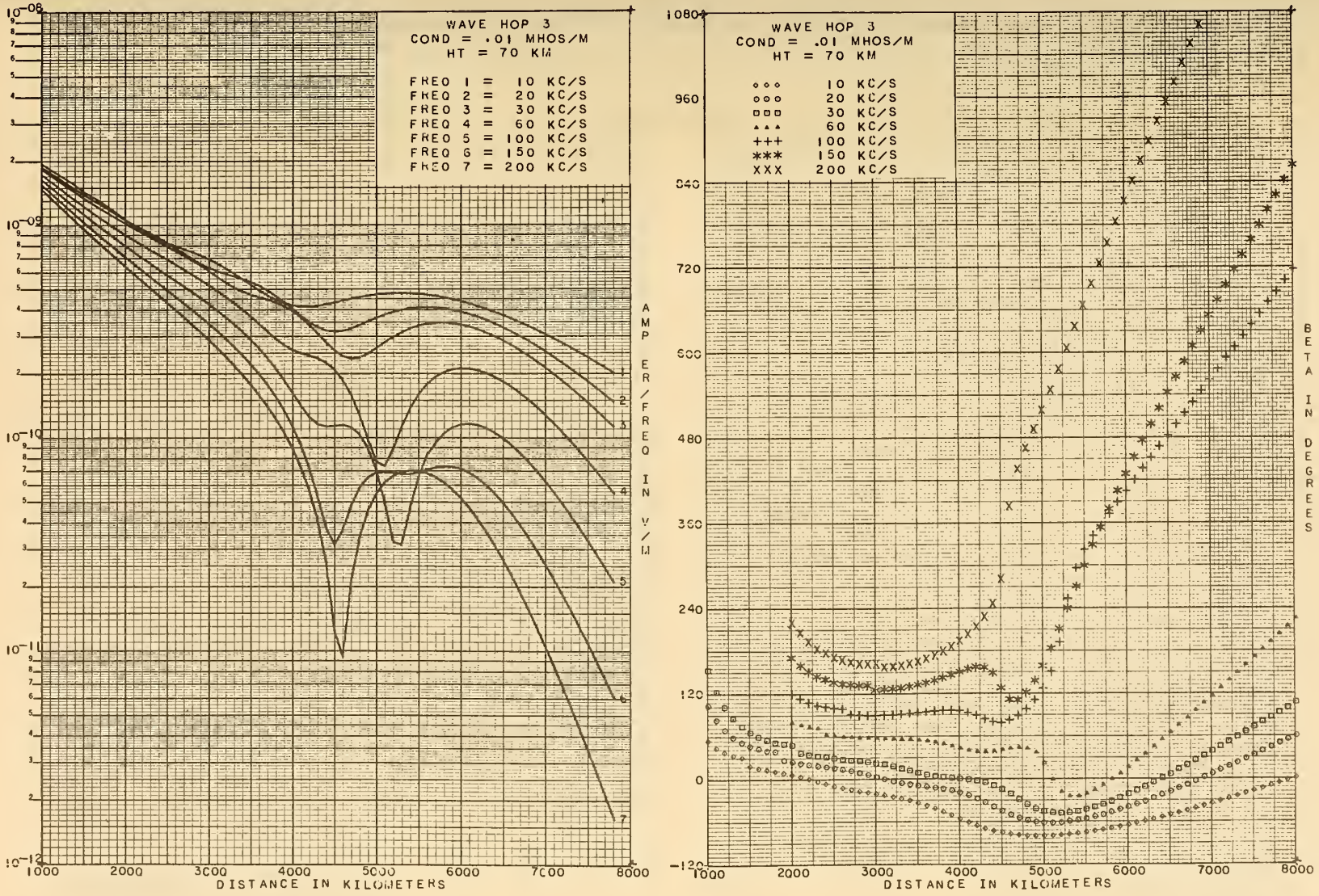

Figure 15.3 Amplitude, $|I_3/f_{kHz}|$, and phase lag, β_3, for parameters shown.

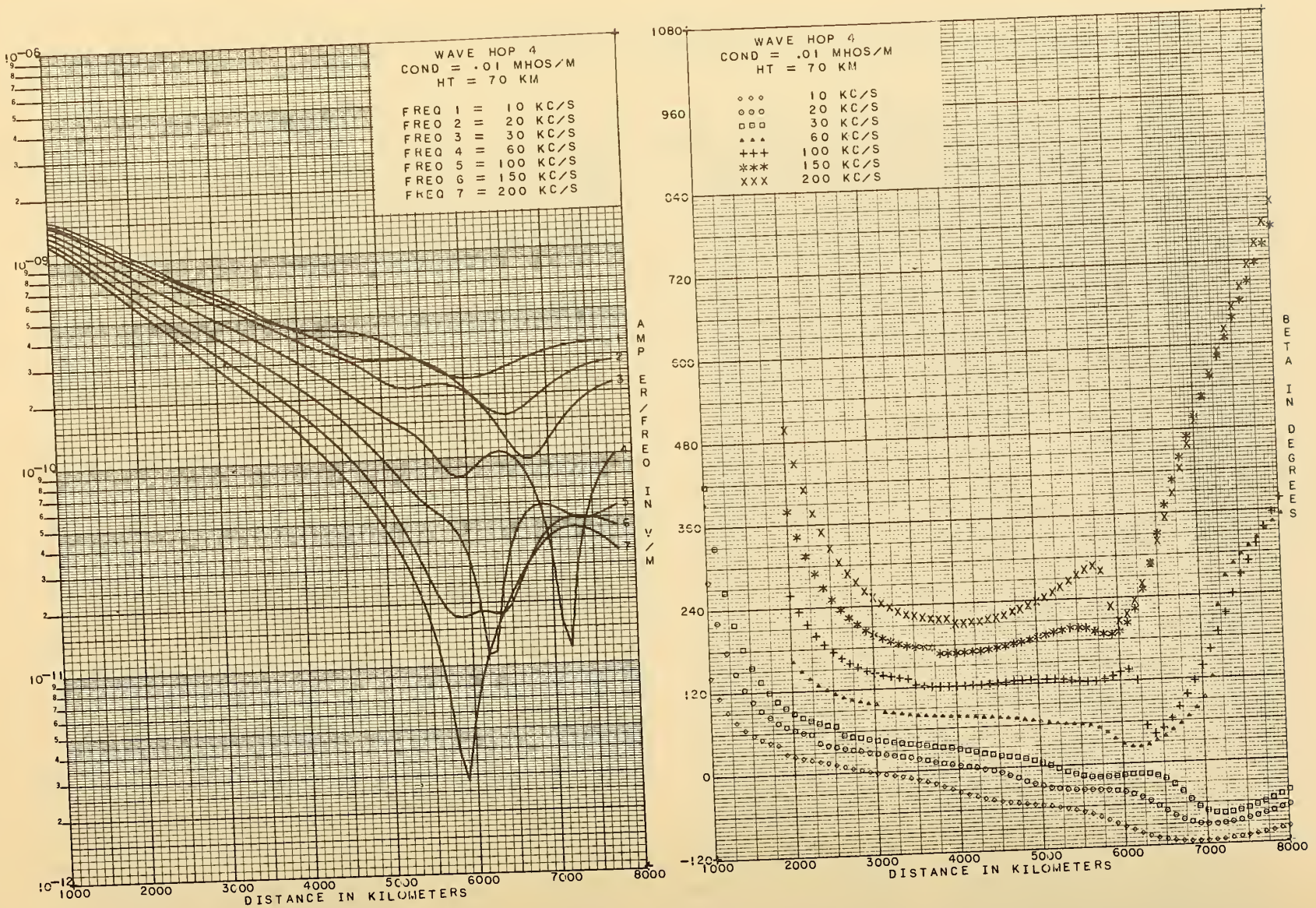

Figure 15.4 Amplitude, $|I_4/f_{kHz}|$, and phase lag, β_4, for parameters shown.

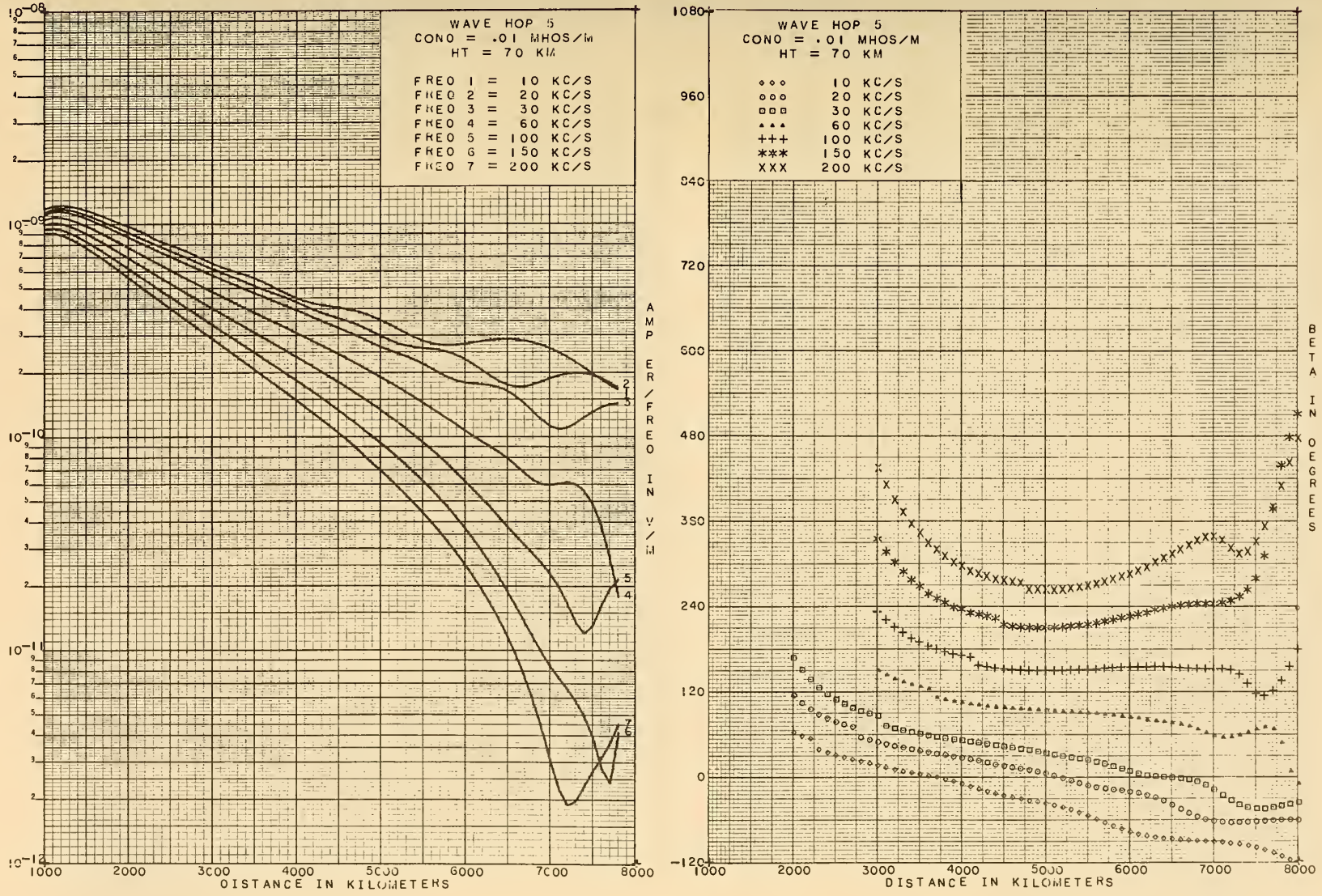

Figure 15.5 Amplitude, $|I_5/f_{kHz}|$, and phase lag, β_5, for parameters shown.

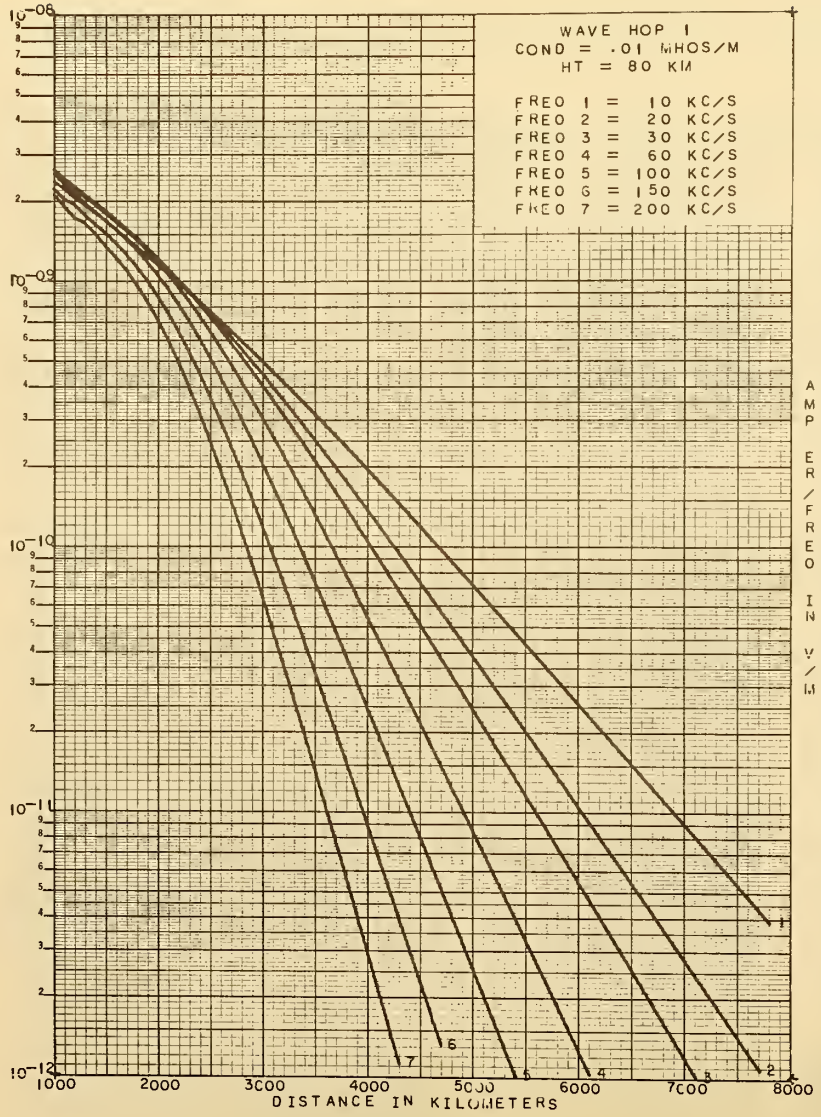

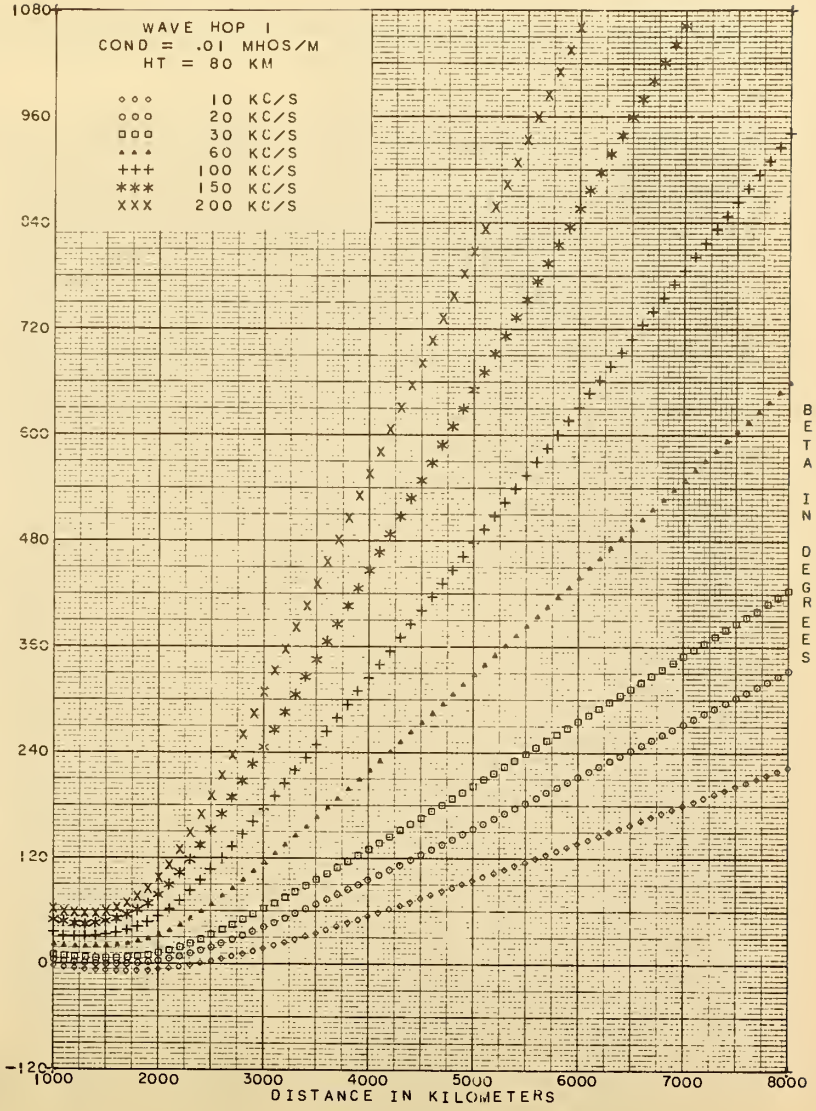

Figure 16.1 Amplitude, $|I_1/f_{kHz}|$, and phase lag, β_1, for parameters shown.

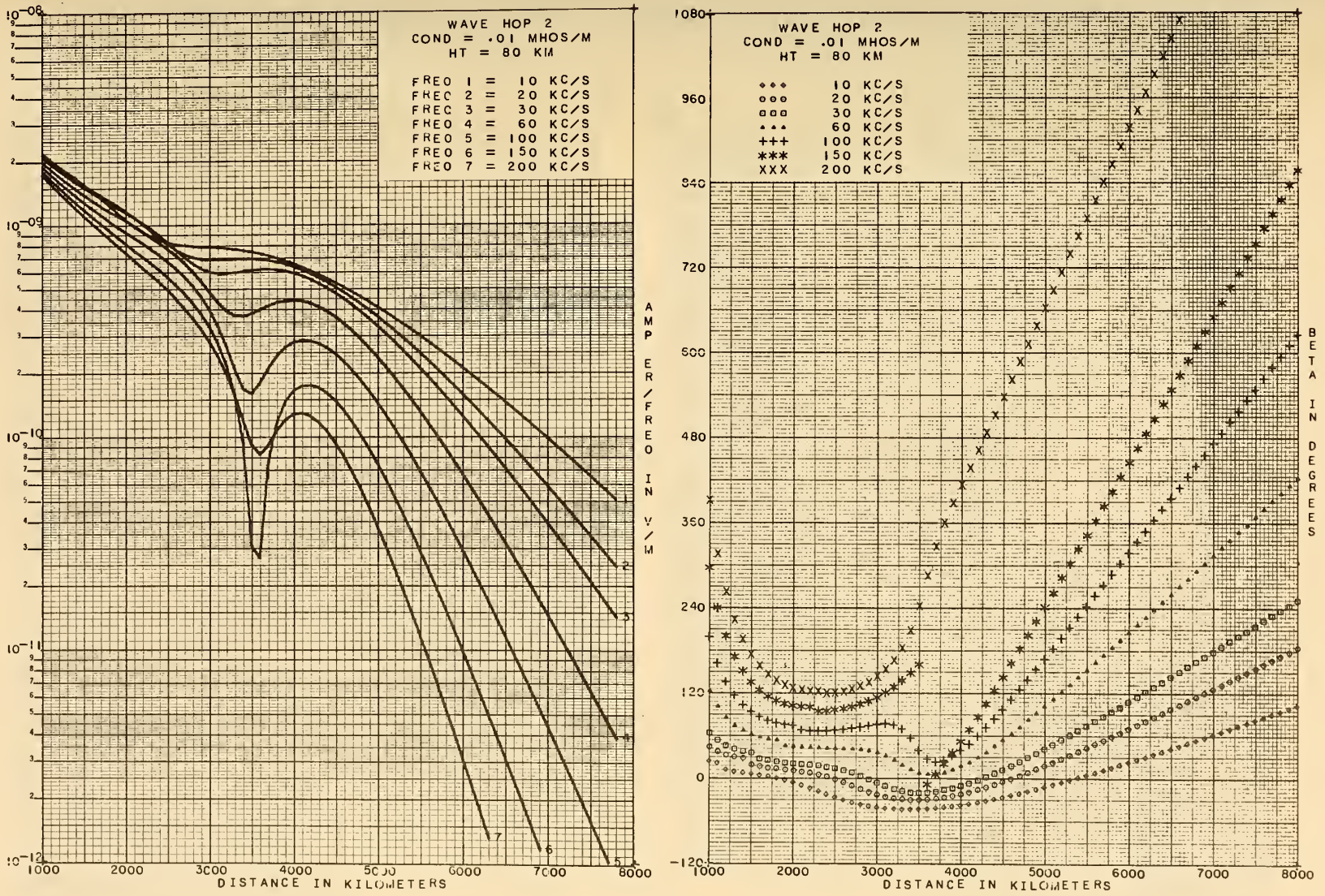

Figure 16.2 Amplitude, $|I_2/f_{kHz}|$, and phase lag, β_2, for parameters shown.

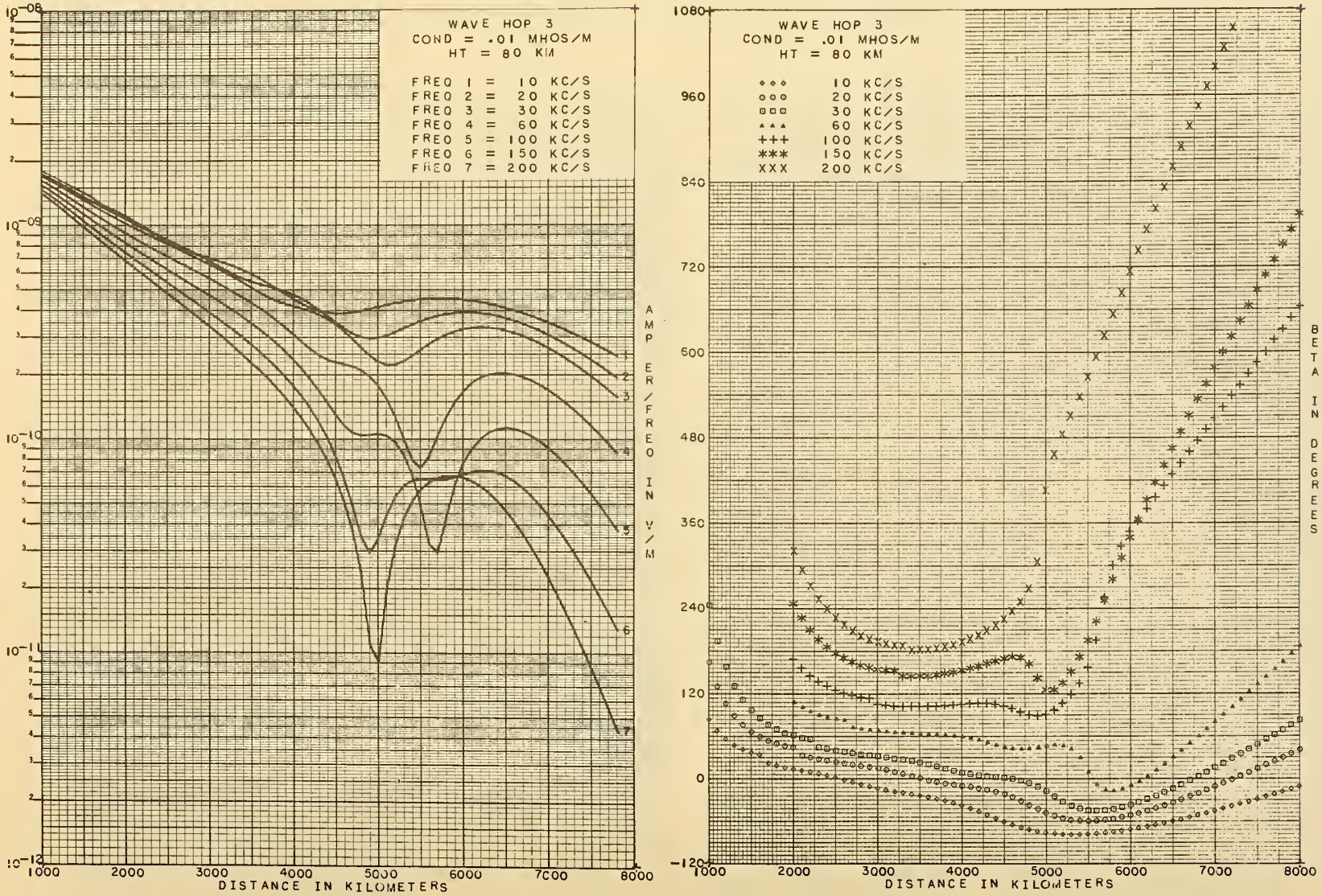

Figure 16.3 Amplitude, $|I_3/f_{kHz}|$, and phase lag, β_3, for parameters shown.

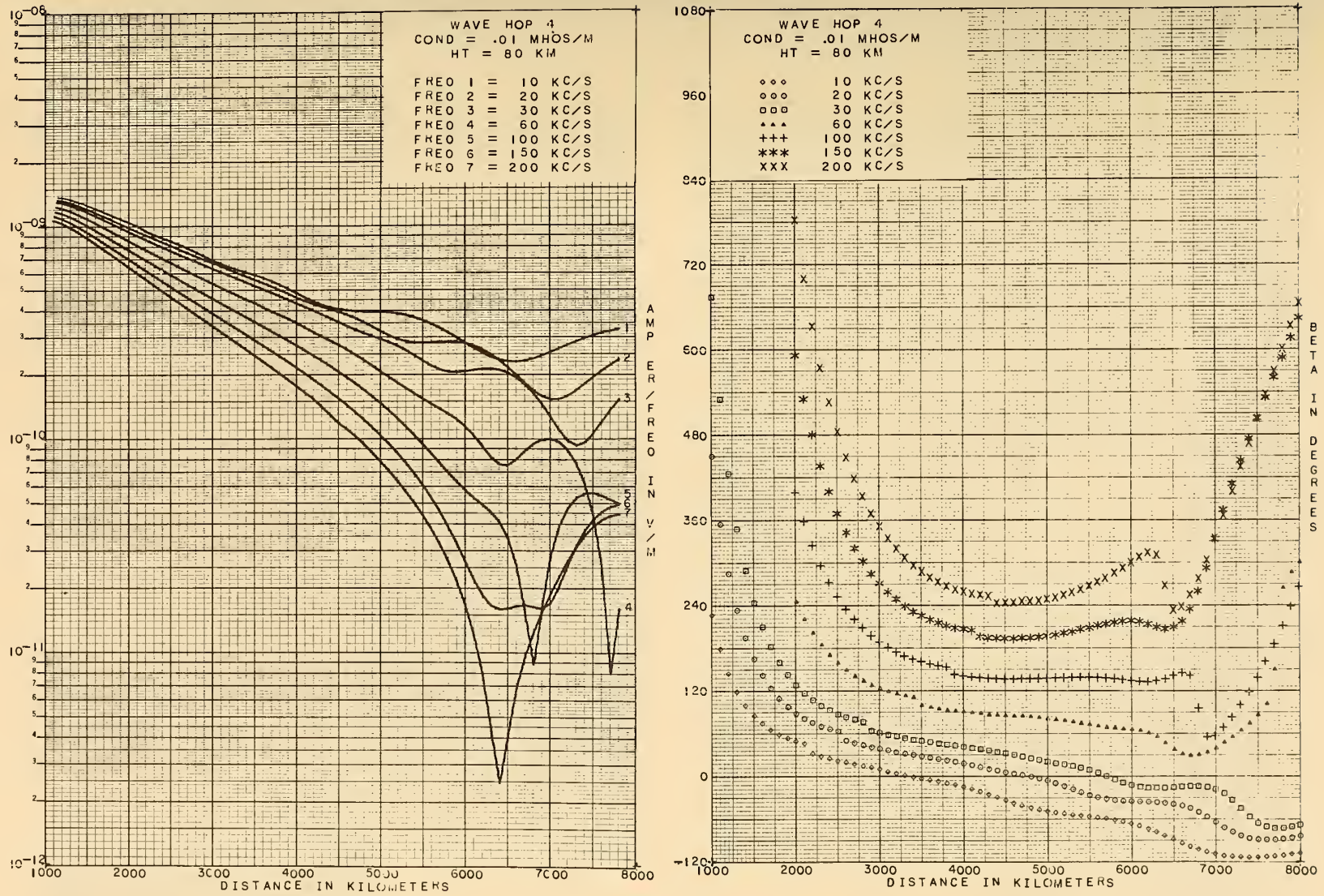

Figure 16.4 Amplitude, $|I_4/f_{kHz}|$, and phase lag, β_4, for parameters shown.

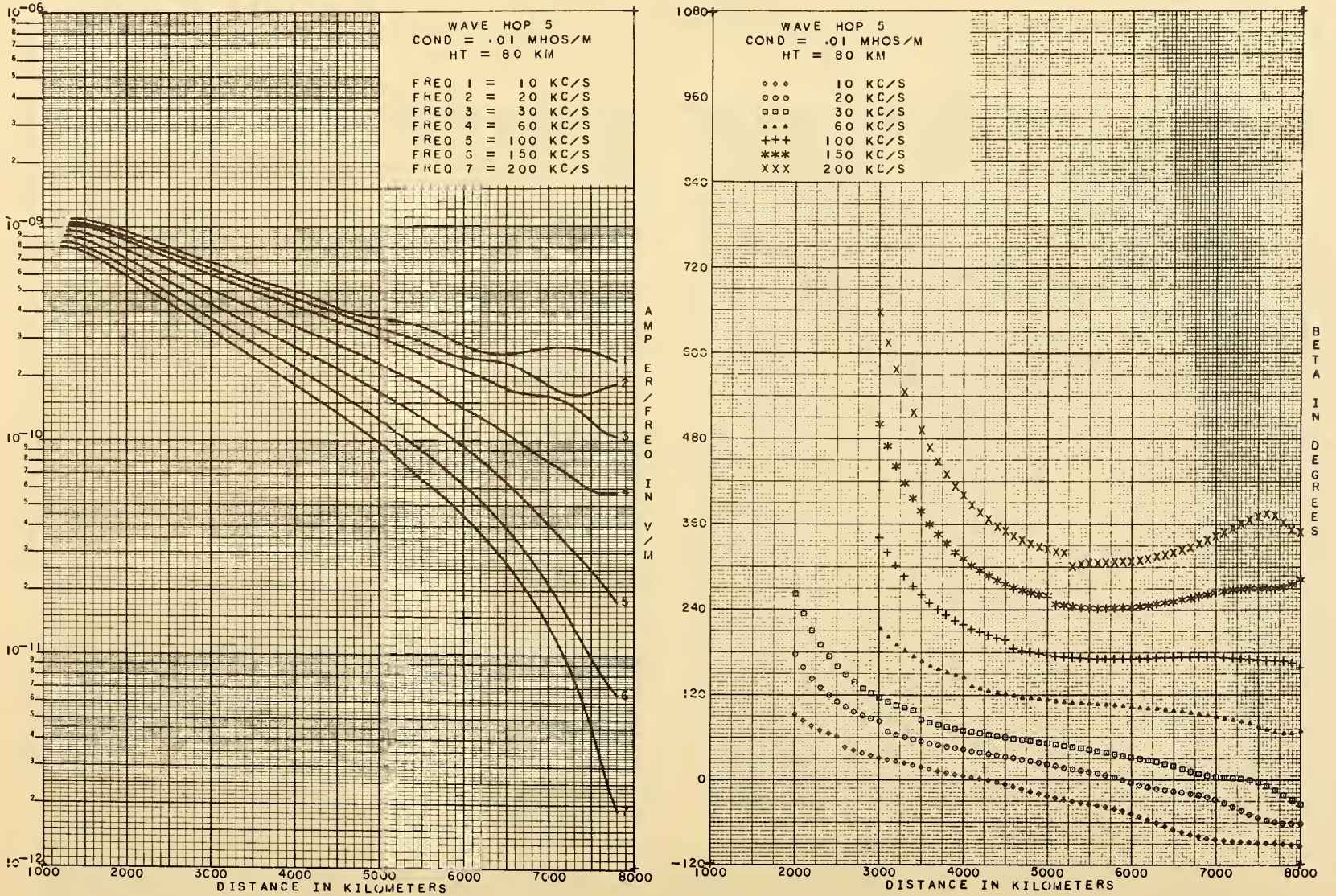

Figure 16.5 Amplitude, $|I_5/f_{kHz}|$, and phase lag, β_5, for parameters shown.

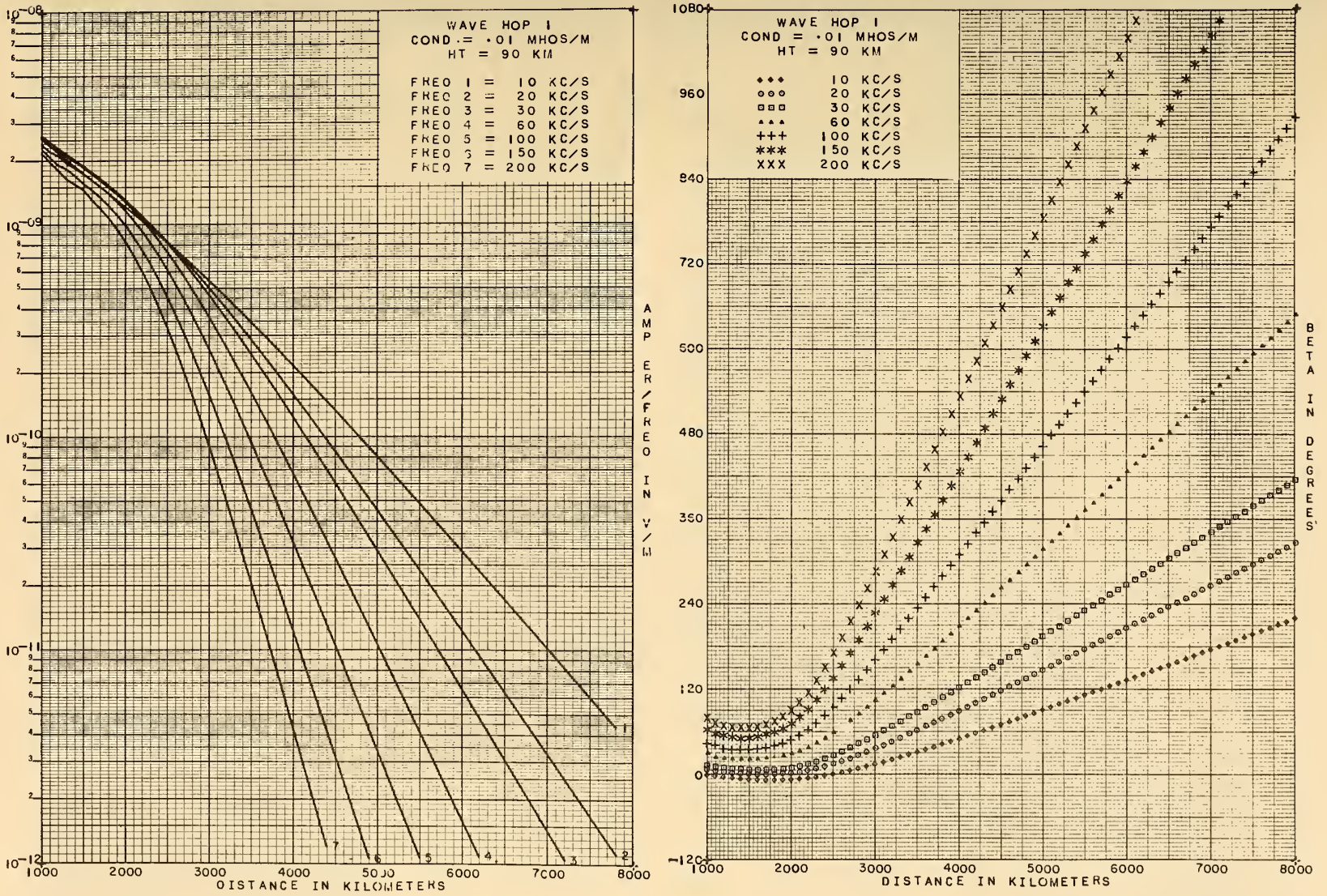

Figure 17.1 Amplitude, $|I_1/f_{kHz}|$, and phase lag, β_1, for parameters shown.

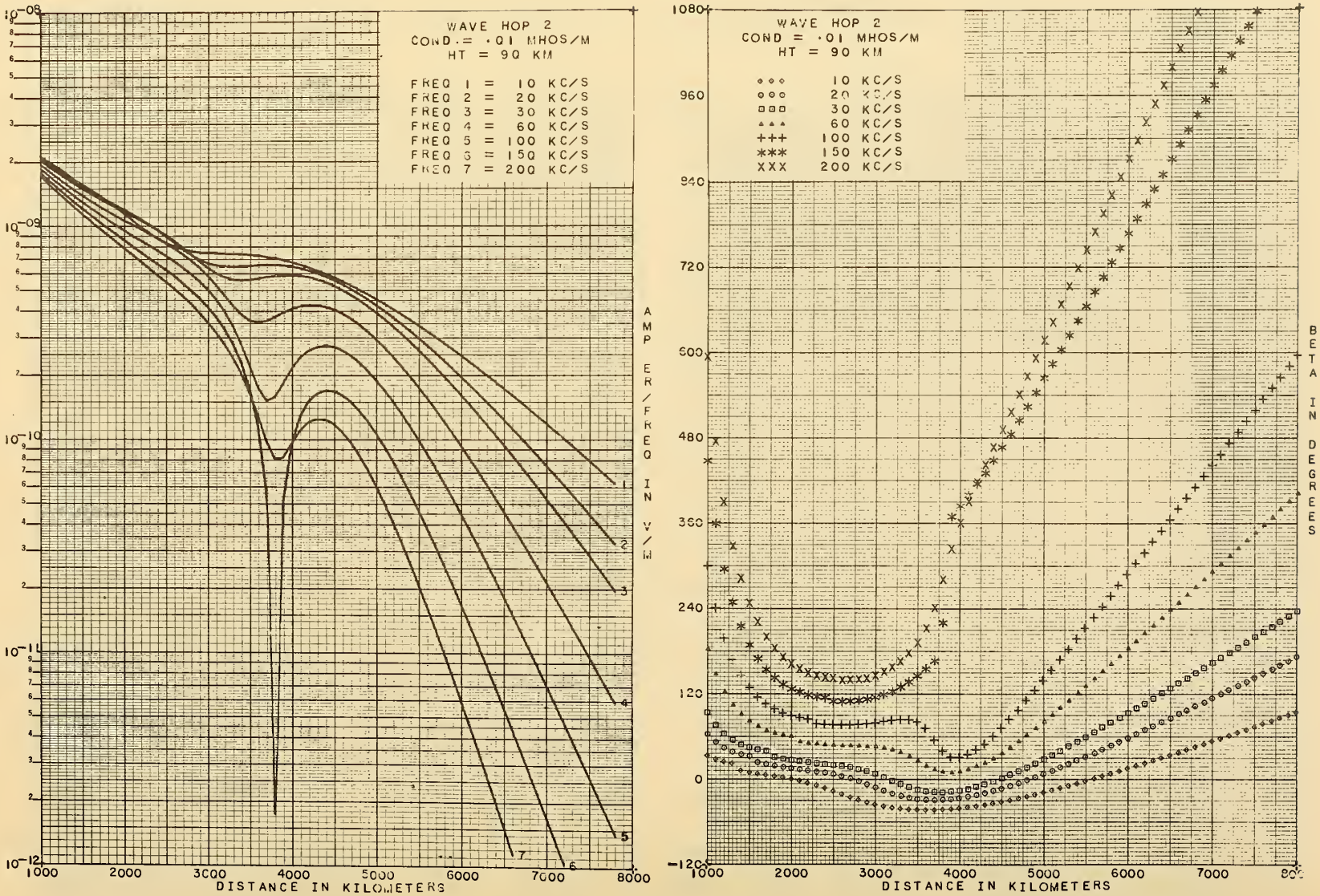

Figure 17.2 Amplitude, $|I_2/f_{kHz}|$, and phase lag, β_2, for parameters shown.

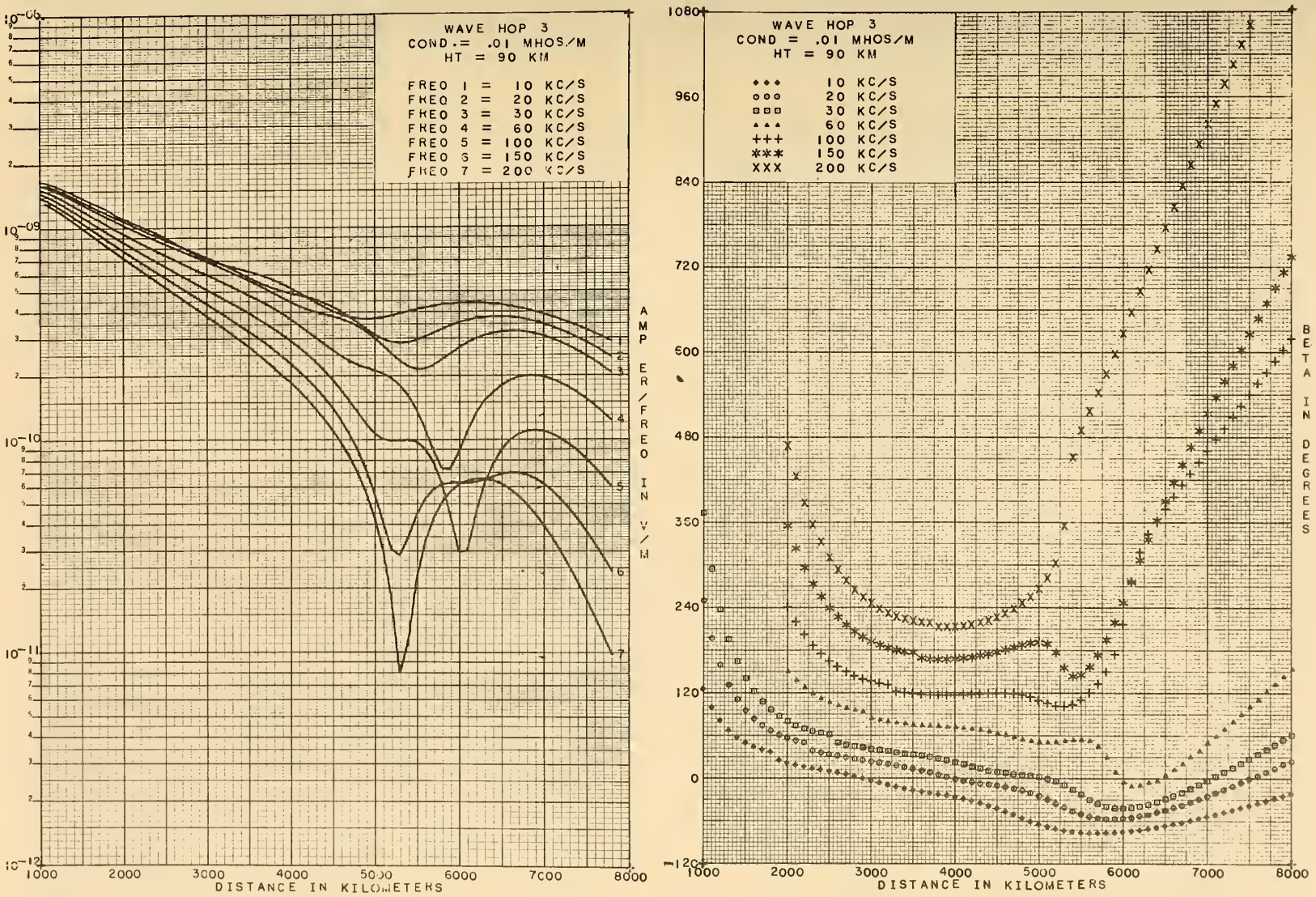

Figure 17.3 Amplitude, $|I_3/f_{kHz}|$, and phase lag, β_3, for parameters shown.

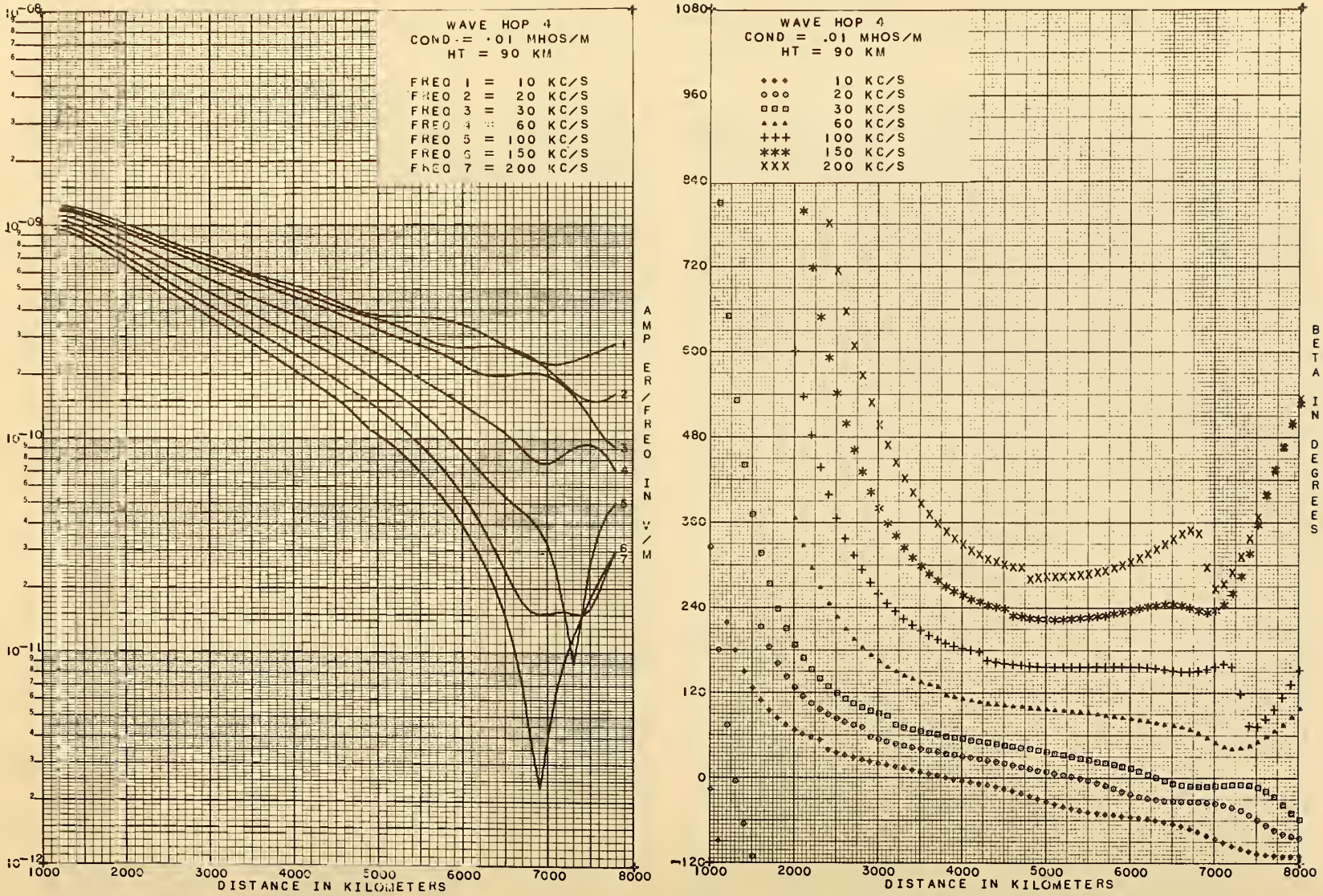

Figure 17.4 Amplitude, $|I_4/f_{kHz}|$, and phase lag, β_4, for parameters shown.

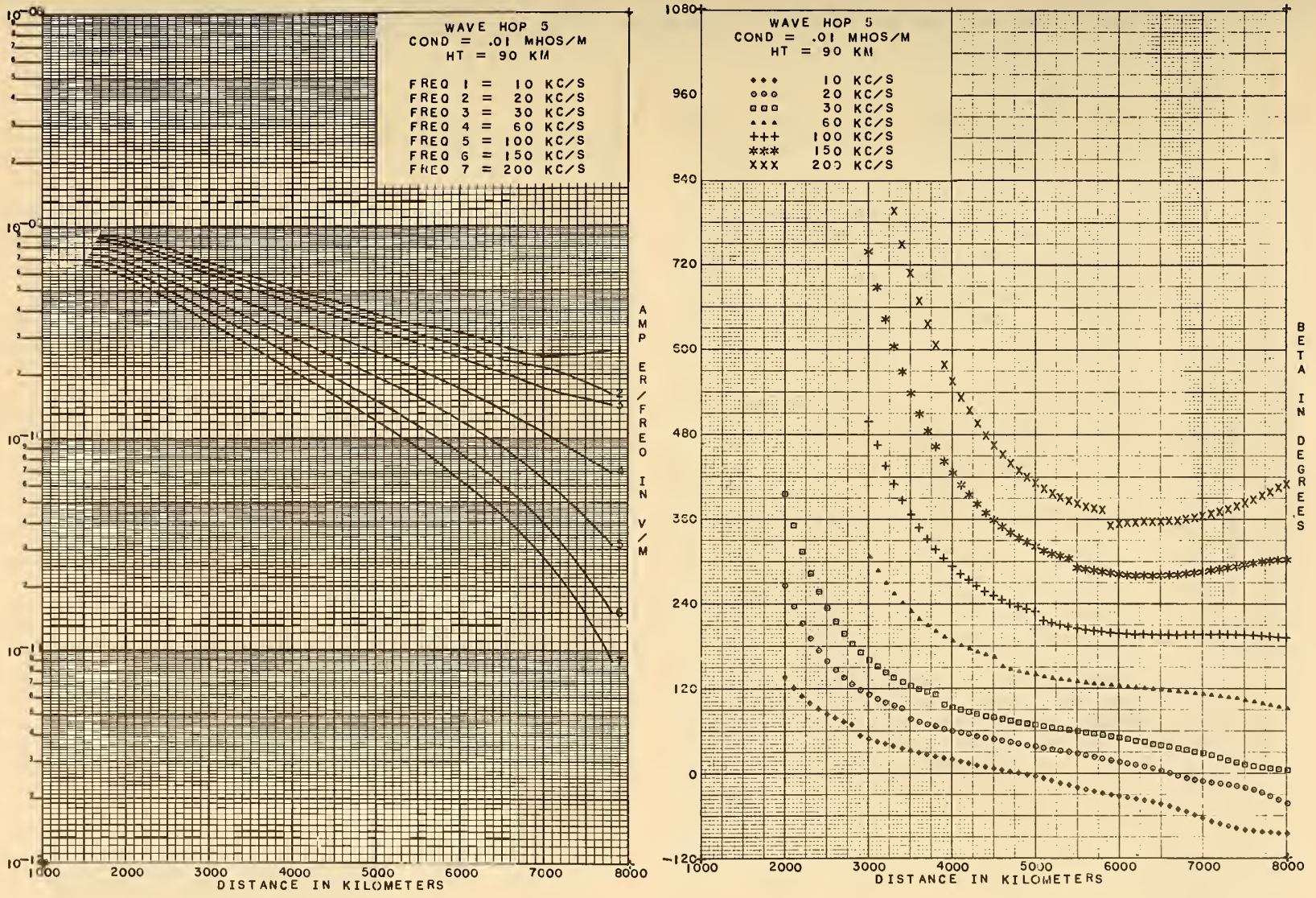

Figure 17.5 Amplitude, $|I_5/f_{kHz}|$, and phase lag, β_5, for parameters shown.

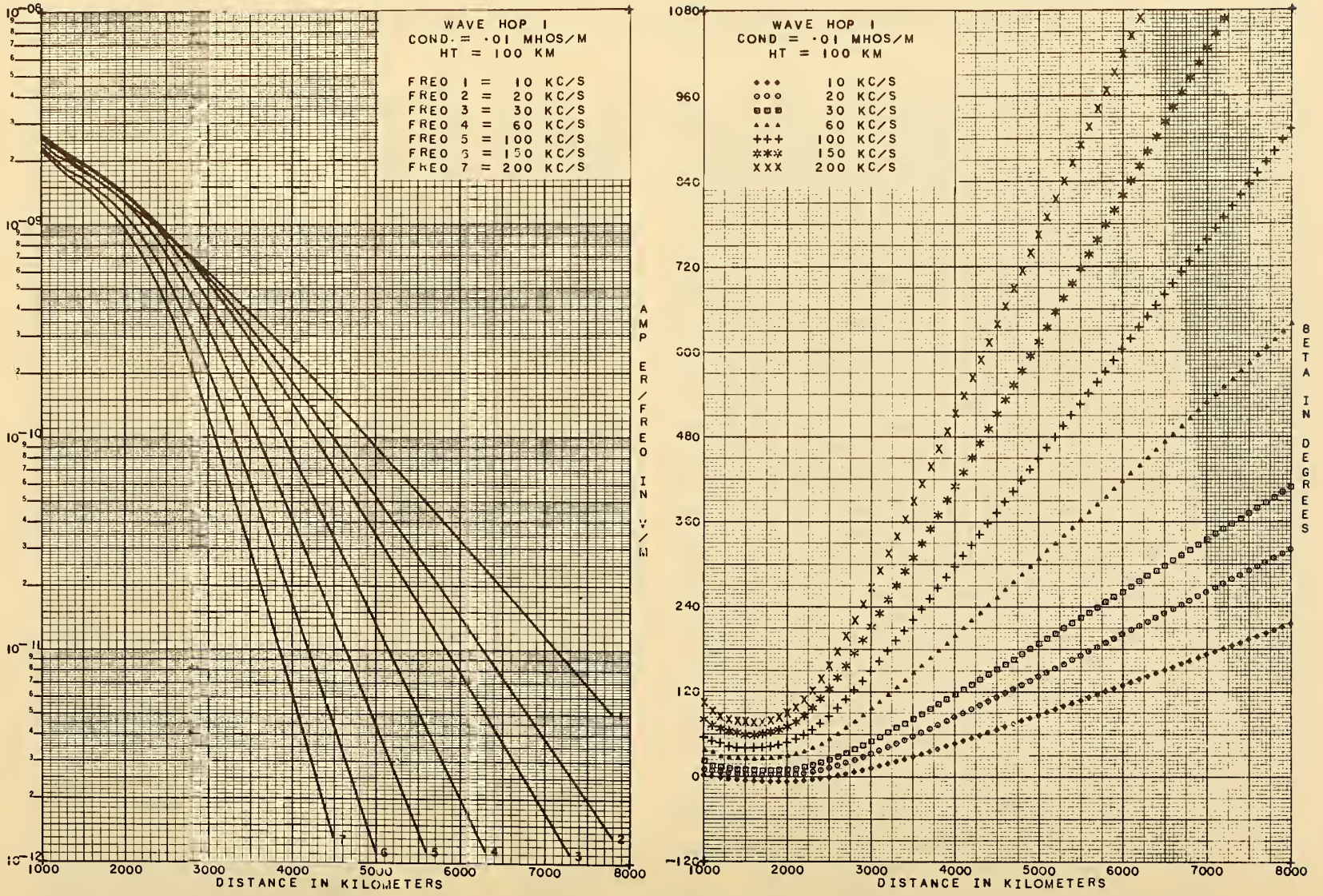

Figure 18.1 Amplitude, $|I_1/f_{kHz}|$, and phase lag, β_1, for parameters shown.

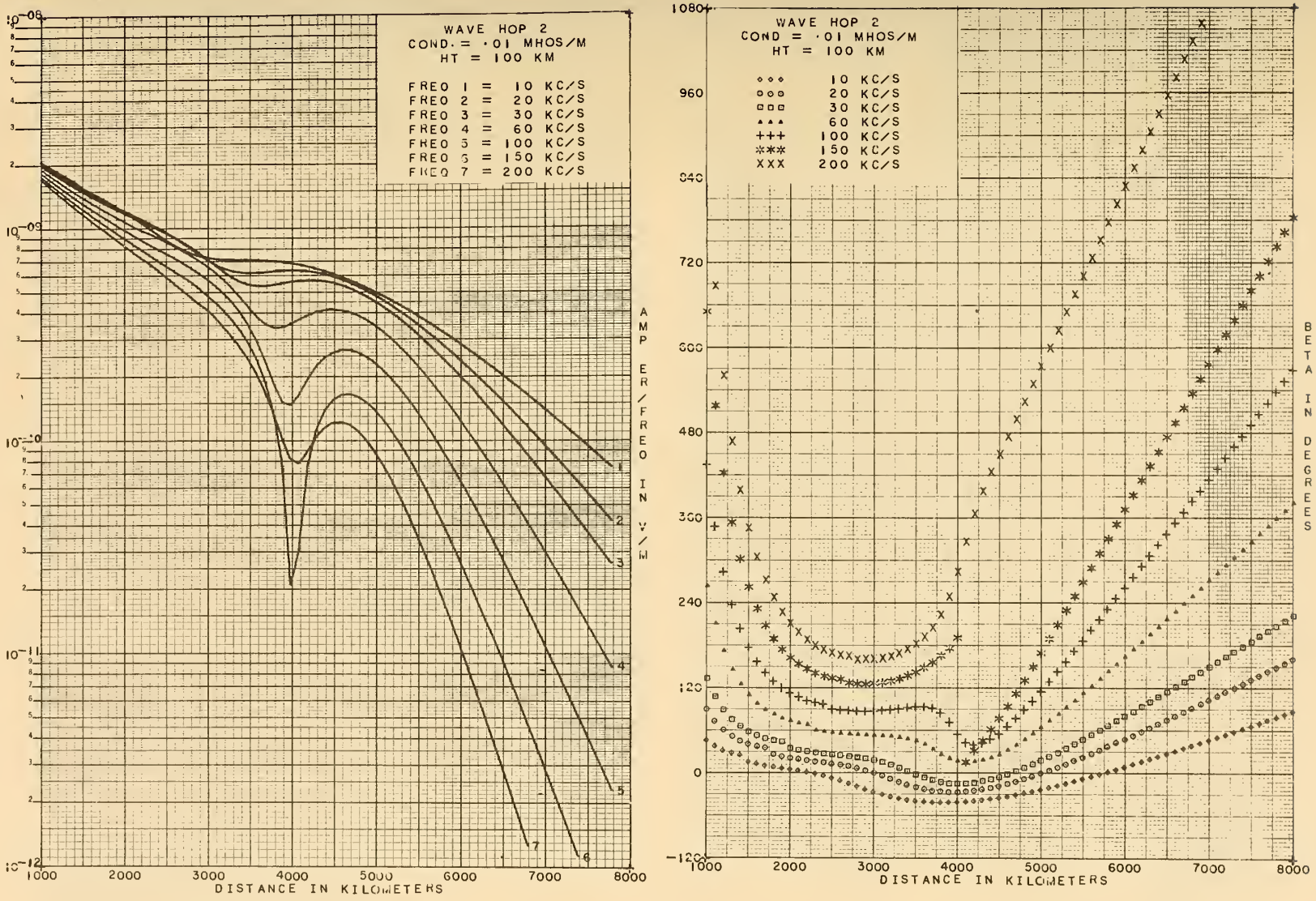

Figure 18.2 Amplitude, $|I_2/f_{kHz}|$, and phase lag, β_2, for parameters shown.

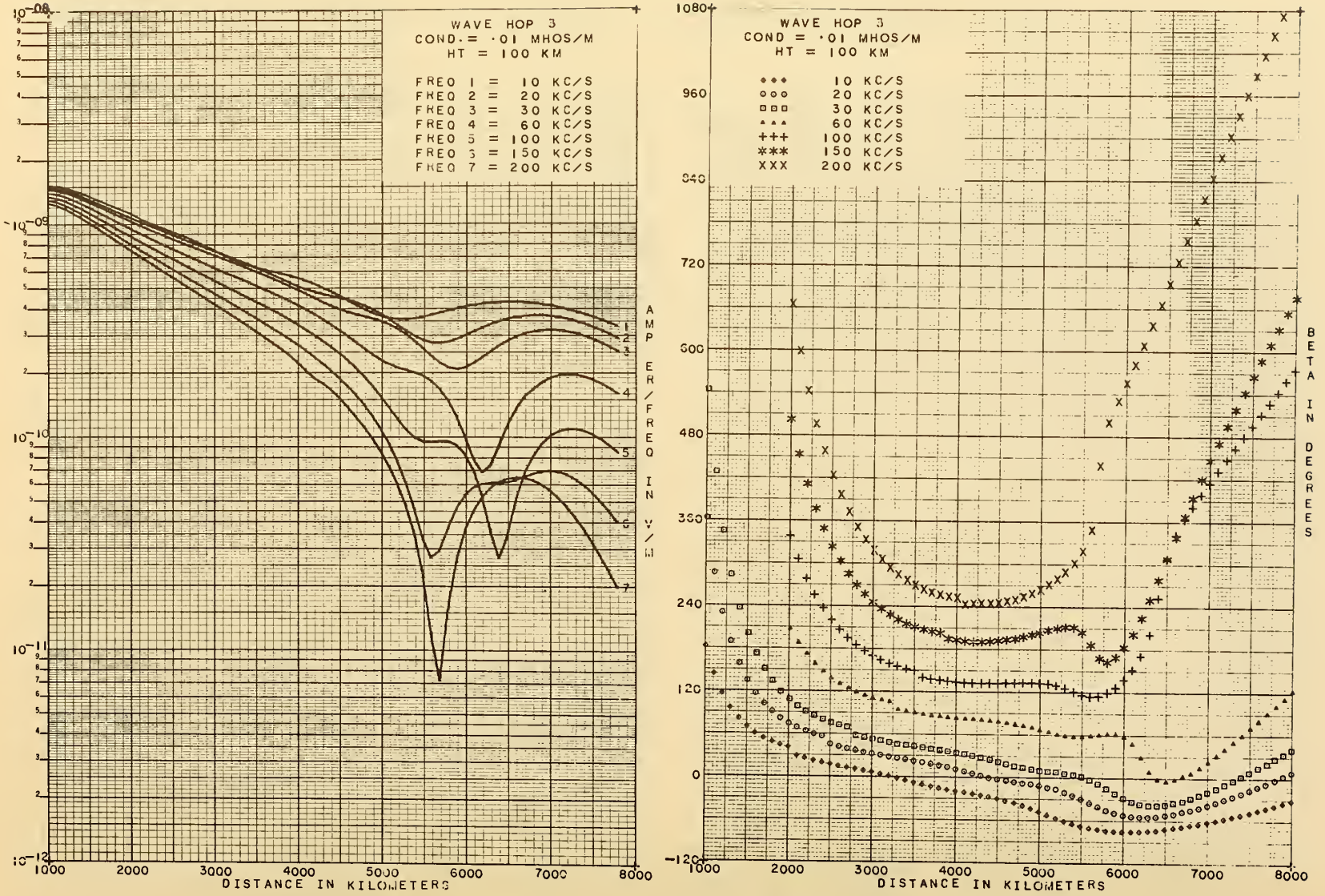

Figure 18.3 Amplitude, $|I_3/f_{kHz}|$, and phase lag, β_3, for parameters shown.

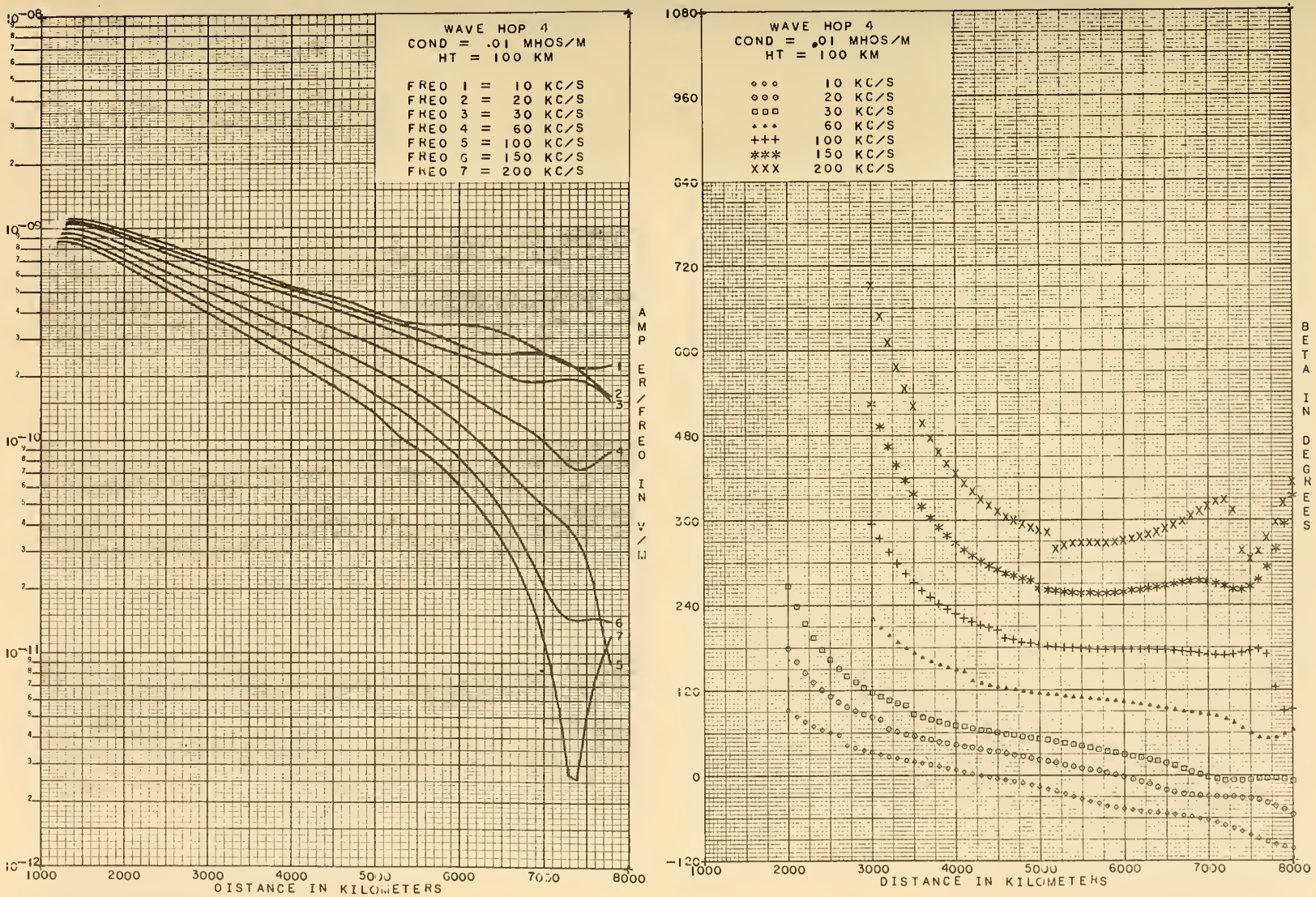

Figure 18.4 Amplitude, $|I_4/f_{kHz}|$, and phase lag, β_4, for parameters shown.

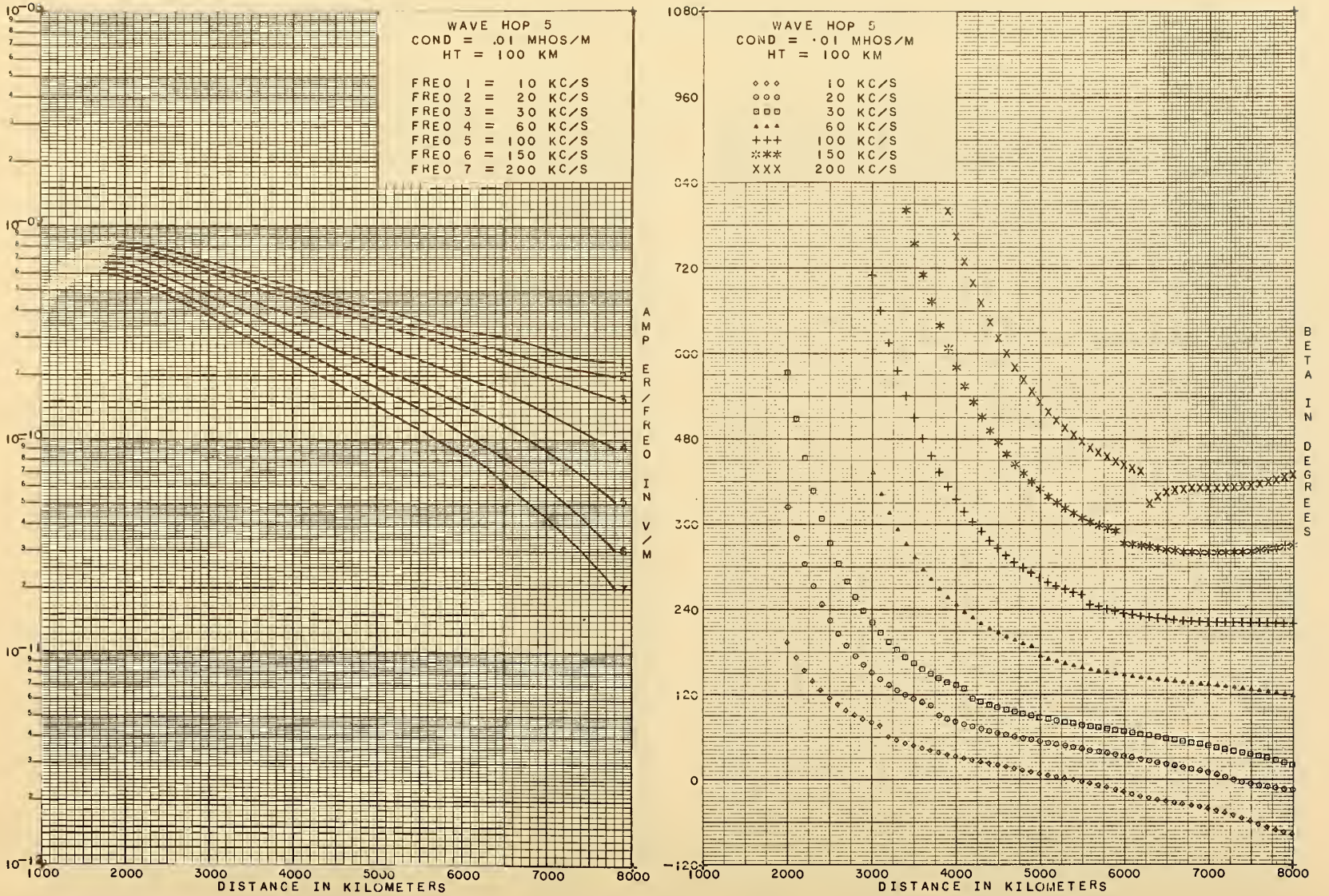

Figure 18.5 Amplitude, $|I_5/f_{kHz}|$, and phase lag, β_5, for parameters shown.

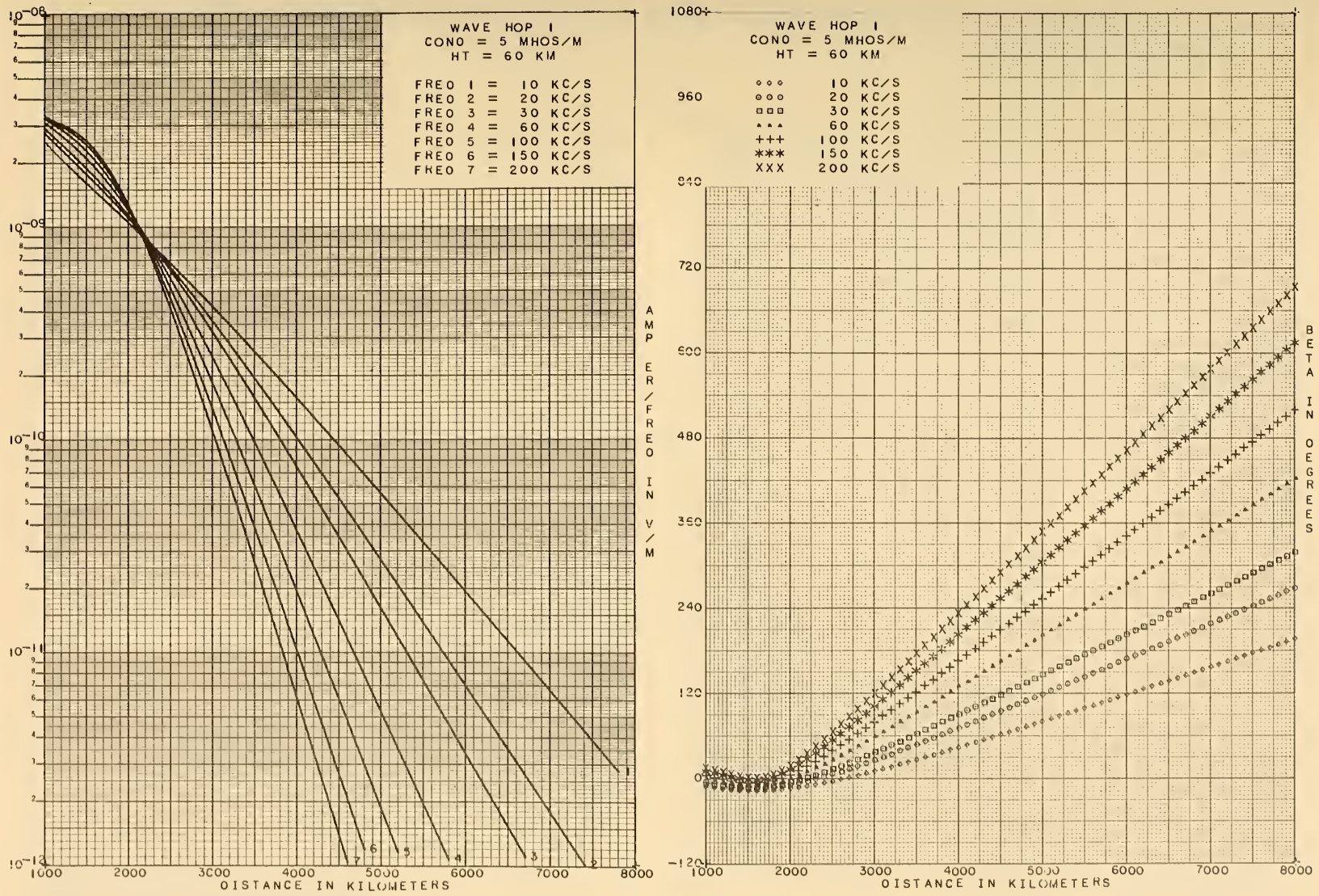

Figure 19.1 Amplitude, $|I_1/f_{kHz}|$, and phase lag, β_1, for parameters shown.

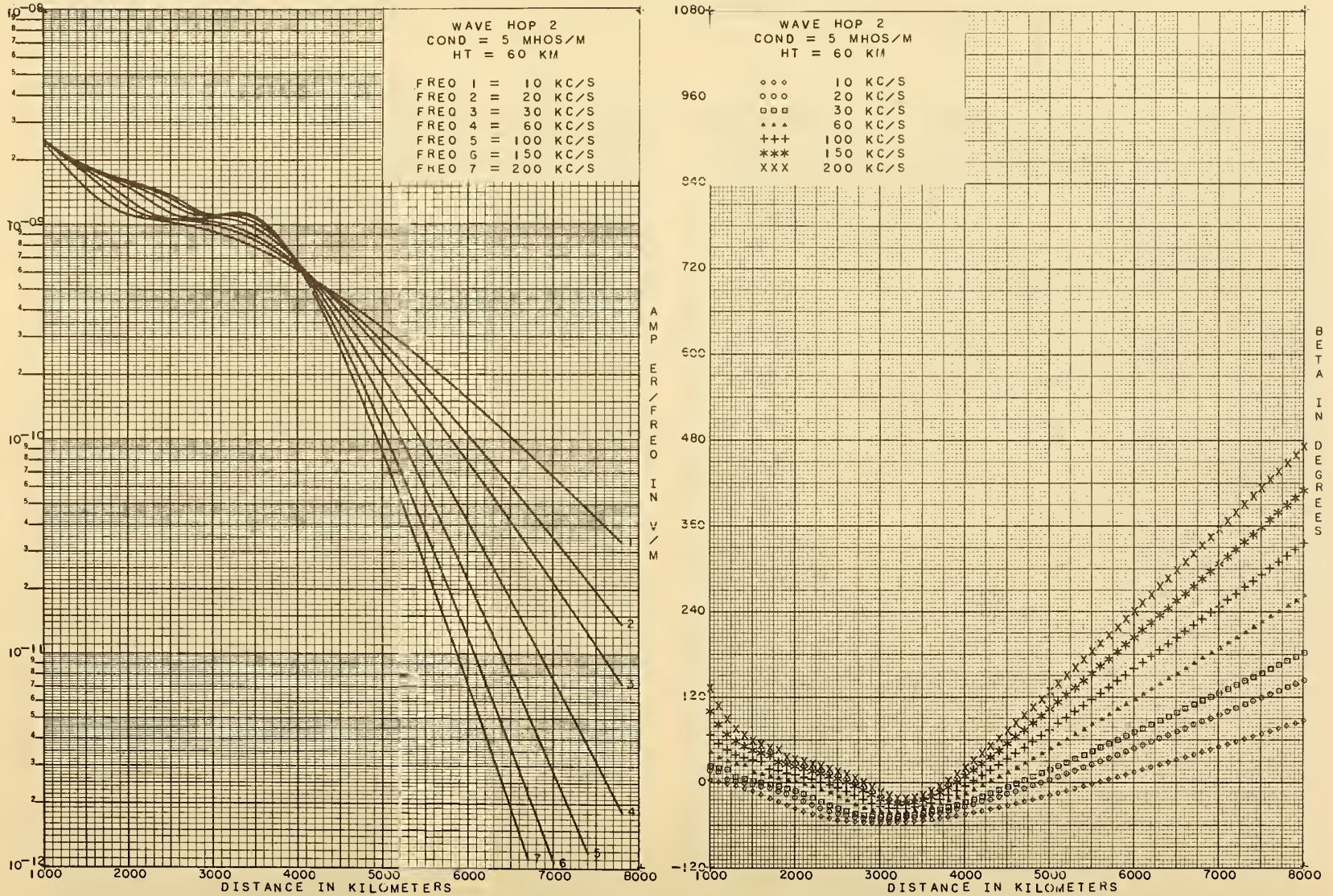

Figure 19.2 Amplitude, $|I_2/f_{kHz}|$, and phase lag, β_2, for parameters shown.

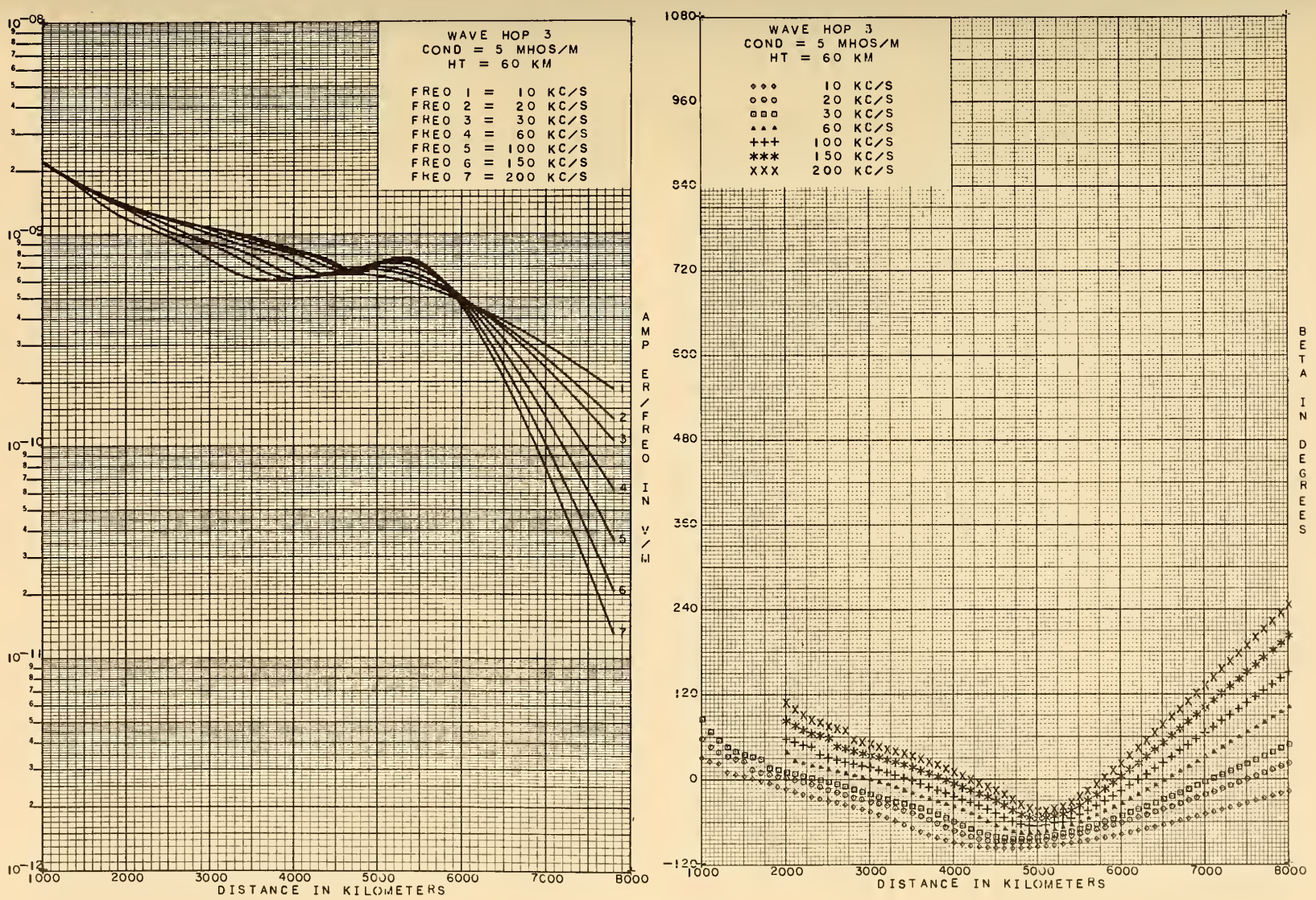

Figure 19.3 Amplitude, $|I_3/f_{kHz}|$, and phase lag, β_3, for parameters shown.

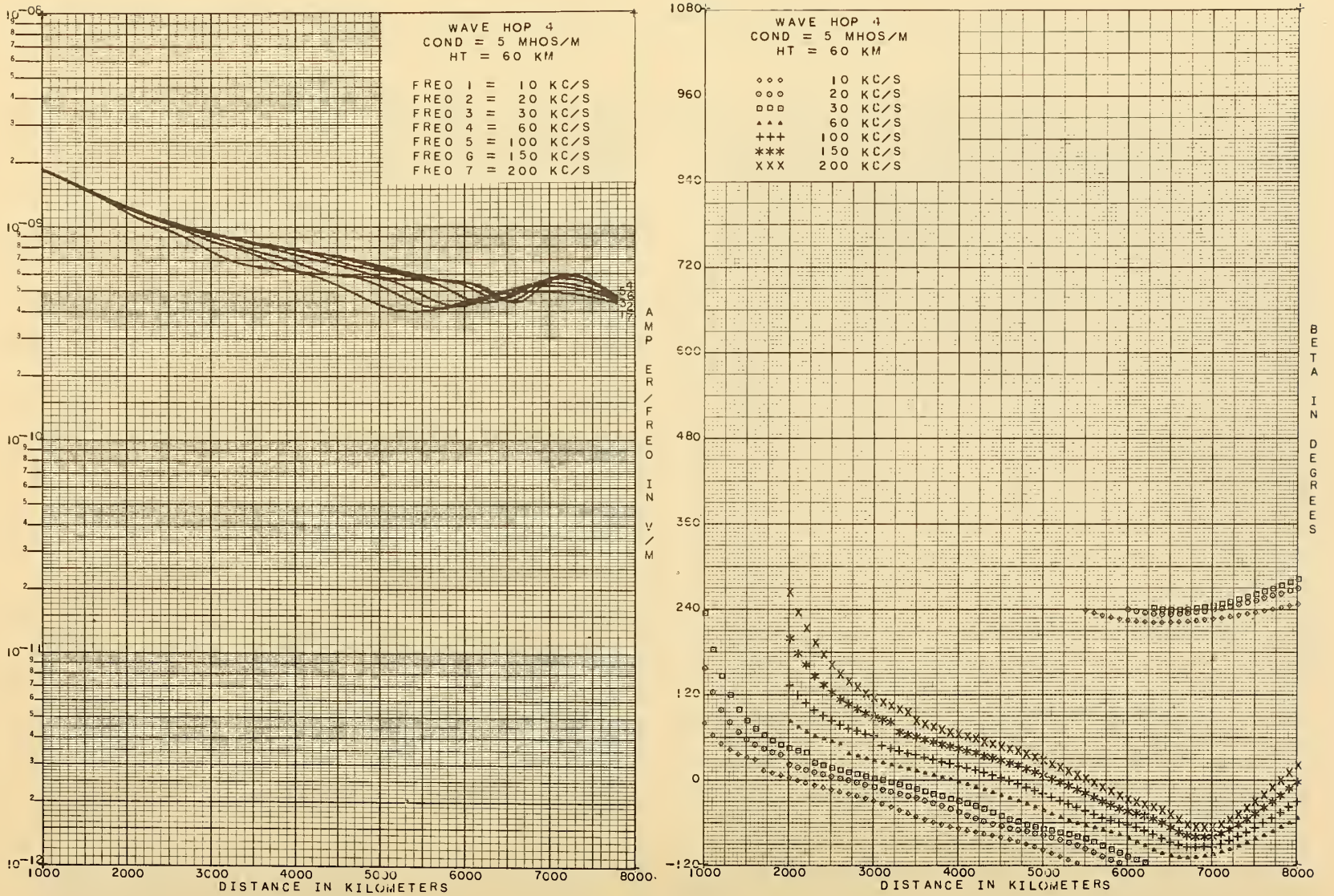

Figure 19.4 Amplitude, $|I_4/f_{kHz}|$, and phase lag, β_4, for parameters shown.

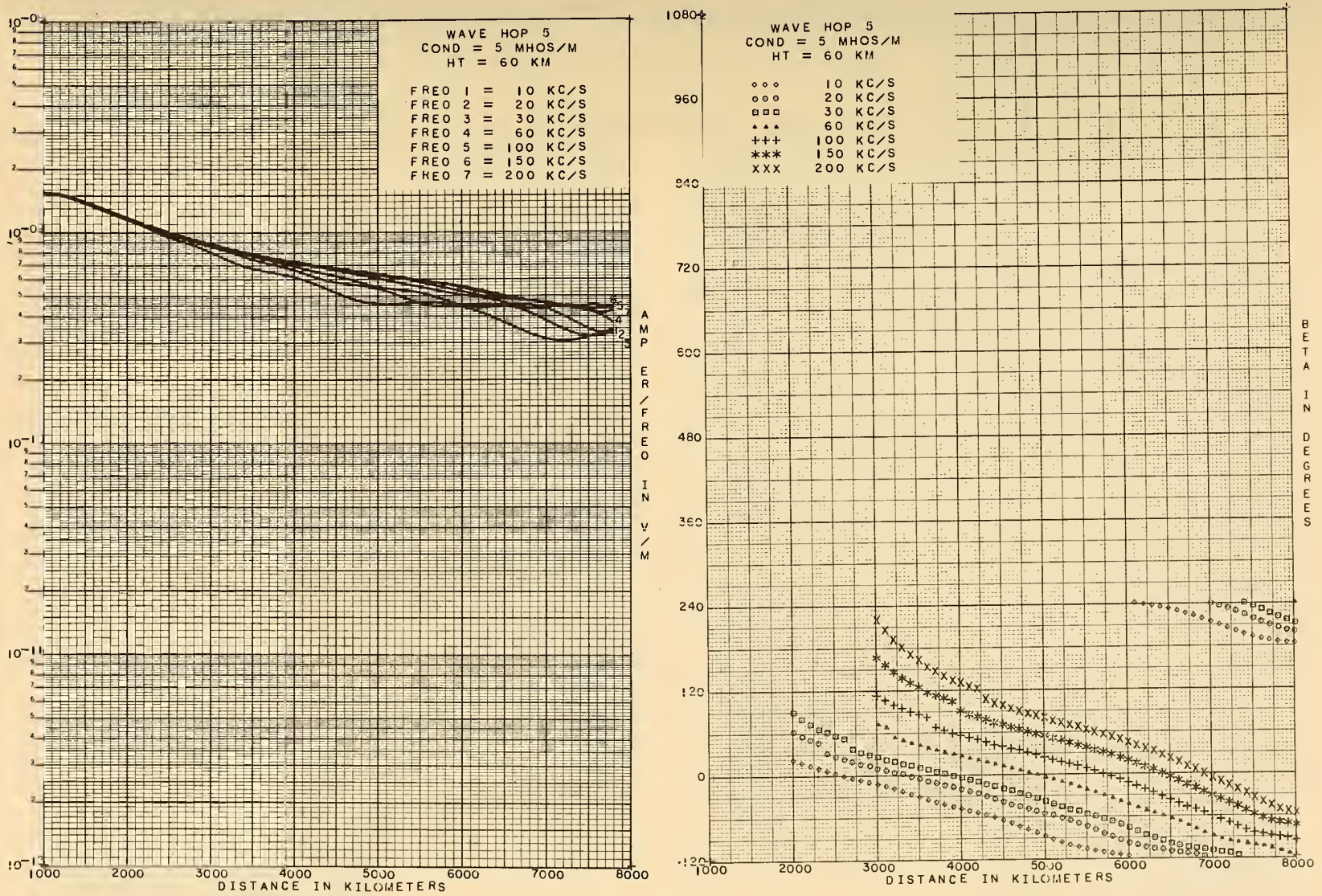

Figure 19.5 Amplitude, $|I_5/f_{kHz}|$, and phase lag, β_5, for parameters shown.

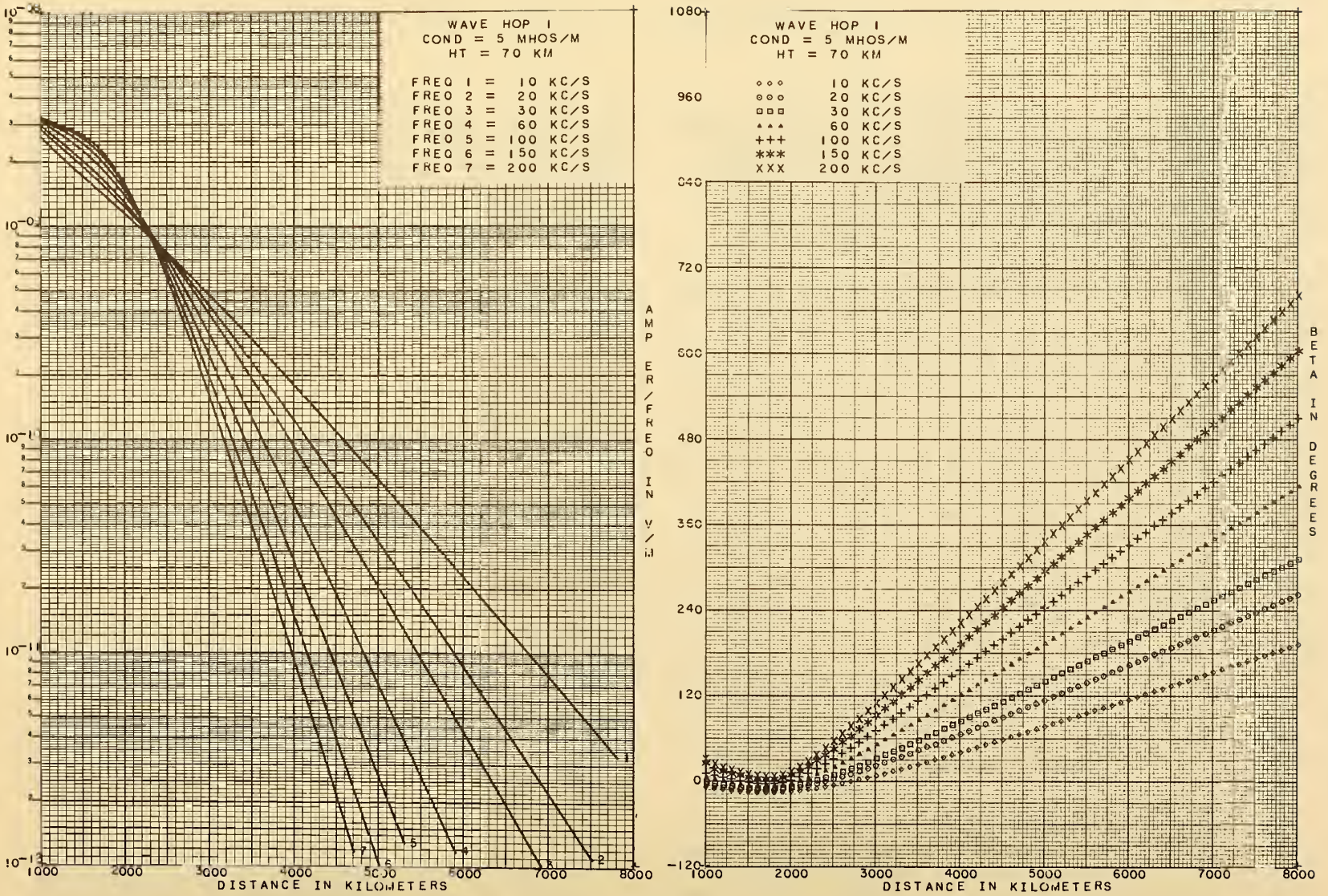

Figure 20.1 Amplitude, $|I_1/f_{kHz}|$, and phase lag, β_1, for parameters shown.

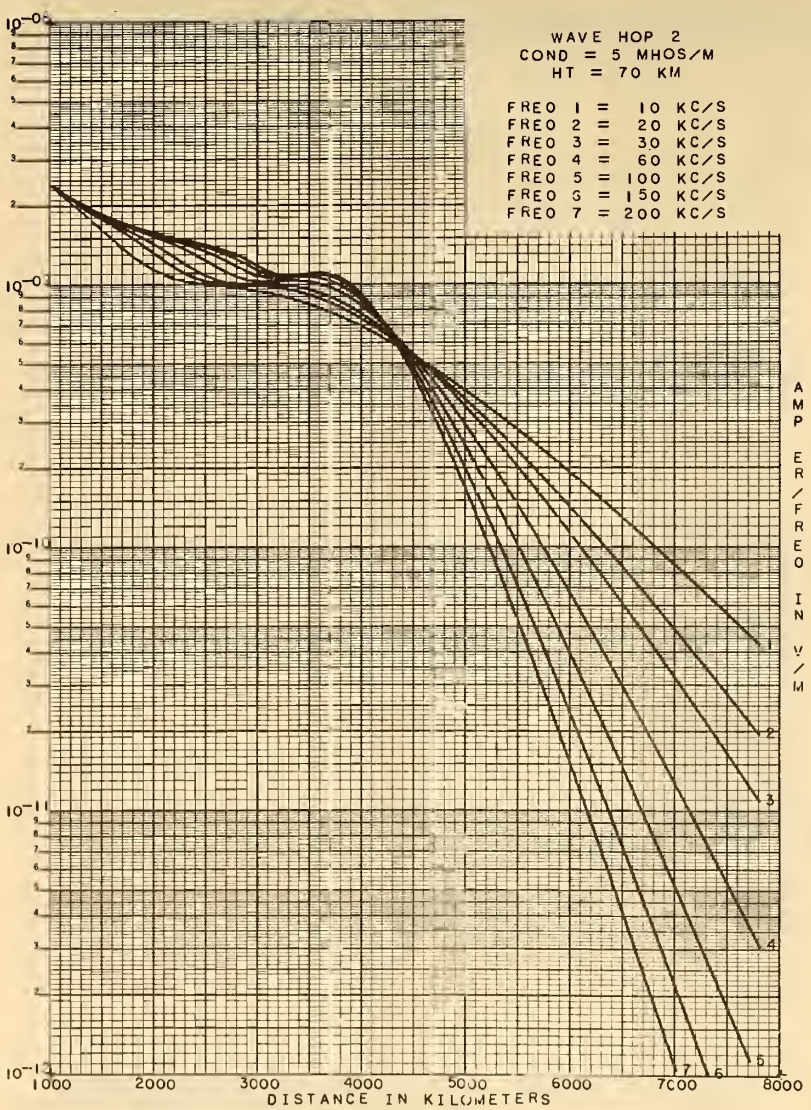

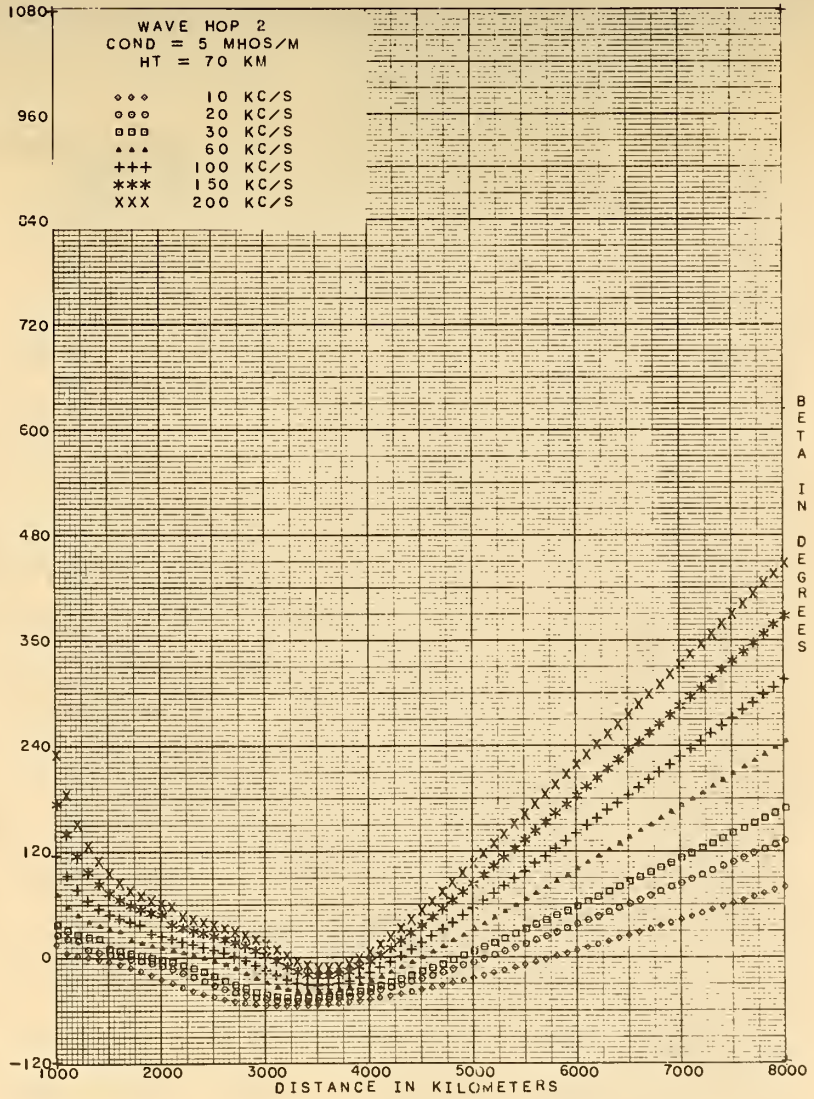

Figure 20.2 Amplitude, $|I_2/f_{kHz}|$, and phase lag, β_2, for parameters shown.

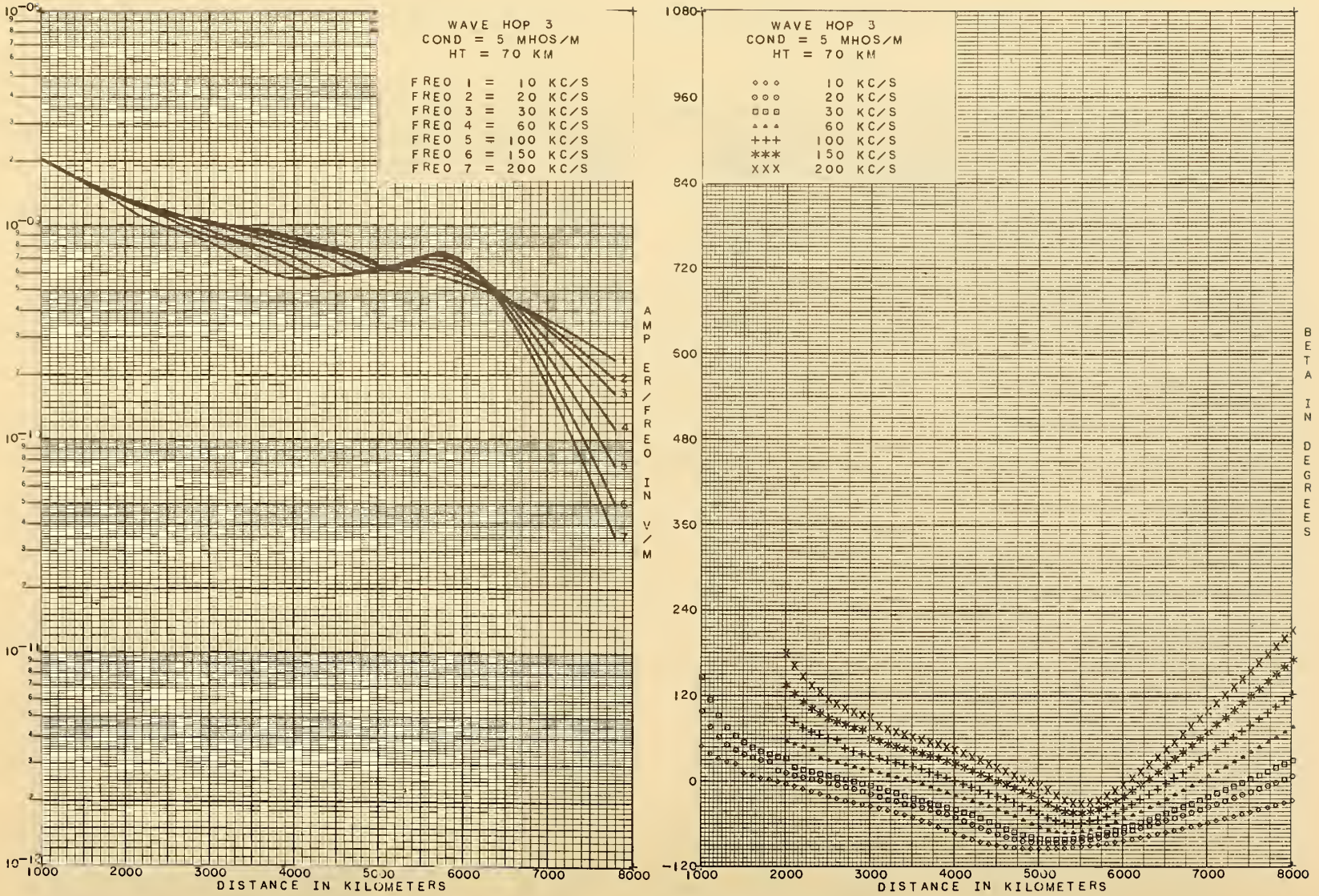

Figure 20.3 Amplitude, $|I_3/f_{kHz}|$, and phase lag, β_3, for parameters shown.

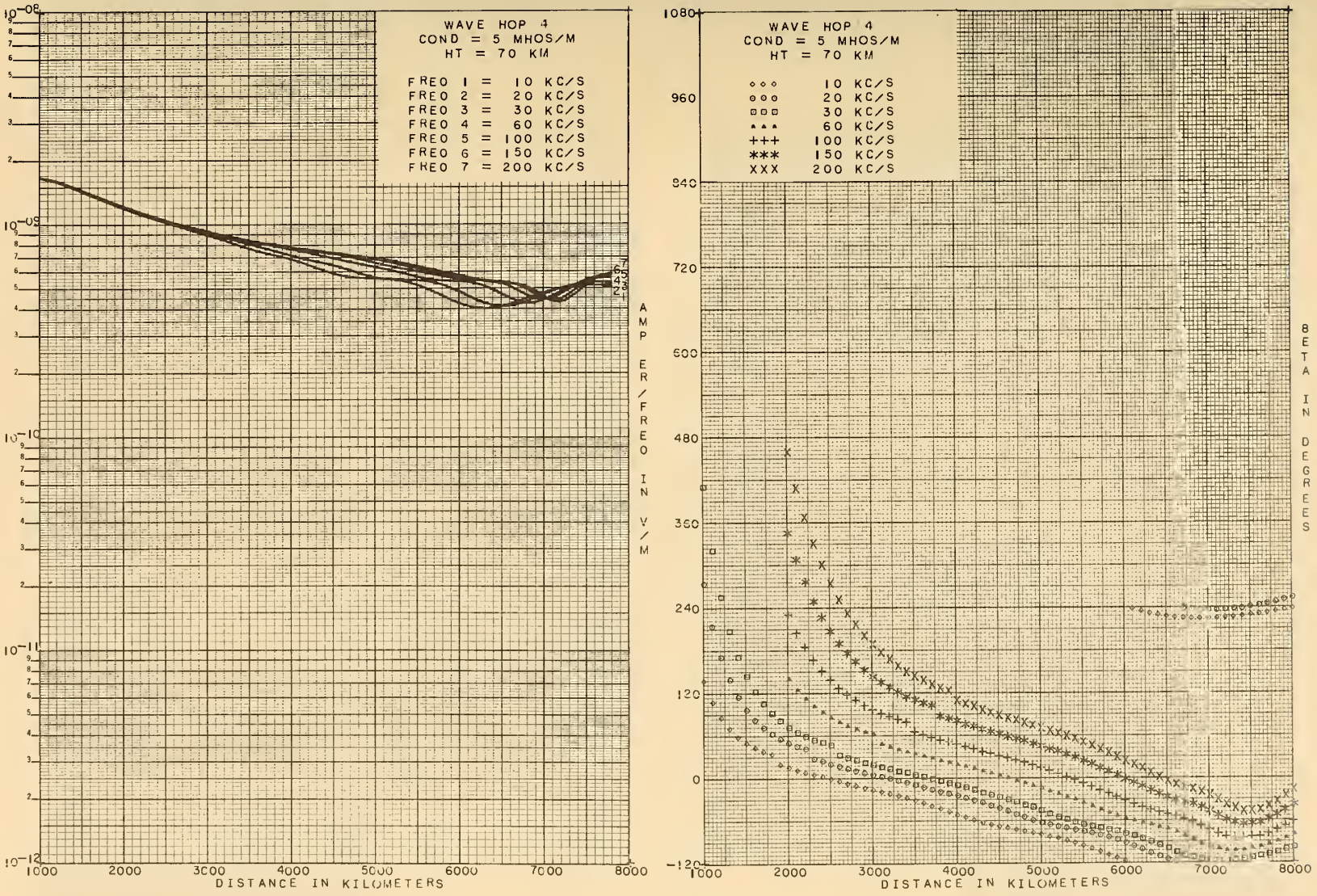

Figure 20.4 Amplitude, $|I_4/f_{kHz}|$, and phase lag, β_4, for parameters shown.

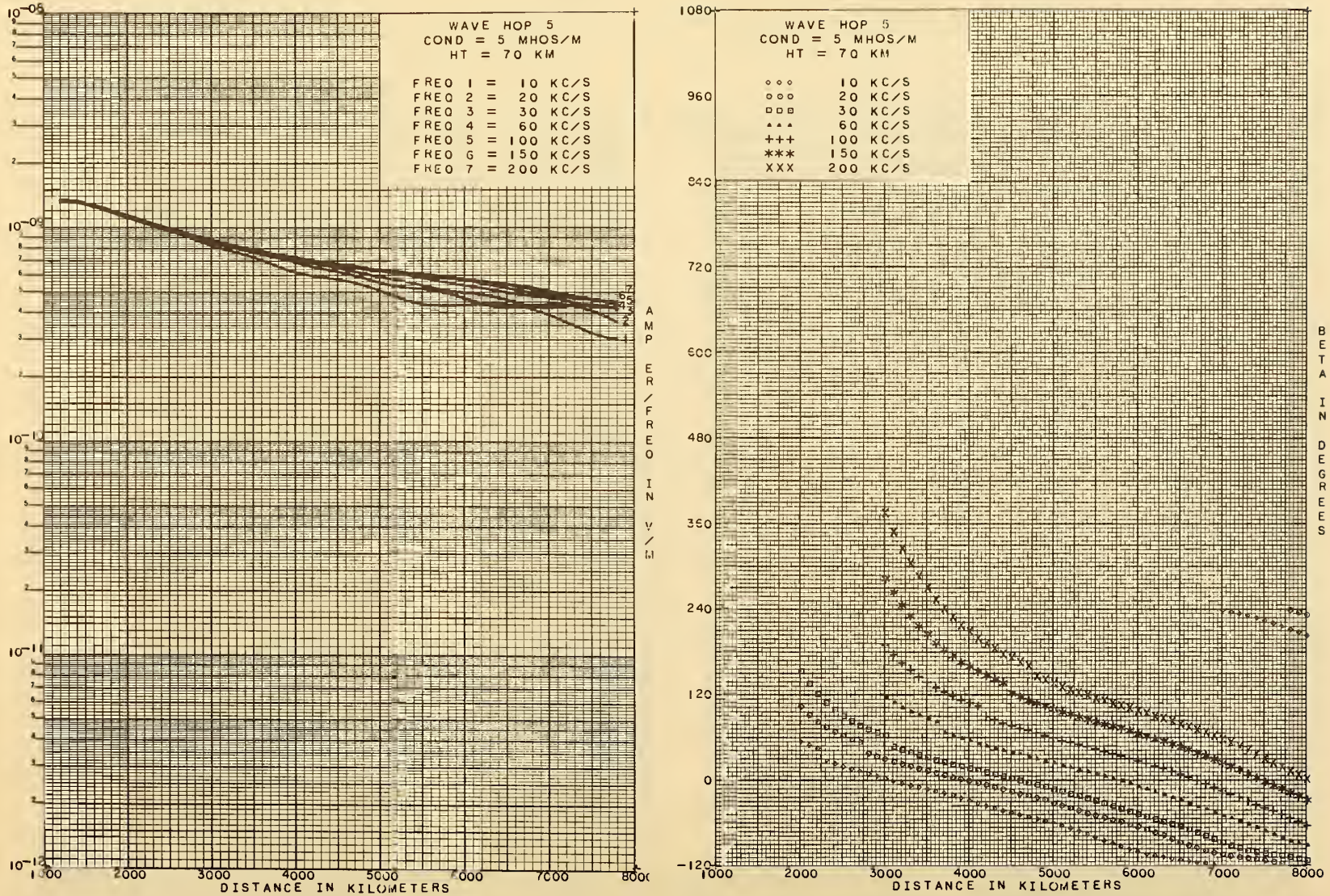

Figure 20.5 Amplitude, $|I_5/f_{kHz}|$, and phase lag, β_5, for parameters shown.

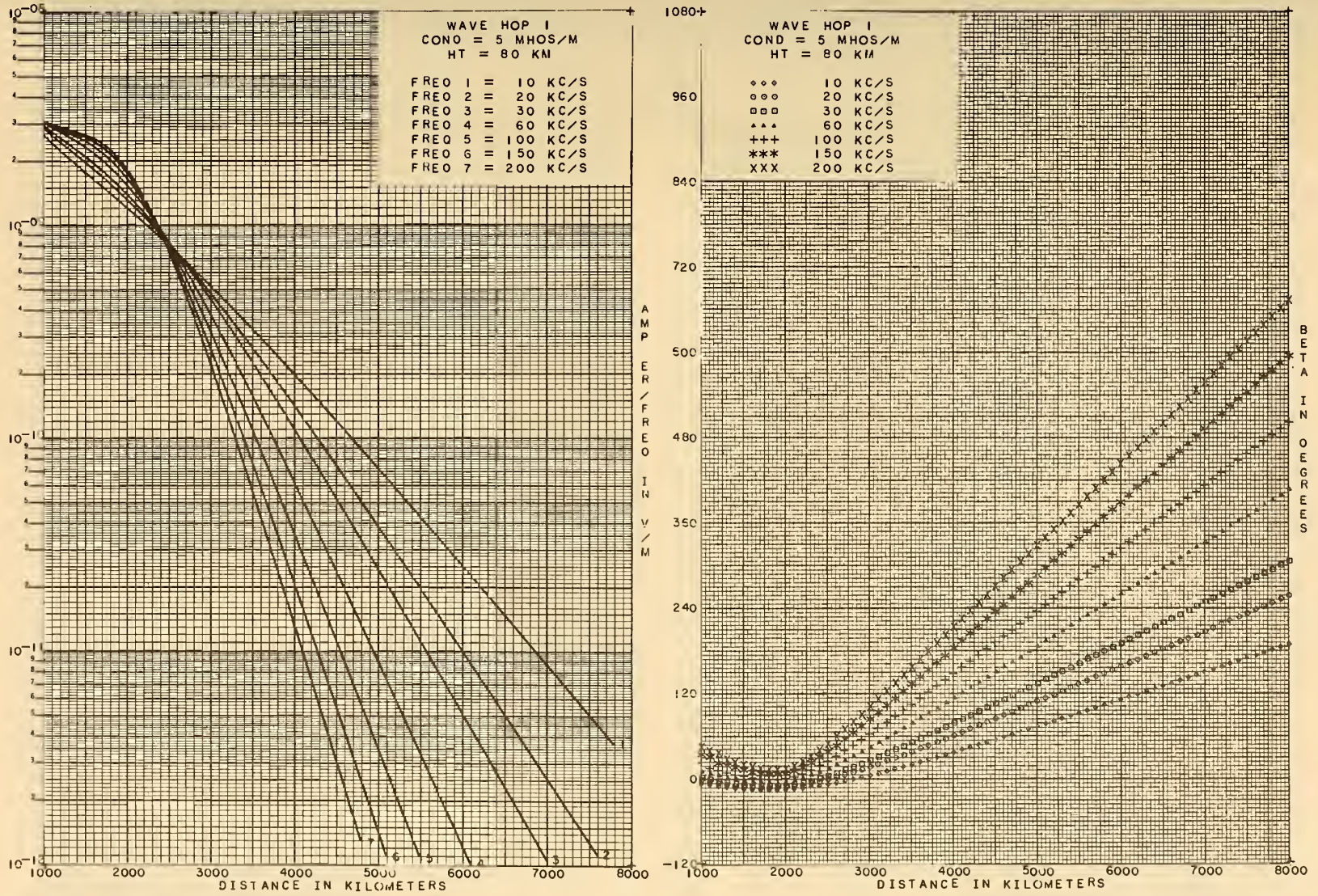

Figure 21.1 Amplitude, $|I_1/f_{kHz}|$, and phase lag, β_1, for parameters shown.

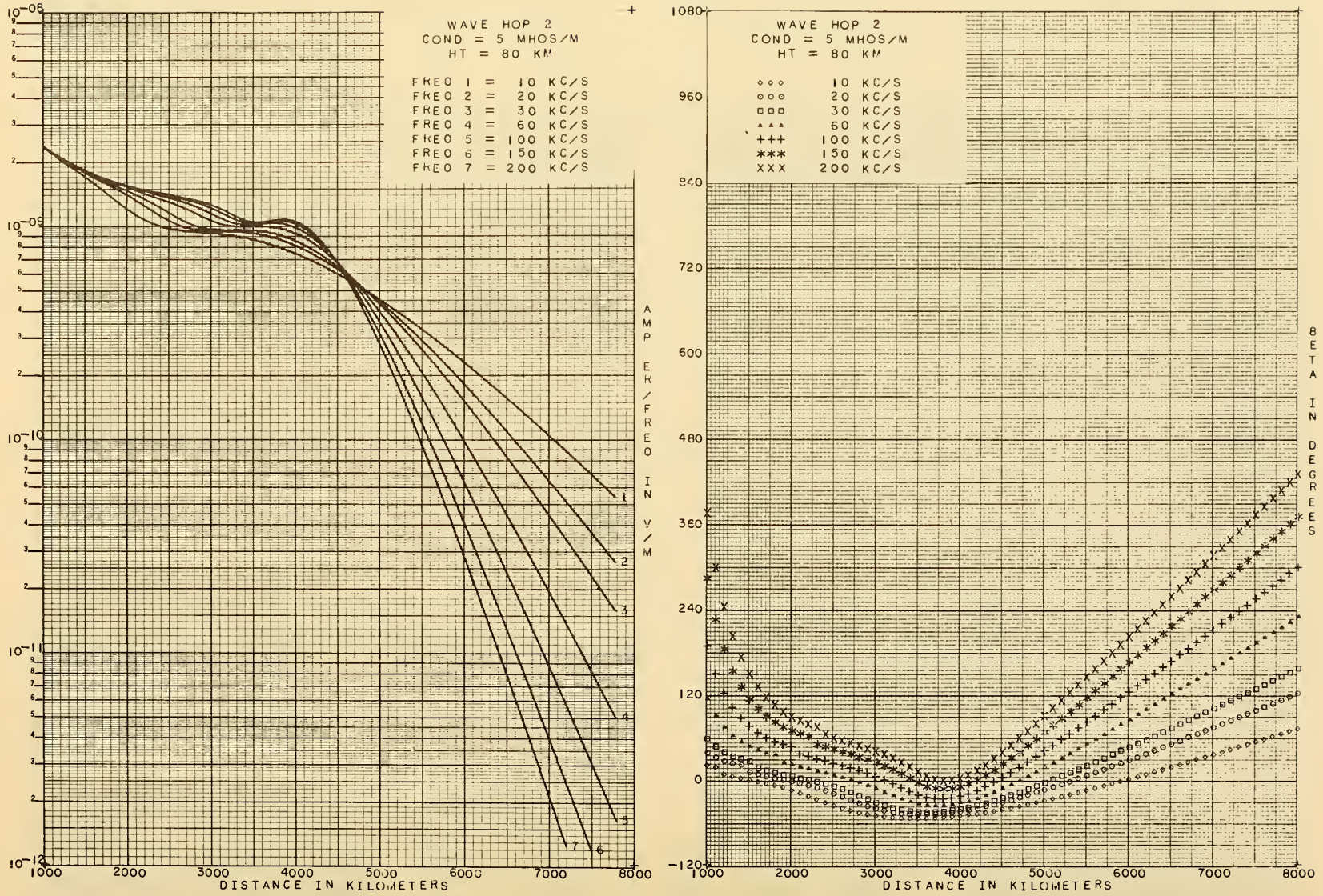

Figure 21.2 Amplitude, $|I_2/f_{kHz}|$, and phase lag, β_2, for parameters shown.

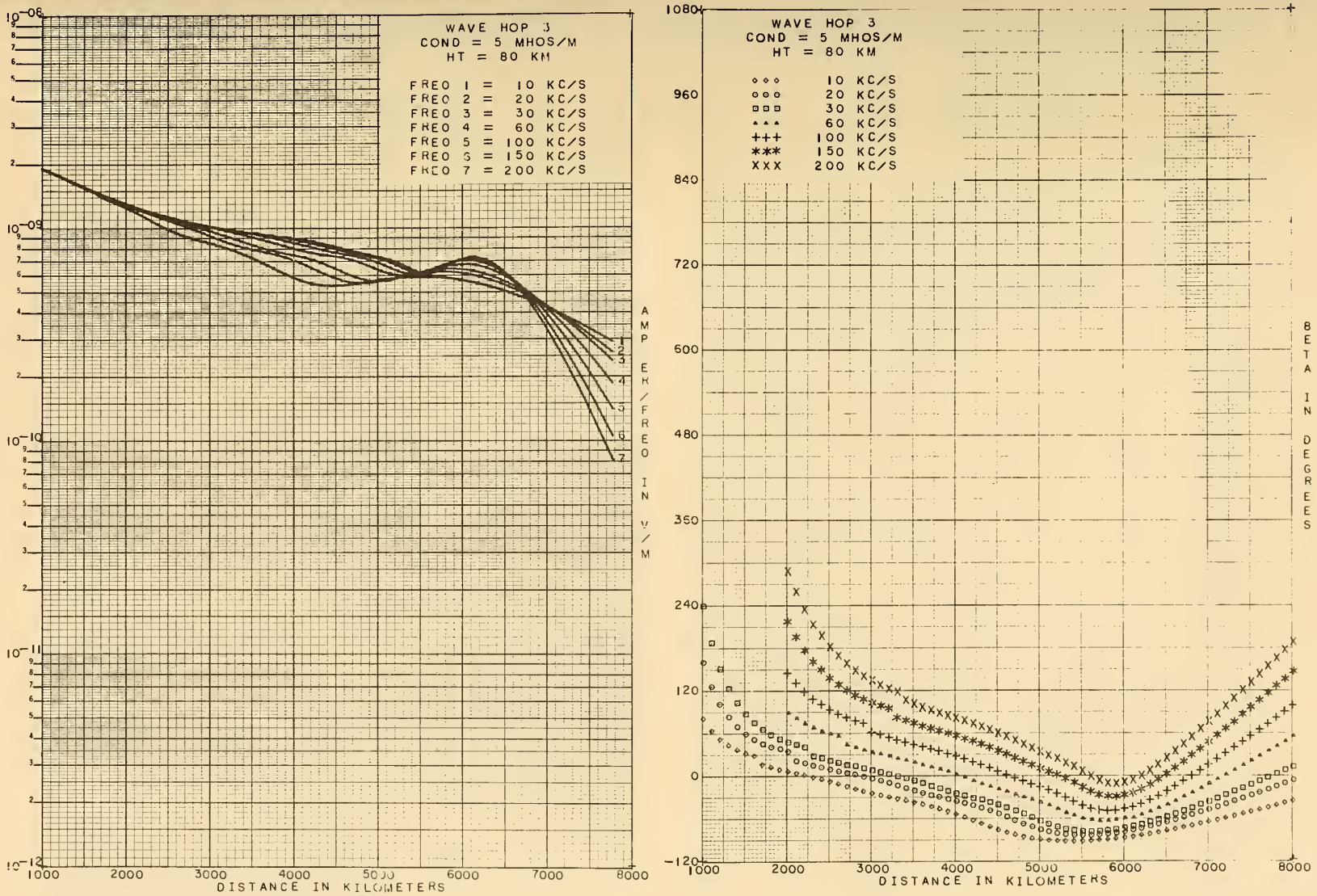

Figure 21.3 Amplitude, $|I_3/f_{kHz}|$, and phase lag, β_3, for parameters shown.

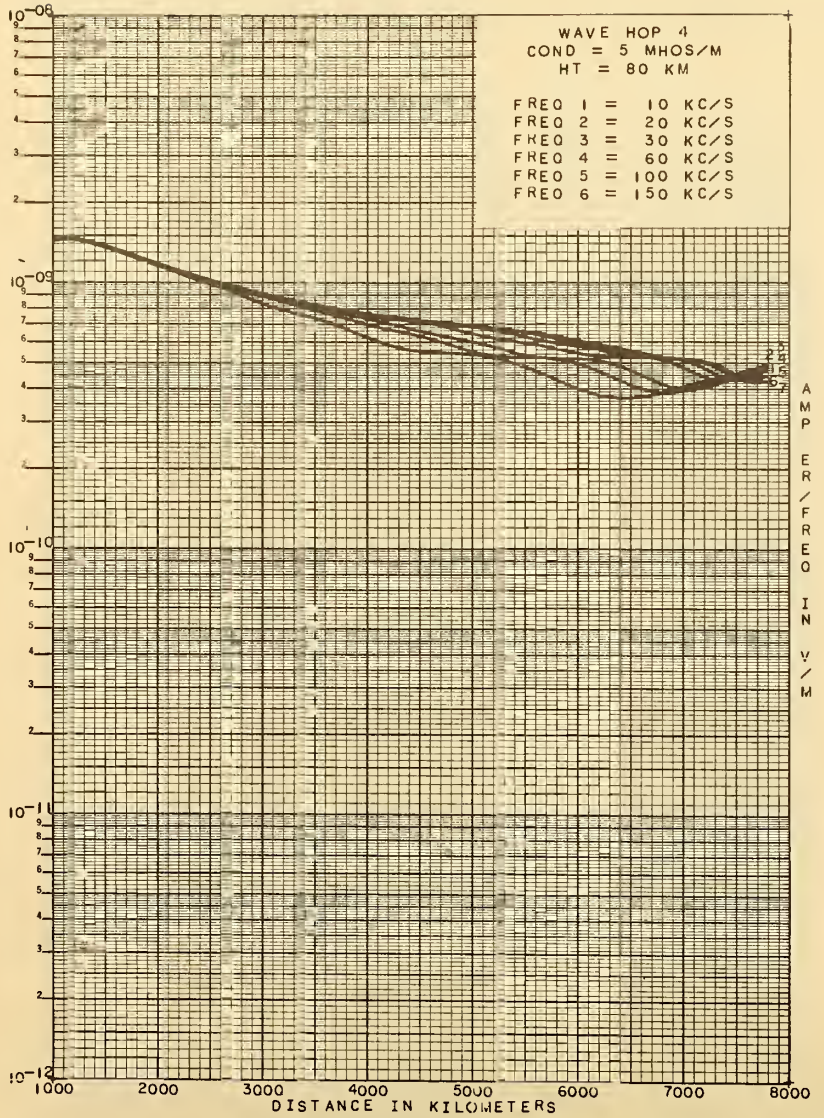

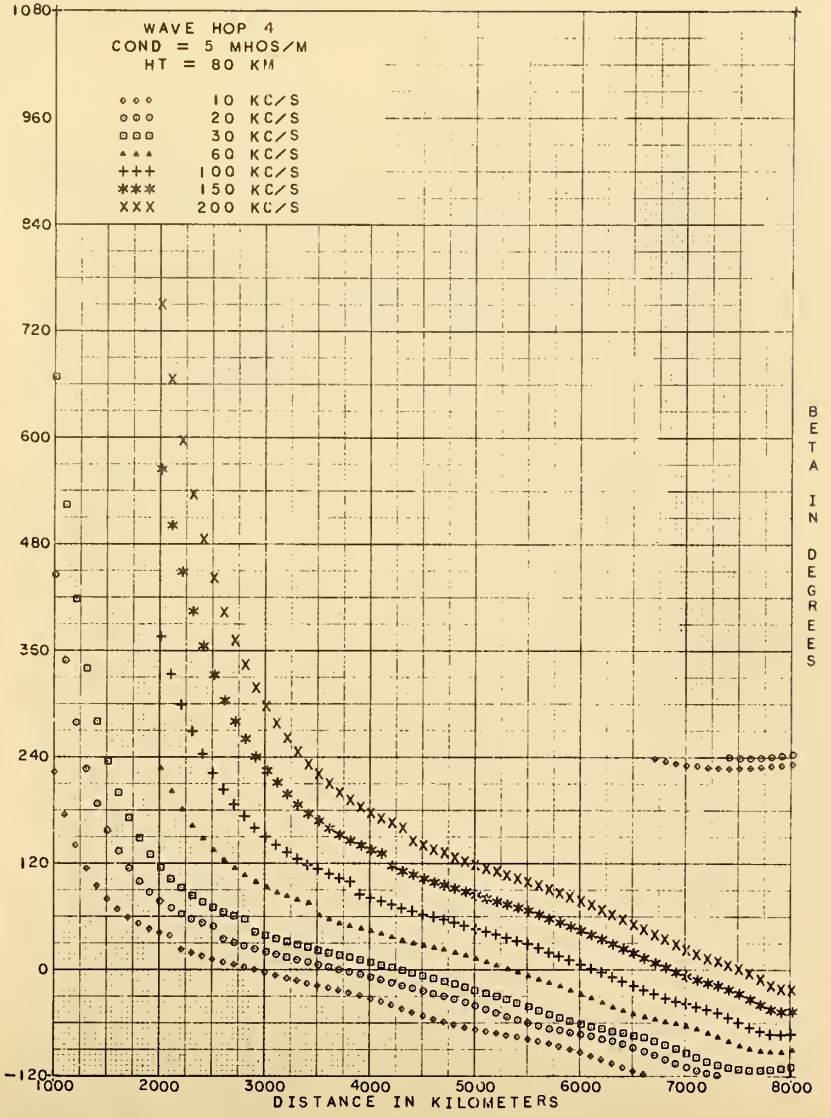

Figure 21.4 Amplitude, $|I_4/f_{kHz}|$, and phase lag, β_4, for parameters shown.

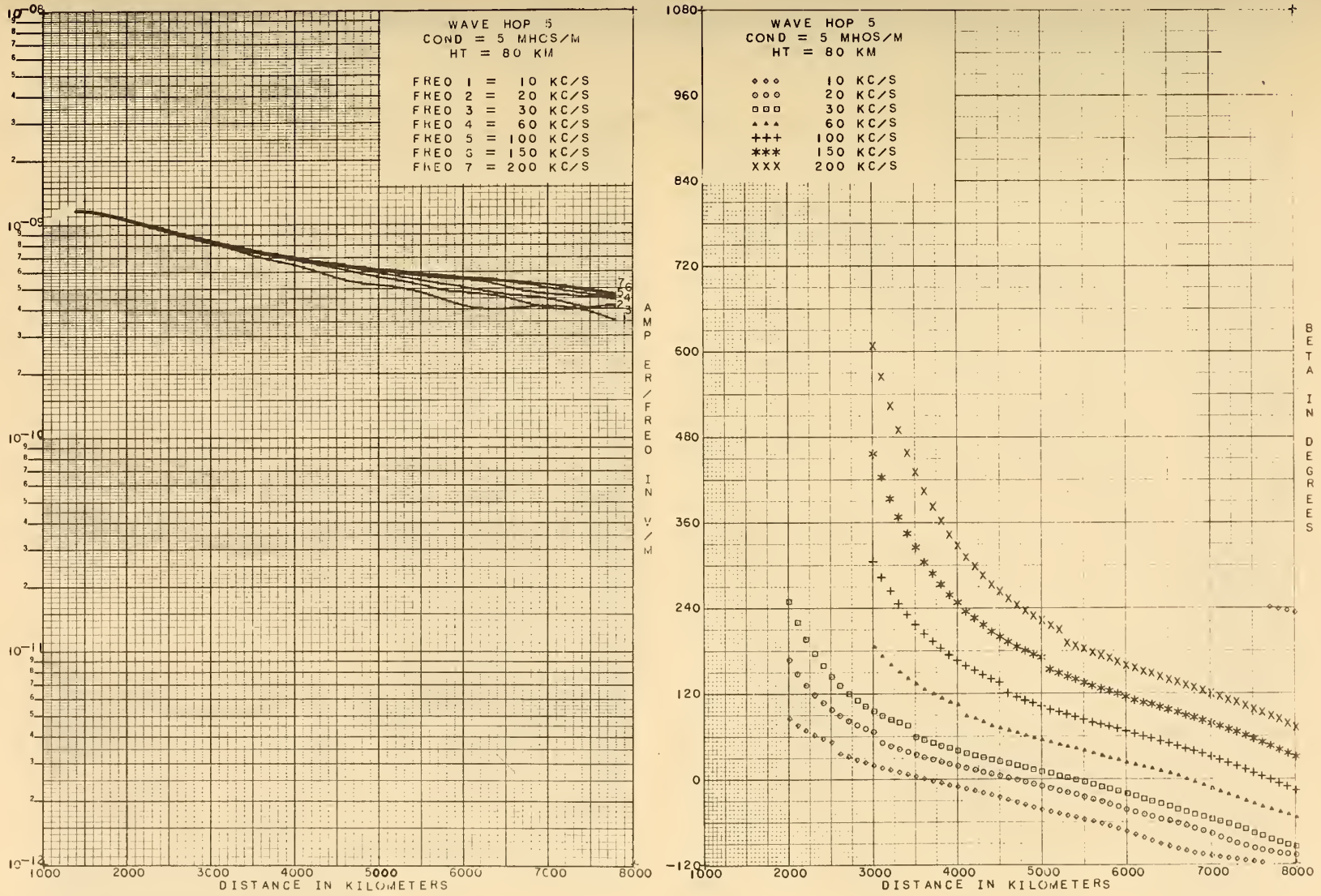

Figure 21.5 Amplitude, $|I_5/f_{kHz}|$, and phase lag, β_5, for parameters shown.

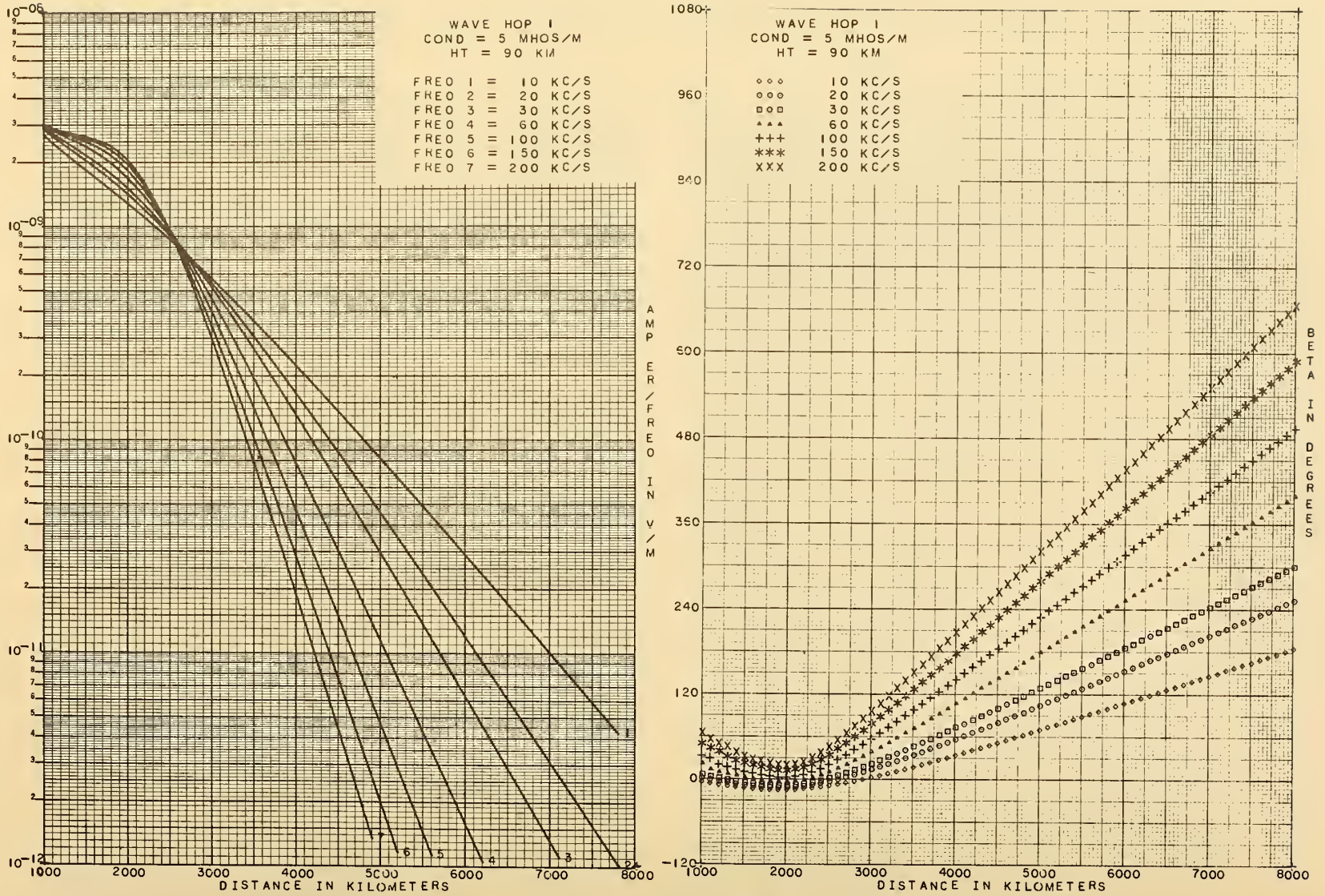

Figure 22.1 Amplitude, $|I_1/f_{kHz}|$, and phase lag, β_1, for parameters shown.

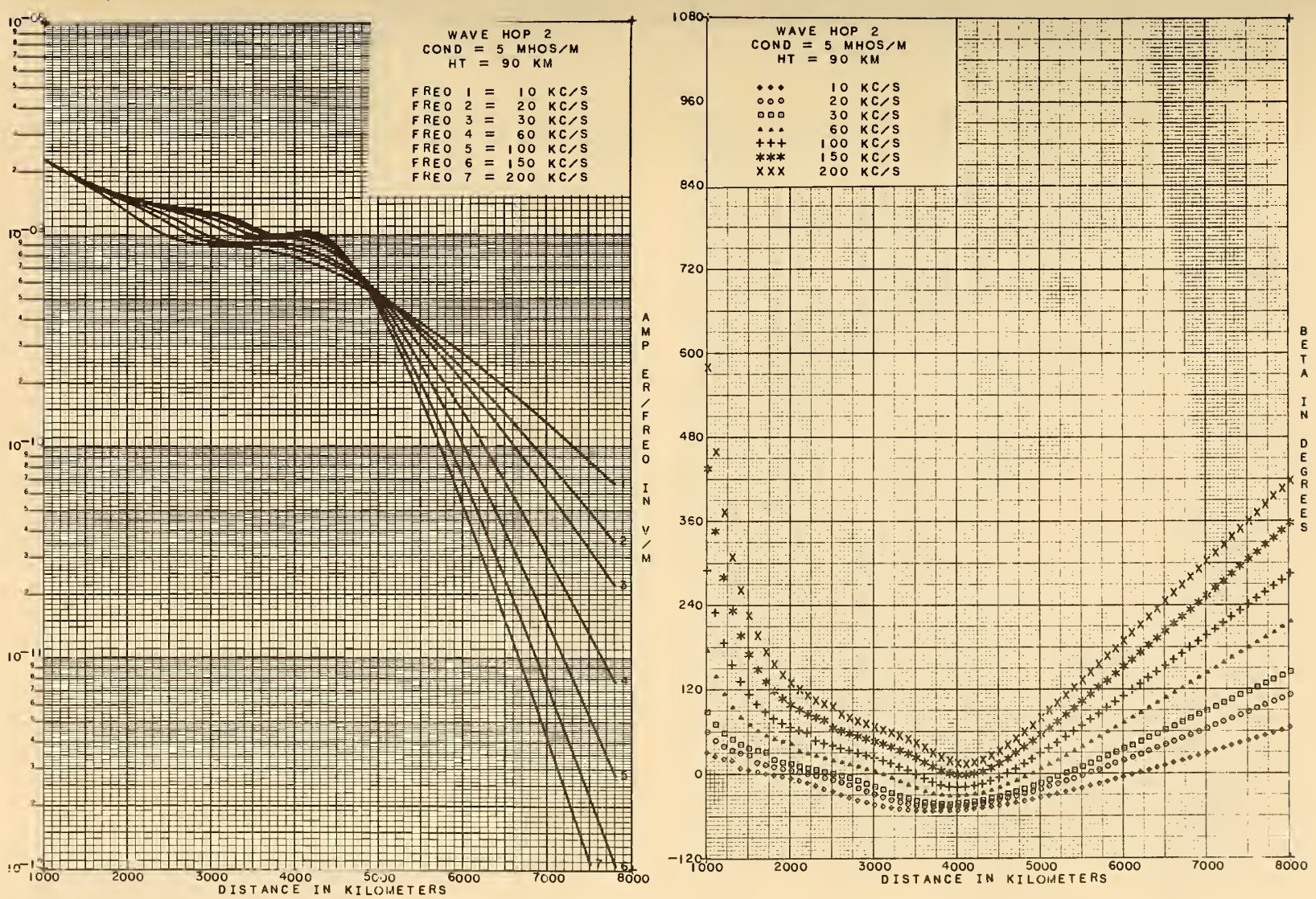

Figure 22.2 Amplitude, $|I_2/f_{kHz}|$, and phase lag, β_2, for parameters shown.

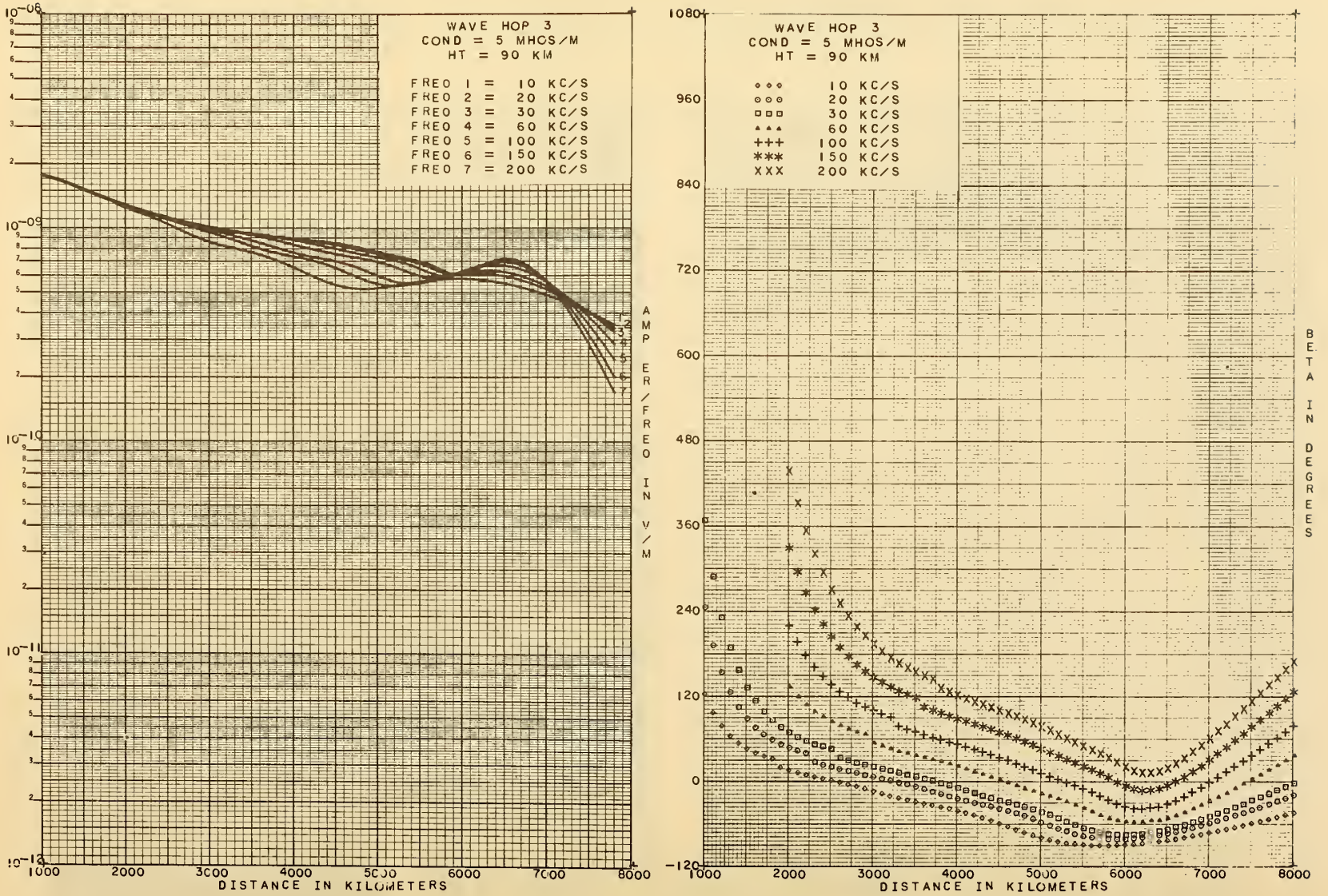

Figure 22.3 Amplitude, $|I_3/f_{kHz}|$, and phase lag, β_3, for parameters shown.

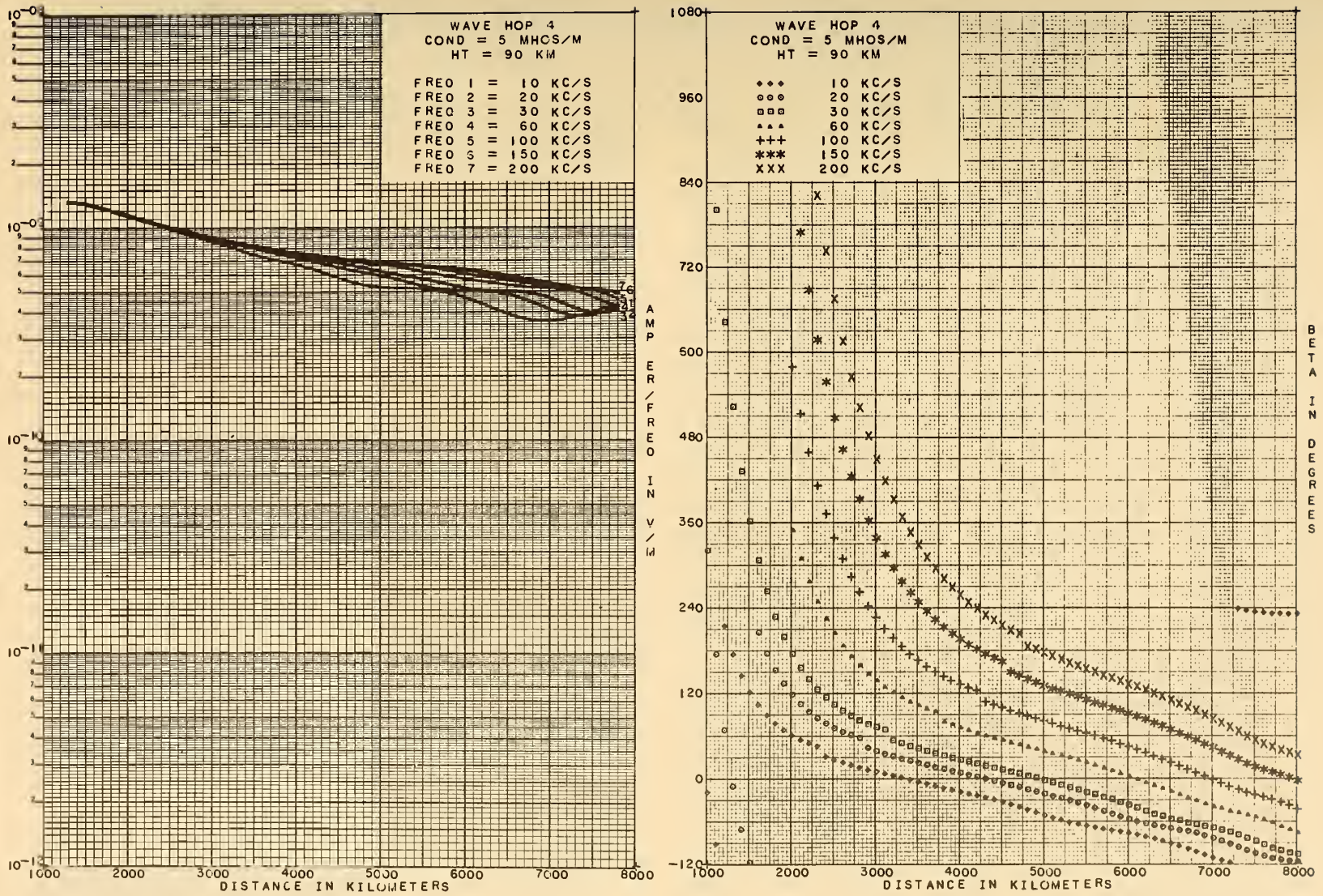

Figure 22.4 Amplitude, $|I_4/f_{kHz}|$, and phase lag, β_4, for parameters shown.

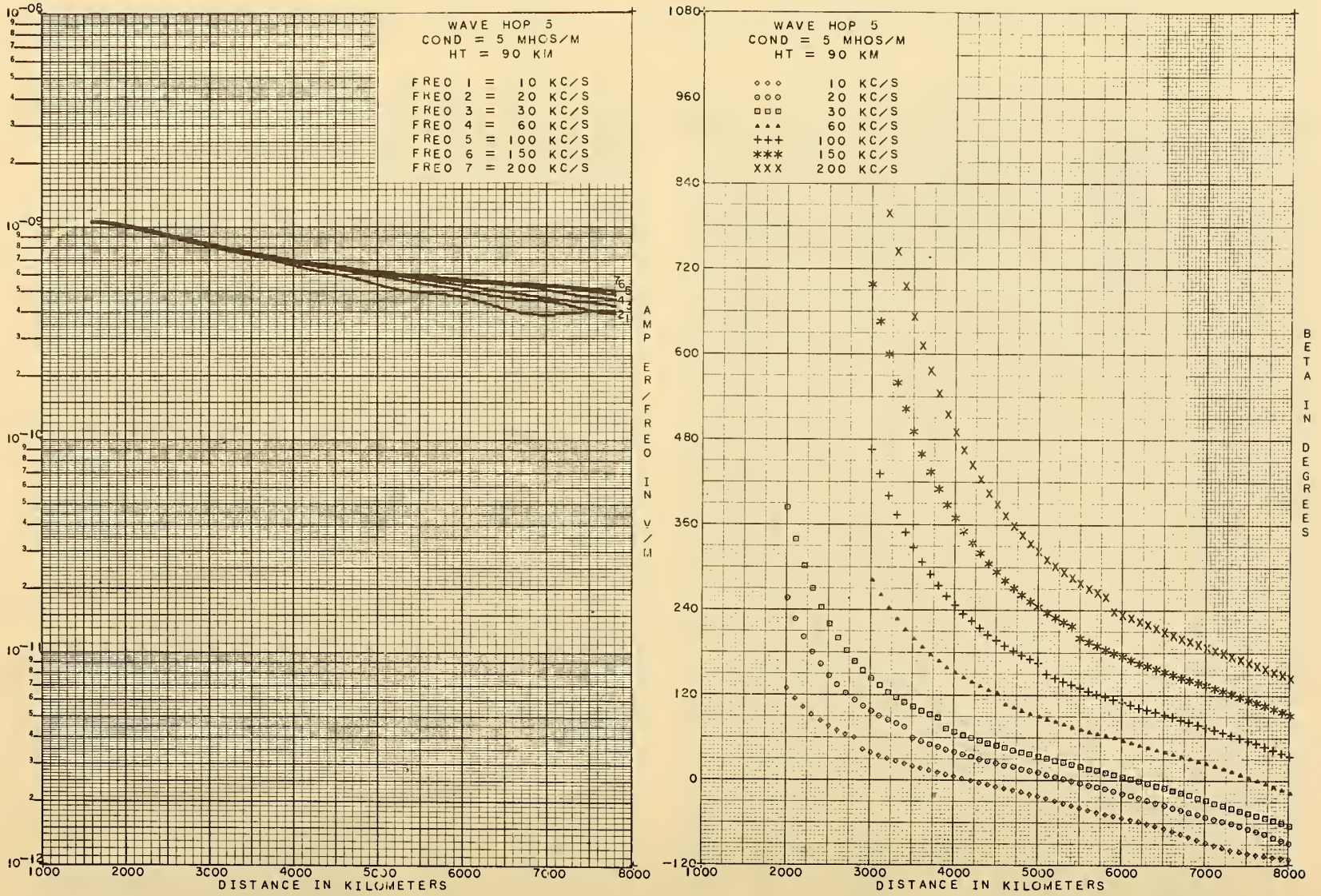

Figure 22.5 Amplitude, $|I_5/f_{kHz}|$, and phase lag, β_5, for parameters shown.

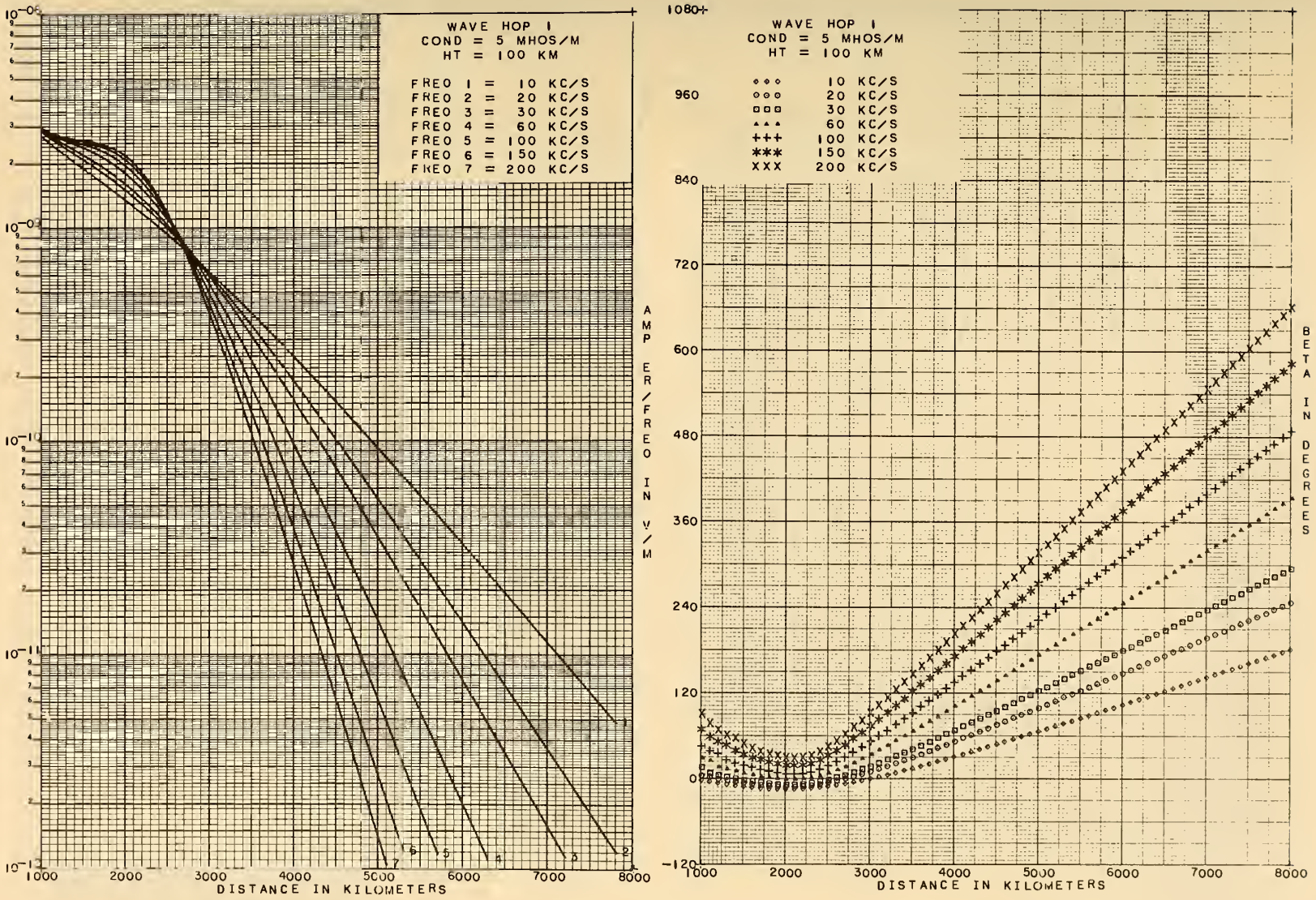

Figure 23.1 Amplitude, $|I_1/f_{kHz}|$, and phase lag, β_1, for parameters shown.

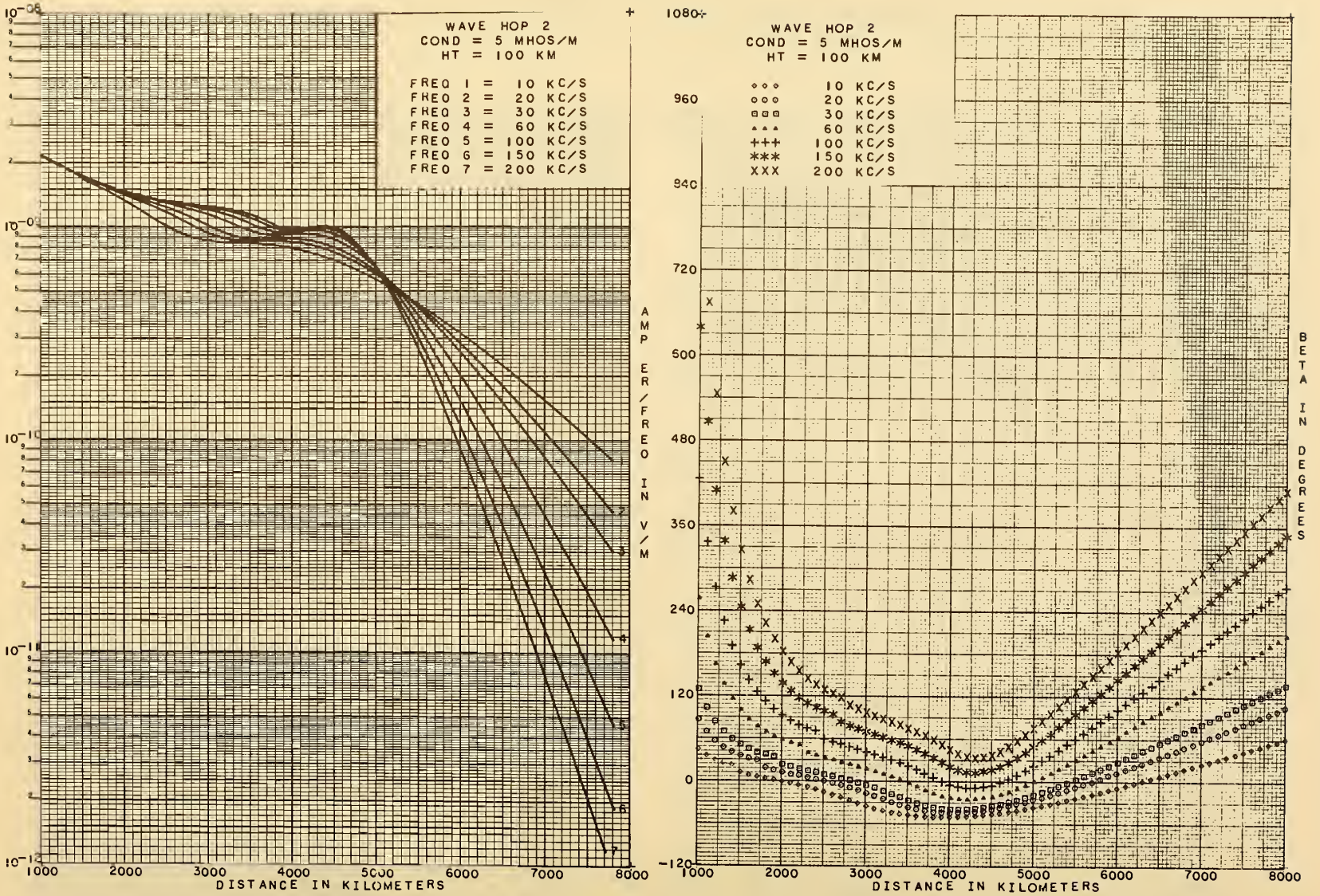

Figure 23.2 Amplitude, $|I_2/f_{kHz}|$, and phase lag, β_2, for parameters shown.

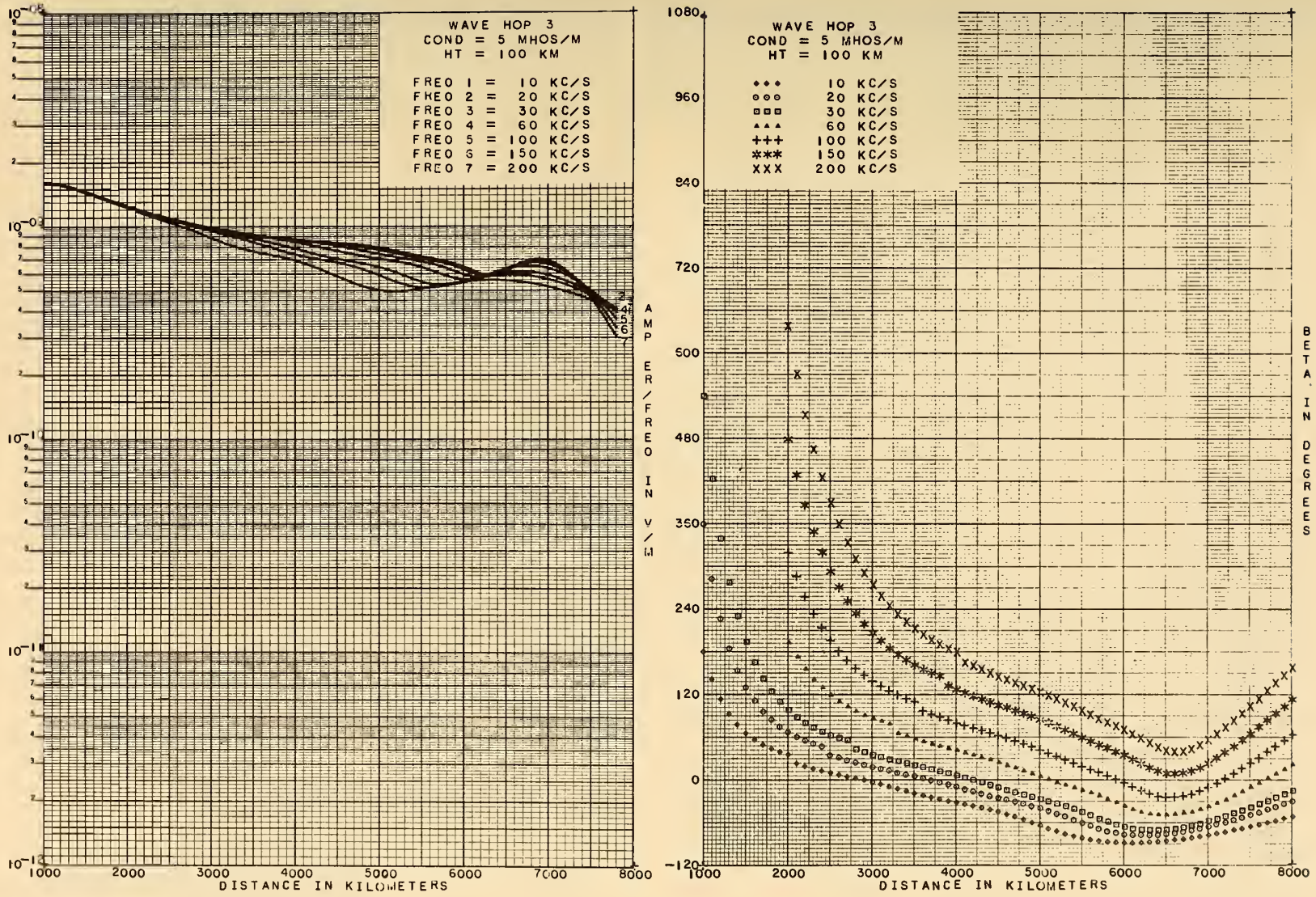

Figure 23.3 Amplitude, $|I_3/f_{kHz}|$, and phase lag, β_3, for parameters shown.

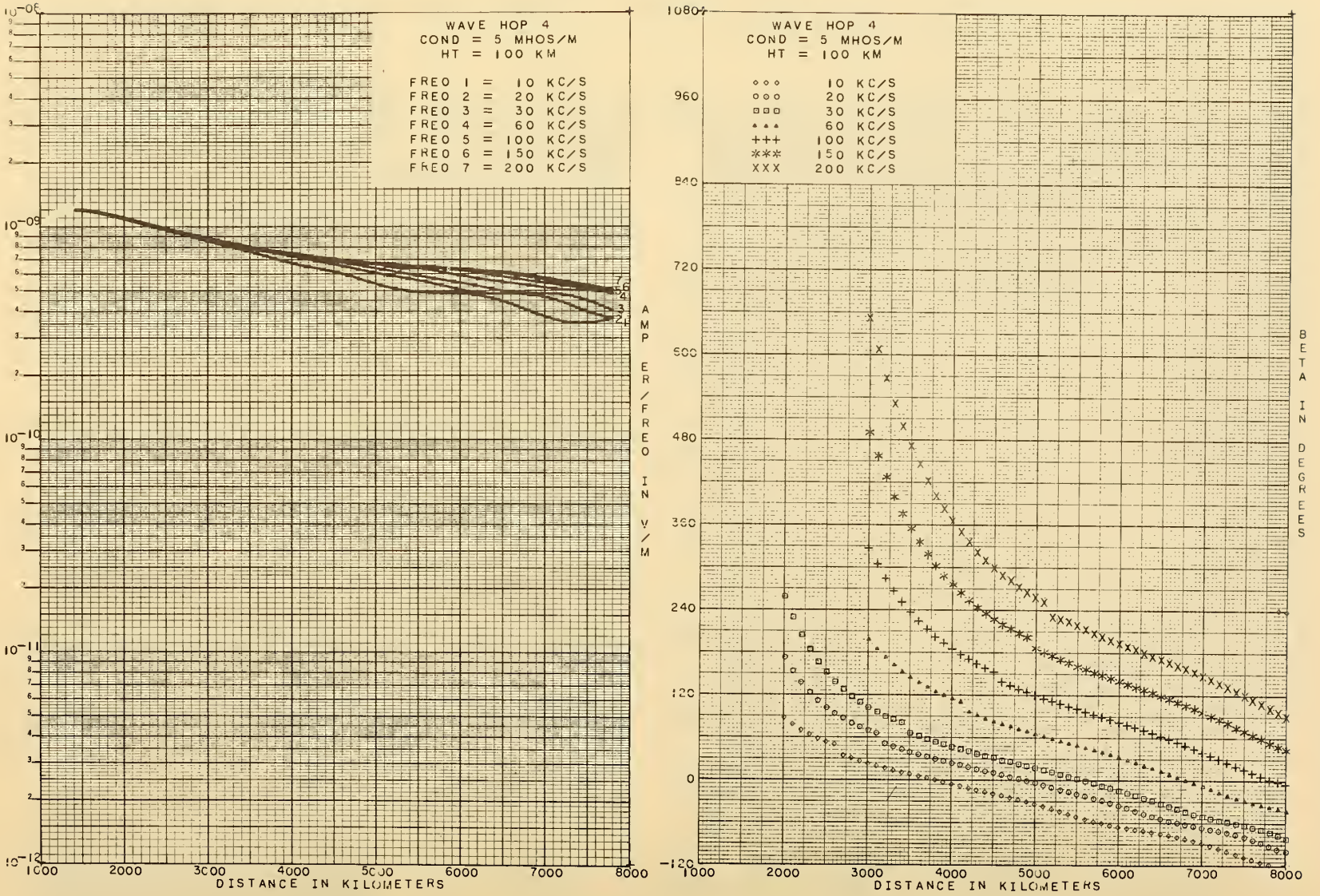

Figure 23.4 Amplitude, $|I_4/f_{kHz}|$, and phase lag, β_4, for parameters shown.

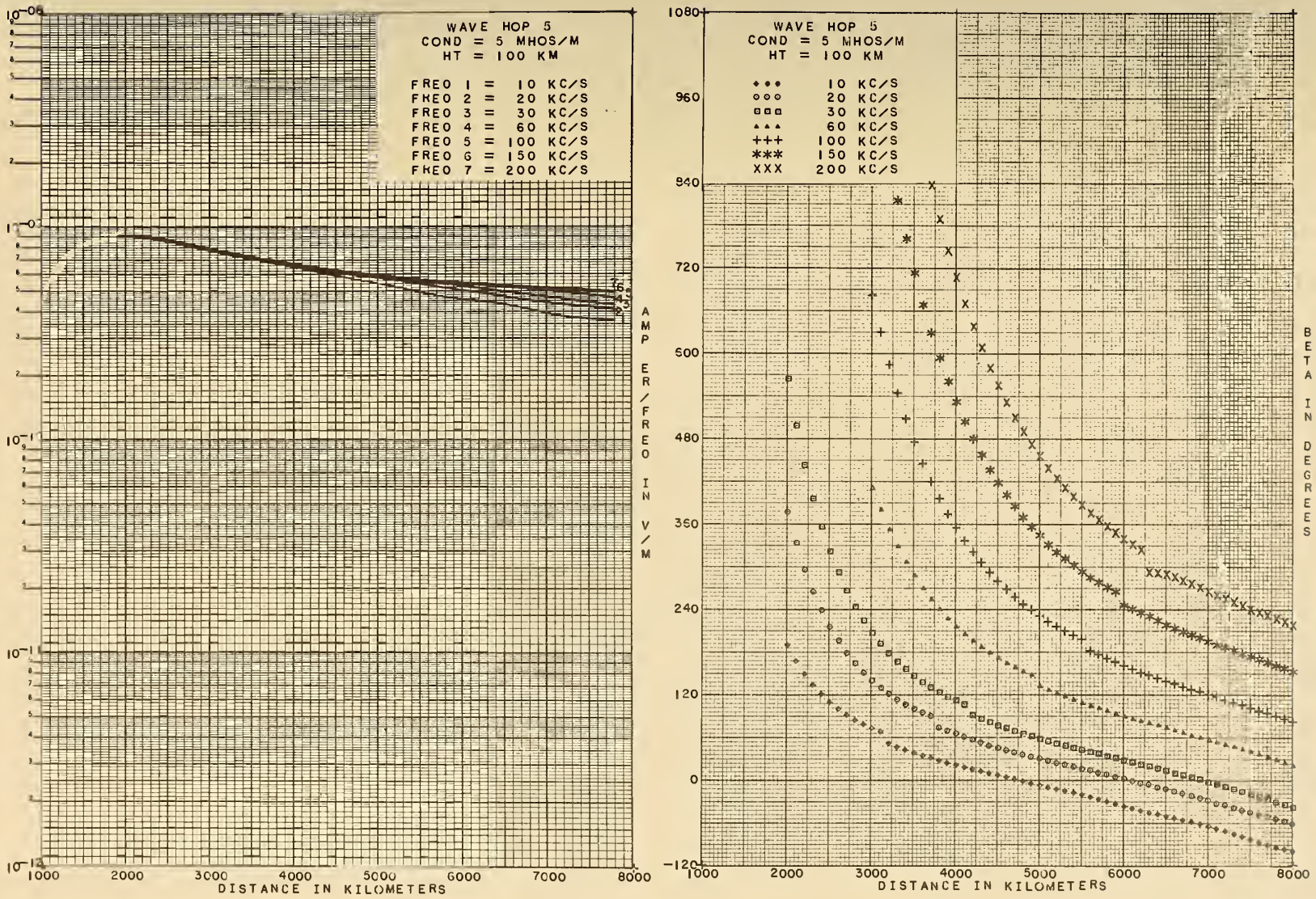

Figure 23.5 Amplitude, $|I_5/f_{kHz}|$, and phase lag, β_5, for parameters shown.

U.S. DEPARTMENT OF COMMERCE
WASHINGTON, D.C. 20230

OFFICIAL BUSINESS

POSTAGE AND FEES PAID
U.S. DEPARTMENT OF COMMERCE